DEPARTAMENTO DE FÍSICA TEÓRICA

EFFECTIVE FIELD THEORIES FOR HEAVY AND LIGHT FERMIONS

PEDRO DAVID RUIZ FEMENÍA

UNIVERSITAT DE VALENCIA
Servei de Publicacions
2004

Aquesta Tesi Doctoral va ser presentada a Valencia el día 11 de Desembre de 2004 davant un tribunal format per:

- D. José Bernabeu Alberola
- D. Vicent Giménez Gómez
- D. Marc Knecht
- D. Joaquín Salvador Prades
- D. Antonio Miguel Pineda Ruiz

Va ser dirigida per:
D. Antonio Pich Zardova
D. Jorge Portolés Ibáñez

Depòsit legal:
I.S.B.N.:84-370-5900-3
Edita: Universitat de València
Servei de Publicacions
C/ Artes Gráficas, 13 bajo
46010 València
Spain
Telèfon: 963864115

VNIVERSITAT DE VALÈNCIA
Departament de Física Teòrica

Effective Field Theories for Heavy and Light Fermions

Tesis Doctoral

Pedro David Ruiz Femenía

SEPTIEMBRE 2003

Consejo Superior de Investigaciones Científicas
Universitat de València
IFIC - INSTITUTO DE FISICA CORPUSCULAR

Effective Field Theories for Heavy and Light Fermions

Pedro David Ruiz Femenía

Departament de Física Teòrica, IFIC
Universitat de València - CSIC

Antonio Pich Zardoya, Catedrático del Departamento de Física Teórica de la Universitat de València, y

Jorge Portolés Ibáñez, Investigador Ramón y Cajal - CSIC en el Instituto de Física Corpuscular de Valencia,

Certifican:

Que la presente memoria, Effective Field Theories for Heavy and Light Fermions, ha sido realizada bajo su dirección en el Instituto de Física Corpuscular de València por *Pedro David Ruiz Femenía*, y constituye su Tesis para optar al grado de Doctor en Ciencias Físicas.

Y para que así conste, en cumplimiento de la legislación vigente, presentan en la Universitat de València la referida Tesis Doctoral, y firman el presente certificado, en

Burjassot, 18 de Septiembre de 2003

Antonio Pich Zardoya

Jorge Portolés Ibáñez

Agradecimientos

Buscando un título con más gancho para esta seción barajé varias posibilidades. Pensé primero en llamarla "Ajuste de Cuentas", pero como podía dar lugar a malentendidos y no tengo afán de revancha, lo descarté rápidamente. Luego se me ocurrió "Cartas al Director", que en mi caso tendría que escribir en plural y dejaría de tener gracia. Quizás lo más ajustado a la realidad hubiera sido lo de "Han intervenido (por orden alfabético)", más que nada para no acumular excesivo protagonismo. Al final, temiendo que la memoria fuese rechazada por no ajustarse a la estricta normativa respecto a encabezados, número de caracteres en castellano, etcétera, he optado por seguir la tradición y lanzarme de cabeza al clásico festival de agradecimientos.

Como este trabajo ha tenido dos directores, me toca agradecer su ayuda por duplicado (el caso es darme faena). Históricamente Toni fue mi primera víctima. Él ha confiado en que ésto podría seguir adelante en momentos en los que yo era un mar de dudas (el sueldo a fin de mes también ayudaba a despejar el horizonte, tengo que reconocerlo), y ha sabido darme más de un tiempo muerto. Buena parte de los contenidos de este trabajo han sido sugerencias suyas y aunque no acabe de creérselo, lo he terminado (ahora sí, de verdad). Tengo la sospecha de que Toni utilizó dobles durante su época de director del instituto para poder atendernos a todos, pero no es más que una hipótesis. Es muy posible que el verdadero Toni se ocultase en su despacho (o estuviese salvando al mundo vestido con un pijama).

Toni tuvo que respirar aliviado cuando apareció la mano salvadora de Jorge a tres despachos de distancia. Yo pronto advertí que su verdadera vocación había sido la de paellero, pero por cosas del destino (pues no quiero dudar de sus habilidades), acabó dedicándose a la física, que exige menos sacrificios. No obstante, su paciencia y su capacidad para salir ileso de mi acoso primero y del de las nuevas generaciones después, demuestran que para ésto le sobran aptitudes. De no ser por Jorge es posible que hubiera tirado la toalla antes de tiempo y quién sabe si no estaría yo ahora en cualquier otro sitio, con un futuro prometedor por delante y un trabajo envidiable. Pero no fué así, y tengo que admitir que ha sido un placer y una suerte encontrarme y colaborar con él.

Para Juanjo reservo unos tacos de jamón y unos buenos pedazos de carnaza de la que le gusta, que sé que lo disfrutará más que mi chachara complaciente. Por mucho que quiera comer este trotamundos, sus tajadas no serán comparables a las que he sacado yo de nuestras conversaciones.

También he disfrutado de las charlas con mi compañero de celda, el Dr. Eidemüller, que despues del Dr. Frankenstein es el doctor con apellido más siniestro

que conozco, aunque la cosa no pasa del nombre dado su buen carácter. Otros doctores que me han atendido gustosamente han sido Carlos (alias Charlie) y Verónica (alias Susy), a los que me alegro de ver cuando se dejan caer por los alrededores.

No me quiero olvidar de los miembros de la Federación de Jovenes Investigadores/ PRECARIOS que han dedicado parte de su tiempo a mejorar las condiciones labores del personal investigador en formación.

A mi familia y amigos, como su apoyo es el mismo con tesis o sin ella, espero haber sabido mostrarles mi aprecio más alla de lo que pueda escribir aquí en unas pocas líneas, y si no ha sido así, aún tengo tiempo para remediarlo. Empezaré contigo Irene, que eres quién más cerca tengo (afortunadamente), aumentando nuestra dosis diaria de besos y abrazotes. Gracias por tu comprensión y por tu cariño.

Contents

Prólogo

La memoria que se presenta a continuación recoge el trabajo de investigación llevado a cabo en el Instituto de Física Corpuscular de Valencia para optar al grado de doctor en Ciencias Físicas. El trabajo se enmarca dentro del campo de la Física de Partículas y más concretamente en el de la Fenomenología del Modelo Estándar.

Bajo el título Teorías de Campos Efectivas para Fermiones Pesados y Ligeros hemos pretendido englobar diversos temas relacionados con la aplicación de las teorías efectivas de QED y QCD a la producción de leptones y quarks a partir de la aniquilación de un par electrón-positrón. Los contenidos de la tesis han sido estructurados en dos bloques: el primero está formado por los Capítulos 2 y 3, que se ocupa de aspectos ligados a la creación de sabores pesados, mientras que el segundo bloque, los dos últimos capítulos, aborda la producción de sabores de quarks ligeros. Como preámbulo, se ha incluido una breve introducción sobre la naturaleza y utilidad de las teorías efectivas en la descripción de la dinámica de quarks y leptones.

El estudio en la producción de fermiones pesados ha sido impulsado en años recientes por el desarrollo de las teorías efectivas no-relativistas de QED y QCD. El interés en estos formalismos ha sido el germen del trabajo que se recoge en el primer bloque de la tesis. En el Capítulo 2 evaluamos la contribución del diagrama caja con dos fotones a la producción de fermiones en la aniquilación de e^+e^-, que proporciona correcciones electromagnéticas $\mathcal{O}(\alpha^2)$ a la sección eficaz de Born. Dicho cálculo está motivado por el estudio de la sección eficaz de producción de $\tau^+\tau^-$ al orden sub-sub-dominante que se inició en trabajos anteriores, y que constituyó el Trabajo de Investigación de Tercer Ciclo resumido en este mismo capítulo, para situar el cálculo del diagrama caja en el contexto adecuado. También se efectúa la expansión no-relativista de la amplitud caja, que es relevante a energías cercanas al umbral de producción, y verificamos que la expansión umbral de las integrales a 1-*loop* reproduce correctamente los resultados obtenidos con teoría de perturbaciones usual.

En el siguiente capítulo pasamos de la producción de leptones pesados a la de quarks pesados, haciendo una revisión profunda de la técnica de las reglas de suma para quarks pesados, utilizadas de forma recurrente para extraer los parámetros de QCD en este sector. Así analizamos nuevas contribuciones en la parte teórica de las reglas de suma y mostramos que la teoría general de las singularidades de las amplitudes perturbativas es el método adecuado para tratar algunos aspectos específicos. En particular se estudia la inclusión de la radiación de quarks ligeros por

quarks pesados a $\mathcal{O}(\alpha_s^2)$, y la de los correladores asimétricos a $\mathcal{O}(\alpha_s^3)$. Íntimamente relacionado con lo anterior, también proponemos una solución para la construcción de los momentos de la densidad espectral a $\mathcal{O}(\alpha_s^3)$ cuando la presencia de contribuciones sin masa invalida el uso de las técnicas estándar. Solucionamos el problema a través de una nueva definición de los momentos, que proporciona un procedimiento consistente y libre de problemas en la zona infrarroja.

La producción electromagnética de hadrones formados por quark ligeros se aborda en la segunda parte de esta tesis. En la región de bajas energías, donde la teoría de perturbaciones de QCD en términos de quarks libres no es aplicable, el uso de teorías efectivas con campos de mesones cuantizados se hace inevitable, y es necesario obtener información sobre los nuevos parámetros antes de que la teoría efectiva sea operativa. El Capítulo 4 presenta el procedimiento para inferir relaciones entre las constantes de baja energía y QCD. Con este fin, analizamos el Lagrangiano efectivo más general con términos de paridad intrínseca negativa, válido para procesos que involucran un pseudoscalar y mesones vectoriales descritos como tensores antisimétricos. Construyendo la función de Green de tres puntos con corrientes de QCD vector-vector-pseudoscalar, al orden dominante en $1/N_C$, y exigiendo que su comportamiento a cortas distancias coincida con el resultado de la OPE, se obtiene información sustancial sobre los acoplamientos de paridad intrínseca negativa. Las condiciones así impuestas por QCD permiten predecir las amplitudes de desintegración $\omega \to \pi\gamma$ y $\rho \to \pi\gamma$, y las correcciones $\mathcal{O}(p^6)$ a $\pi \to \gamma\gamma$. También se extraen del análisis anterior consecuencias importantes sobre la hipótesis de *vector meson dominance* (VMD) en la desintegración $\omega \to 3\pi$.

El siguiente capítulo constituye el inicio de un proyecto que pretende obtener una descripción teórica de la sección eficaz de producción de hadrones en la región de las resonancias utilizando únicamente la información que proporcionan las simetrías de QCD y su comportamiento a cortas distancias, tal y como se ejemplifica en el capítulo anterior. En esta primera etapa de la investigación se ha diseñado la estrategia general a seguir. De esta forma, en el Capítulo 5 se deriva una expresión teórica para el correlador de dos corrientes vectoriales en la región energética entre 1 y 2 GeV, cuya parte imaginaria se relaciona con la sección eficaz hadrónica, empleando la Teoría de Resonancias Quiral (RχT) con términos de paridad intrínseca negativa a 1-*loop*. Las partes absortivas así incluidas están motivadas por la fenomenología, con el objetivo de incorporar sucesivamente los estados exclusivos que aparecen en el espectro hadrónico en la zona de las resonancias. La regularización de los polos de las resonancias queda garantizada mediante una resumación de los diagramas a 1-*loop*. Finalmente se comentan las limitaciones de los resultados anteriores y se sugieren las lineas de investigación a seguir en el futuro.

Salvo la introducción sobre teorías efectivas que viene a continuación y las conclusiones finales, el resto de la tesis está escrita en inglés. De esta forma se cumplen los requisitos exigidos por la normativa del Doctorado Europeo.

Oscuro para que todos atiendan.
Claro como el agua, claro,
para que nadie comprenda.

Antonio Machado, *haiku japonés.*

Breve Introducción sobre las Teorías de Campo Efectivas

Seguramente la primera pregunta que formularía un recien llegado a la Física de Partículas dentro del Modelo Estándar sobre las Teorías de Campo Efectivas (EFTs) sería: "¿Para qué trabajar con Lagrangianos aproximados si se conoce el exacto?". Y de hecho la pregunta no carece de sentido ya que la situación dentro del Modelo Estándar es precisamente esa: el contenido de partículas fundamentales en la teoría ha sido establecido tras más de medio siglo de investigación tanto experimental como teórica, y se ha logrado desarrollar un formalismo matemático en términos de campos cuantizados que permite explicar gran parte de la dinámica de los constituyentes básicos de la naturaleza. Sabemos que el Modelo Estándar no es la teoría definitiva, pero nos ha servido como armazón teórico para abordar gran parte de los problemas que han ido surgiendo en la Física de Partículas durante las últimas decadas.

Sin embargo, el hechizo se rompe tan pronto como empezamos a hacer cálculos con el Modelo. La respuesta a la pregunta formulada arriba acaba con nuestro entusiasmo: o bien no somos capaces de resolver la teoría en aquellos regímenes donde los estados físicos son sistemas compuestos de las partículas fundamentales, o bien nos vemos forzados a realizar cálculos engorrosos que involucran a todos los grados de libertad cuando en realidad sólo algunos de ellos pueden aparecer como estados asintóticos en la región de energías que nos interesa.

Estos problemas no son en modo alguno nuevos en Física. Por ejemplo, tendríamos serias dificultades para derivar el espectro atómico del hidrógeno considerando la interacción electromagnética de los electrones con los quarks que forman el protón dada por la Electrodinámica Cuántica y, lo que es más, si finalmente consiguieramos encontrar la solución, descubriríamos que los grados de libertad ligados al movimiento del protón apenas corrigen la posición de los niveles energéticos. De hecho, la física que gobierna el sistema se entiende tomando la interacción electromagnética del electrón con un núcleo estático (de masa infinita), es decir la interacción de Coulomb, tal y como se describe en la Teoría de Schrödinger para átomos hidrogenoides.

Las dos dificultades mencionadas anteriormente aparecen en el ejemplo anterior: la descripción de sistemas compuestos a partir de las interacciones de sus constituyentes fundamentales puede estar fuera de nuestro alcance y, además, tener en cuenta la dinámica concreta de algunos grados de libertad de la teoría completa

puede ser irrelevante al final o, en cualquier caso, podría simplificarse con un método alternativo. La observación crucial en lo que concierne al papel de las Teorías Efectivas es pues evidente: deben servirnos para estudiar el comportamiento dinámico de un sistema a una escala determinada de forma más simple que la teoría fundamental que está por encima. El precio a pagar es que para alcanzar una precisión dada se necesita ir añadiendo más y más términos a la teoría efectiva, generando así una expansión controlada típicamente por un parámetro Λ característico de un escala más alta. A medida que aumentamos la potencia de Λ en el denominador, operadores de dimensiones más altas son introducidos en la teoría efectiva y, la teoría deja de ser renormalizable en el sentido clásico. Este hecho es inevitable; piénsese por un momento que nuestro problema físico involucra partículas ligeras que interaccionan entre sí a través del intercambio de otra partícula de masa M mucho mayor. Si la energía característica es mucho menor que M, podemos reemplazar el intercambio no-local de la partícula pesada (es decir el propagador) por una torre de interacciones locales entre las partículas ligeras. El conjunto de operadores así generado es en principio infinito en número, y de dimensión creciente, de forma que se requieren infinitos contratérminos para absorber las divergencias. Afortunadamente, la no-renormalizabilidad de la teoría efectiva no supone el fin de la historia, ya que podemos recuperar el poder predictivo de la teoría si nos contentamos con tener resultados con una precisión limitada. A un determinado orden en $1/\Lambda$ sólo un número finito de operadores de la expansión del Lagrangiano efectivo contribuyen al proceso físico, con lo que un número finito de contratérminos es suficiente.

Tres son los pasos fundamentales a seguir en el proceso de construcción de las EFTs:

i/ Identificar las diferentes escalas y variables relevantes que gobiernan el problema físico;

ii/ Construir los términos de interacción entre los estados asintóticos presentes a esas escalas, que satisfagan analiticidad, unitariedad y el resto de requisitos que imponen las simetrías de la teoría subyacente;

iii/ Restaurar la información contenida en los grados de libertad descartados de forma que se puedan reproducir (hasta una cierta precisión) los resultados de la teoría completa.

El primer paso es crucial y altamente no trivial en algunos casos[1]. En ocasiones, la teoría efectiva se obtiene eliminando una partícula pesada de la teoría (lo que se conoce como "integrar" una partícula pesada en la terminología de las EFTs). Un ejemplo de lo anterior es la construcción de una teoría efectiva de QCD con $N_f - 1$ sabores de quarks ligeros a partir de QCD con N_f sabores (veáse la discusión introductoria sobre este tema en la Referencia [2]), o el Lagrangiano de Euler-Heisenberg que describe la dispersión de luz por luz a bajas energías ($E_\gamma \ll m_e$), donde los

[1]Tómense como ejemplo las dificultades encontradas en identificar los modos relevantes en las versiones no-relativistas de QED y QCD [1]

fermiones han sido integrados. Puede darse el caso de que la partícula pesada sí aparezca entre los estados asintóticos, pero sólo en algún determinado régimen cinemático (como una fuente estática o a bajas velocidades, por ejemplo), lo cuál permite simplificar la dinámica integrando los modos irrelevantes. Sirvan como ejemplos de este caso la Teoría Efectiva de Quarks Pesados y la Electrodinámica y la Cromodinámica Cuántica No-Relativistas (denotadas como NRQED y NRQCD respectivamente).

En otros regímenes, la construcción de la teoría efectiva no se reduce simplemente a eliminar alguno de los grados de libertad de la teoría subyacente, y la idea de integrar modos fuera de la teoría con el formalismo de integrales de camino deja de ser aplicable. Esto es lo que ocurre en el mundo hadrónico a bajas energías, donde los grados de libertad activos no son quarks y gluones libres sino un amplio espectro de mesones. La simetría quiral aparece en esta región, sirviéndonos de guía para escribir el Lagrangiano efectivo adecuado para describir las interacciones entre mesones.

De hecho las simetrías son una herramienta muy valiosa para construir una EFT. Aparte de los ingredientes de analiticidad, unitariedad, invariancia Lorentz, invariancia gauge, etc, puede existir alguna simetría adicional (total o parcialmente realizada) de la teoría completa capaz de explicar los aspectos más importantes de la dinámica a una cierta escala. Imponiendo esta simetría en la acción efectiva se garantiza que las interacciones a bajas energías guardan información de la teoría completa, aún incluso si los parámetros son desconocidos. Desde un punto de vista práctico, las simetrías representan un método para diseñar la teoría efectiva cuando se carece de un procedimiento analítico para derivar el Lagrangiano efectivo directamente del Lagrangiano completo (como sí se puede hacer, por ejemplo, para obtener la acción de NRQED a partir del Lagrangiano de QED mediante una transformación de Foldy-Wouthuysen).

Por construcción, la teoría efectiva hereda de la teoría completa la física correcta para los grados de libertad activos. Sin embargo, los modos de las regiones por encima de la escala de alta energía que han sido descartados, tambien contribuyen a los procesos físicos a escalas inferiores, teniendo que ser sus efectos correctamente implementados en la acción efectiva. El procedimiento de *matching* entre las dos teorías traslada la información de los modos integrados a los valores concretos que toman los coeficientes de los operadores presentes en la EFT. Las condiciones de *matching* exigen que los resultados de la teoría subyacente y de la EFT coincidan en un determinado punto cinemático (en la frontera entre ambas teorías, por ejemplo), o en un cierto régimen asintótico. Este procedimiento puede, en principio, determinar los parámetros de bajas energías que no quedan fijados únicamente por las simetrías, o por la expansión directa del Lagrangiano completo. Además, el *matching* nos permite relacionar las dos teorías más alla del orden árbol, una vez que se ha regularizado convenientemente el cálculo de *loops* en la EFT. De esta forma, la EFT se ajusta para reproducir, en su región de validez, los resultados de la teoría completa a través de una expansión bien definida respecto a una escala característica.

Mostramos a continuación cómo los aspectos mencionados se implementan en algunos ejemplos de teorías efectivas que se usarán en este trabajo.

NRQED (NRQCD)

La interacción de Coulomb gobierna la dinámica de un par de partículas cargadas cuando su velocidad es pequeña. La escala $|\boldsymbol{p}| \sim Mv$, típica de estas interacciones, es mucho menor que la escala asociada a la masa de los fermiones M, y la evolución es pues claramente no-relativista. Una descripción adecuada provendría de una teoría simplificada que mantuviera la física relevante del sistema a esta escala, permitiendo así identificar de forma clara y sistemática las contribuciones dominantes.

NRQED [3] fue precisamente diseñada con este fin. Es una teoría efectiva de campos de QED a bajas energías, aplicable a fermiones en un régimen no-relativista, es decir con una velocidad no-relativista típica $|\boldsymbol{p}|/M \sim v \ll 1$. Se puede obtener una expansión en potencias de $1/M$ mediante una transformación de Foldy-Wouthuysen del Lagrangiano de QED. De este modo, la teoría relativista que describe fermiones en términos de espinores de Dirac (de 4 componentes) queda reemplazada por una teoría de Schrödinger no-relativista con dos campos de Pauli (espinores de dos componentes) distintos para el fermión y el antifermión. También es posible definir el lagrangiano de NRQED sin conocimiento previo de QED imponiendo restricciones cuyo origen sean las simetrías que debe obedecer la teoría, tales como invariancia gauge, localidad, hermiticidad, conservación de paridad, invariancia bajo inversión temporal e invariancia Lorentz para el término cinético del fotón. Las partículas con masas $m \ll M$ que se incorporen a esta descripción siguen comportándose como relativistas dentro incluso de la teoría efectiva y por tanto deben describirse por la acción de QED.

Los primeros términos en el Lagrangiano de NRQED son [3, 5]

$$\begin{aligned}
\mathcal{L}_{\text{NRQED}} \;=\; & \frac{1}{2}\,(\,\boldsymbol{E}^2 - \boldsymbol{B}^2\,) + \psi^\dagger \Big[\, iD_t + c_2\,\frac{\boldsymbol{D}^2}{2\,M} + c_4\,\frac{\boldsymbol{D}^4}{8\,M^3} + \ldots \\
& + \frac{c_F\,e}{2\,M}\,\boldsymbol{\sigma}\cdot\boldsymbol{B} + \frac{c_D\,e}{8\,M^2}\,(\,\boldsymbol{D}\cdot\boldsymbol{E} - \boldsymbol{E}\cdot\boldsymbol{D}\,) + \frac{c_S\,e}{8\,M^2}\,i\,\boldsymbol{\sigma}\,(\,\boldsymbol{D}\times\boldsymbol{E} - \boldsymbol{E}\times\boldsymbol{D}\,) + \ldots \Big]\,\psi \\
& - \frac{d_1\,e^2}{4\,M^2}\,(\psi^\dagger\boldsymbol{\sigma}\sigma_2\chi^*)\,(\chi^T\sigma_2\boldsymbol{\sigma}\psi) - \frac{d_2}{M^2}\,(\psi^\dagger\sigma_2\chi^*)\,(\chi^T\sigma_2\psi) \;+ \\
& + \frac{d_3\,e^2}{6\,M^4}\,\Big[\,(\psi^\dagger\boldsymbol{\sigma}\sigma_2\chi^*)\,(\chi^T\sigma_2\boldsymbol{\sigma}(-\tfrac{i}{2}\overleftrightarrow{\boldsymbol{D}})^2\psi) + \text{h.c.}\,\Big] + \ldots
\end{aligned} \tag{1}$$

El fermión y el antifermión se describen por los espinores de Pauli ψ and χ, respectivamente; D_t y $\boldsymbol{D}$ son las componentes temporal y espacial de la derivada covariante gauge $D_\mu = \partial_\mu + ieA_\mu$, y $E^i = F^{0i}$ y $B^i = \frac{1}{2}\epsilon^{ijk}F^{jk}$ son las componentes eléctrica y magnética del tensor campo electromagnético (con e la carga eléctrica). Se han omitido los biliniales en el campo del antifermión χ (que salvo signo se

obtienen de los escritos para ψ) y términos de orden superior. La primera línea está relacionada con el término cinético del Lagrangiano de QED, donde los términos bilineales en ψ se pueden extraer de la expansión de la fórmula para la energía relativista en función del trimomento hasta orden $1/M^3$ (el operador $\boldsymbol{D}^4/8M^3$ es fácilmente reconocible como la primera corrección relativista a la energía cinética de la mecánica cuántica). En la segunda fila se recogen los posibles acoplamientos eléctricos y magnéticos de los leptones con los fotones de energía menor que M hasta un cierto orden en la expansión no-relativista. Los subíndices F, D, S en los acoplamientos hacen referencia a los téminos de Fermi, Darwin y espin-órbita, términos bien conocidos de la mecánica cuántica. Los operadores de cuatro fermiones de las lineas finales reproducen la aniquilación y creación de un par f^+f^- en estado de espín triplete (d_1 y d_3) y singlete (d_2) con momento angular orbital más bajo, *i.e.* en onda S. Desde el punto de vista de NRQED, la aniquilación de un par f^+f^- es un proceso de alta energía que sólo puede describirse por un término de interacción de contacto (el fotón que se intercambia en un proceso $f^+f^- \to f^+f^-$ en el canal s involucra necesariamente cuadrimomentos del orden de M). Además, nuevos términos de interacción entre los fotones se han de introducir para simular la inserción de *loops* fermiónicos como la polarización del vacío y la dispersión de luz por luz. Los coeficientes de cortas distancias c_i, d_i, que recogen los efectos de momentos del orden de M, han de ser determinados siguiendo el procedimiento de *matching* a un determinado orden en α y v, con el fin de reabsorber los infinitos que surgen en los cálculos más allá de orden árbol.

Qué interacciones tienen que considerarse para alcanzar una precisión dada (en α y en $v \sim |\boldsymbol{p}|/M$) viene dictado por las reglas de recuento. La presencia de dos escalas dinámicas en la teoría, el trimomento de los fermiones $|\boldsymbol{p}| \simeq Mv$, y su energía cinética $E_c \simeq Mv^2$, provoca que las reglas de recuento de NRQED sean más complicadas de establecer que en la mayoría de teorías de campos efectivas. Es evidente que en el caso en que $v \lesssim \alpha$, el orden de importancia de un diagrama ya no viene dictado por las potencias de α que contiene sino también por los factores de la velocidad. Mientras que las potencias de α de un diagrama pueden inferirse directamente de los coeficientes de los vértices, las potencias de v pueden generarse en los propagadores y en la integración de los *loops*. En años recientes ha surgido un controvertido debate sobre la manera de organizar los cálculos dentro de NRQED/NRQCD (ésta última la versión no-relativista de QCD) mediante una expansión sistemática en v [1], especialmente en el contexto de la regularización dimensional. La situación parece haberse clarificado notablemente con las nuevas formulaciones propuestas en las Referencias [4].

Previamente, y siguiendo un esquema de regularización con un corte ultravioleta en la integración de momentos, Labelle [5] derivó unas reglas de recuento para la velocidad empleando teoría de perturbaciones ordenada temporalmente junto al *gauge* de Coulomb para separar los fotones blandos (con energía $E_\gamma \simeq Mv$) de los ultra-blandos ($E_\gamma \simeq Mv^2$). Aunque algo enfarragosas para cálculos que van más alla del orden sub-sub-dominante (NNLO) en la expansión de las velocidades, estas reglas nos proporcionan por simple análisis dimensional el orden en v de aquellos

diagramas que contienen únicamente fotones blandos.

Con estas reglas puede probarse que los diagramas recién mencionados son suficientes para describir la interacción no-relativista entre un par de fermiones hasta NNLO. Además, dado que los fotones blandos tienen un propagador independiente de la energía se tiene que todas las interacciones hasta NNLO pueden escribirse en términos de potenciales, siendo éste un resultado altamente no-trivial que no puede derivarse en el contexto de la teoría de perturbaciones covariante de QED [2]

Algunos resultados originales sobre las propiedades de los estados ligados (estructura hiperfina, anchura total de desintegración, desplazamiento Lamb en el átomo de hidrógeno, etc), tanto para sistemas $\ell^+\ell^-$ ($\ell = e, \mu$) como para estados ligados de quarks pesados, han sido obtenidos en el marco de NRQED y NRQCD, esencialmente usando la prescripción de Labelle.

Otra aplicación importante de este formalismo en QCD ha sido el cálculo de la sección eficaz total de producción de $Q\overline{Q}$ cerca del umbral hasta orden sub-subdominante en la expansión no-relativista, que se discutirá para el caso de leptones τ en el Capítulo 2. También se abordará en este mismo capítulo la técnica de la expansión umbral, especialmente adecuada para el cálculo de *loops* en las regiones no-relativistas. El lector puede remitirse a las Referencias [6, 7] para encontrar un análisis bien fundamentado sobre el desarrollo de NRQED y NRQCD y sus aplicaciones recientes.

La Teoría de Perturbaciones Quiral

QCD se comporta de forma muy distinta en los dominios de altas y de bajas energías; mientras que los quarks disfrutan de libertad asintótica a cortas distancias y la teoría de perturbaciones es aplicable, a largas distancias quedan confinados dentro de hadrones y su evolución se vuelve altamente no-perturbativa. La fenomenología queda entonces inundada por un vasto espectro de estados compuestos por hadrones, y nos vemos obligados a renunciar al modelo quark en nuestros cálculos.

La simetría quiral acude entonces en nuestro auxilio. Aunque las raíces de esta simetría hay que buscarlas en el Álgebra de Corrientes y en la clasificación de hadrones de Gell-Mann, hoy en día se entiende como aquella simetría del Lagrangiano de QCD con N_f sabores de quarks diferentes, $q = (u, d, \ldots)$,

$$\mathcal{L}_{\rm QCD} = -\frac{1}{4}\, G^a_{\mu\nu} G_a^{\mu\nu} + i\, \bar{q}_L \not{D}\, q_L + i\, \bar{q}_R \not{D}\, q_R\,,$$

bajo transformaciones globales del grupo $G \equiv {\rm SU}(N_f)_{\rm L} \otimes {\rm SU}(N_f)_{\rm R}$ actuando sobre los campos de quarks con helicidad positiva y negativa. Dado que las masas de los quarks ligeros (u, d, s) son pequeñas, la simetría quiral debería estar realizada

[2] En términos de diagramas este hecho se traduce en que sólo aquellos de tipo escalera con fotones culombianos o interacciones de contacto contribuyen a las amplitude físicas hasta NNLO. Asímismo puede demostrarse que los diagramas escalera con fotones blandos cruzados se anulan.

al menos de forma aproximada para este sector. Sin embargo, cuando tratamos de clasificar a los hadrones en representaciones del grupo completo encontramos que no hay multipletes degenerados con paridades opuestas. Si el vacío no es simétrico bajo la acción del grupo quiral, el mecanismo de rotura espontánea de la simetría nos da una posible solución: el grupo $\mathrm{SU(3)_L} \otimes \mathrm{SU(3)_R}$ queda roto al subgrupo de tranformaciones vectoriales $\mathrm{SU(3)_V}$, y el teorema de Goldstone predice que un octete de bosones pseudoscalares sin masa debería existir en la teoría, uno por cada generador roto del grupo quiral. El octete de bosones de Goldstone adquiere los números cuánticos de los ocho estados hadrónicos más ligeros ($\pi^+,\ \pi^-,\ \pi^0,\ \eta,\ K^+,\ K^-,\ K^0$ y $\bar{K^0}$) y, consecuentemente se identifica con ellos. El operador más simple que puede tomar un valor esperado en el vacio (invariante bajo el subgrupo que no se rompe) es el operador bilineal en el campo de quarks, $\langle 0|\bar{q}q|0\rangle \neq 0$.

La identificación de los grados de libertad asintóticos de QCD a bajas energías como los modos de Goldstone de una simetría rota proporciona un método para implementar sus interacciones en forma de teoría efectiva. El formalismo general para construir Lagrangianos efectivos con simetrías rotas espontáneamente fué desarrollado por Callan, Coleman, Wess y Zumino [8]. En la referencia [9] se señaló que la transformación del campo del pion[3] bajo la acción de los generadores axiales debe ser no-lineal. Las transformaciones lineales podían ser permitidas a expensas de introducir un campo escalar extra, denotado usualmente por σ en la literatura. Sin embargo, mientras que el llamado modelo-σ tiene serios problemas para describir la fenomenología, el Lagrangiano quiral que se construye a partir del formalismo no-lineal de Callan *et al.* ha sido aplicado con gran éxito a muchos procesos de bajas energías en QCD.

La realización no-lineal de la rotura de simetría quiral tiene una elegante interpretación en teoría de grupos (veáse, por ejemplo, la Referencia [10]). Los modos de Goldstone parametrizan la variedad formada por los estados de vacío ($G/H = \mathrm{SU(3)_L} \otimes \mathrm{SU(3)_R}/\mathrm{SU(3)_V}$), y representan fluctuaciones alrededor de la configuración de vacío estándar $\langle \phi^a \rangle$. Otras parametrizaciones (*i.e.* una elección de la base de generadores rotos distinta) debe proporcionar los mismos resultados para los observables. Una de las bases usadas comúnmente define los elementos pertenecientes al espacio cociente G/H como

$$U(\phi) = \exp\left\{ i\frac{\sqrt{2}\Phi}{F} \right\},$$

siendo F la constante de desintegración del pion y

$$\Phi(x) \equiv \frac{\lambda^a}{\sqrt{2}}\,\phi^a = \begin{pmatrix} \frac{1}{\sqrt{2}}\pi^0 + \frac{1}{\sqrt{6}}\eta_8 & \pi^+ & K^+ \\ \pi^- & -\frac{1}{\sqrt{2}}\pi^0 + \frac{1}{\sqrt{6}}\eta_8 & K^0 \\ K^- & \bar{K}^0 & -\frac{2}{\sqrt{6}}\eta_8 \end{pmatrix}.$$

[3]Podemos pensar por un momento en el caso más sencillo de simetría $\mathrm{SU(2)_L} \otimes \mathrm{SU(2)_R}$, donde los 3 bosones de Goldstone de la rotura espontánea de la simetría se identifican con las partículas $\pi^+,\ \pi^-$ and π^0.

La matriz U se transforma linealmente bajo la acción del grupo completo,

$$U(\phi) \xrightarrow{G} g_R\, U(\phi)\, g_L^\dagger\,,$$

de forma que es inmediato escribir el Lagrangiano efectivo de QCD a bajas energías. Nótese que los términos de la forma $\langle UU^\dagger \dots UU^\dagger \rangle$ son todos constantes. Esto es equivalente a considerar términos en la acción efectiva con campos de Goldstone constantes, que representan una rotación del vacío estándar de un mismo ángulo en todos los puntos del espacio tiempo y no afectan a la dinámica. Sólo son relevantes para el Lagrangiano de la EFT los gradientes de los campos de Goldstone ϕ^a. De esta forma, los acoplamientos de los bosones de Goldstone son proporcionales a su momento, lo que les hace interaccionar débilmente a baja energía. Esta propiedad permite que la teoría que describe las interacciones entre los campos de Goldstone a largas distancias pueda obtenerse como una expansión en número de derivadas. La contribución de orden más bajo, $\mathcal{O}(p^2)$, es [11, 12, 13]

$$\mathcal{L}_\chi^{(2)} = \frac{F^2}{4} \langle \partial_\mu U \partial^\mu U^\dagger \rangle\,.$$

Pueden ir añadiéndose sistemáticamente términos de orden superior con mayor número de derivadas, y se genera así una expansión en momentos sobre una escala Λ_χ dictada por la rotura de simetría quiral, que del análisis de las amplitudes a 1-*loop* resulta ser $\Lambda_\chi \simeq 4\pi F \sim 1$ GeV. Si expandimos U en una serie de potencias de los campos de Goldstone encontramos que $\mathcal{L}_\chi^{(2)}$ contiene términos de interacción entre 4Φ, 6Φ,..., de forma que amplitudes de dispersión con diferente número de partículas se relacionan entre sí, un rasgo característico de los Lagrangianos no-lineales.

Junto a los pseudoscalares, se pueden acomodar en el formalismo quiral campos externos para generar los acoplamientos de los bosones de Goldstone con las corrientes electrodébiles y para introducir la rotura explícita de la simetría través de las masas de los quarks. El procedimiento se describe en el Capítulo 4. También se pospone para este capítulo la discusión acerca del papel de las resonancias en la teoría quiral.

En la literatura se pueden encontrar excelentes resúmenes sobre simetría quiral y su enorme campo de aplicaciones y resultados relevantes, veánse *e.g.* las referencias [2, 10, 14].

Límite de gran número de colores de QCD

La expansión en el número de colores (N_C) [15, 16] no es una teoría de campos efectiva de QCD, sino un esquema sistemático para acercarse al estudio de los aspectos no-pertubativos de la cromodinámica desde una teoría que se asemeja a QCD en un determinado límite.

Uno comienza considerando QCD con N_C colores y el grupo de gauge SU(N_C), e intenta resolver la teoría en el límite en que N_C se hace muy grande (manteniendo el producto $\alpha_s N_C$ constante). En dicho límite, la teoría se simplifica enormemente y pueden extraerse resultados muy interesantes acerca de la dinámica de mesones y bariones. En este formalismo aparece de forma natural una expansión de las amplitudes físicas en potencias de $1/N_C$. De vuelta a la teoría con $N_C = 3$ esperamos que se mantenga el comportamiento encontrado para N_C grande tanto cualitativa como cuantitativamente.

Las características principales de la expansión $1/N_C$ se deducen del análisis de los factores combinatorios de los diagramas de Feynman. El resultado general es que los diagramas dominantes para N_C grande son los diagramas planares con un sólo *loop* de quarks corriendo por el borde del diagrama. Del papel dominante de esta topología específica se extraen muchas de las propiedades de los mesones, asumiendo que confinamiento persiste en el límite de N_C grande. Entre éstas, resaltamos a continuación las que serán relevantes para nuestro trabajo:

i/ Los mesones en el límite de $N_C = \infty$ son libres, estables y no interaccionan entre sí. Sus masas presentan limites suaves y el espectro de la teoría tiene un número infinito de estados mesónicos.

ii/ La física de mesones a primer orden en la expansión $1/N_C$ viene dada por los diagramas de orden árbol de un Lagrangiano local efectivo escrito en términos de campos de mesones locales.

iii/ Las funciones de n-puntos construídas a partir de los corrientes de quarks se calculan como suma de diagramas de orden árbol con campos de mesones y vértices locales; en particular, para correladores de dos puntos solo pueden existir polos con un mesón en el límite de gran N_C (no hay cortes con varias partículas), y para funciones generales de n-puntos las únicas singularidades permitidas en cualquier canal son polos simples. En principio se deben considerar un número infinito de mesones en la construcción del correlador.

iv/ La regla de Zweig es exacta para N_C grande, de forma que se suprime la mezcla singlete-octete (ya que los diagramas que separan singletes de octetes involucran la aniquilación de un par $q\bar{q}$). Como consecuencia, los mesones se clasifican en nonetes de sabor, y el Lagrangiano de QCD_∞ obedece la simetría $\mathrm{U(3)_R} \otimes \mathrm{U(3)_L}$.

Algunos resultados de la expansión $1/N_C$ permiten entender aspectos cruciales observados en la fenomenología de hadrones. Por ejemplo, en el formalismo de gran número de colores podemos entender que los mesones aparezcan como estados $q\bar{q}$ aproximadamente porque la física hadrónica del "mar" de pares $q\bar{q}$ está suprimida, y la dominancia de estados finales de dos cuerpos en la desintegración de mesones inestables (cuando está permitida cinemáticamente), surge como consecuencia del contaje en $1/N_C$. También hay argumentos teóricos que sustentan la validez de la

expansión $1/N_C$ y su extrapolación a la teoría de tres colores, siendo el más importante el que, bajo hipótesis razonables, se puede probar que el grupo de simetría de QCD en el límite $N_C \to \infty$, $\mathrm{U}(N_f)_\mathrm{R} \otimes \mathrm{U}(N_f)_\mathrm{L}$, se rompe espontáneamente a $\mathrm{U}(N_f)_\mathrm{V}$ [17].

A nivel práctico, los resultados de la expansión $1/N_C$ se pueden extrapolar al mundo tricolor cuando se dispone de un Lagrangiano efectivo en términos de campos de mesones y bariones. Tal es el caso, por ejemplo, de RχT, donde podemos invocar el comportamiento dominante del límite de N_C grande como un punto de partida conveniente en nuestros cálculos. En este sentido, el formalismo de $1/N_C$ proporciona un esquema de recuento bien definido para seleccionar las contribuciones dominantes en la expansión perturbativa de la EFT. Por ejemplo, el límite de gran N_C nos dice que en la amplitud de dispersión elástica de dos piones, los diagramas a un *loop* con estados intermedios de dos mesones están suprimidos con respecto al intercambio de resonancias, que sólo involucra polos de una partícula, y así otros tantos resultados.

Chapter 1

A Few Words about Effective Field Theories

Surely the first question a newcomer to Particle Physics within the Standard Model may ask about Effective Field Theories (EFT's) is "why should we work with approximate Lagrangians if we do know the complete one?". And indeed the question makes sense because the situation within the Standard Model is precisely that one: we have set up a fundamental particle content in the theory after half a century of both experimental and theoretical research and we have managed to write down a mathematical framework in terms of quantum fields which explains the dynamics of the basic constituents of nature. Certainly, the Standard Model is not the final theory of everything, but it appears to be a compelling framework to deal with most of the problems arisen in Particle Physics during the last decades.

However, the spell is broken soon after we start doing calculations with the Model. The answer to the above question hopelessly emerges: we are not able to solve the theory in those regimes where the physical states are compound systems of the fundamental particles, or we are forced to perform cumbersome calculations considering all degrees of freedom (d.o.f.) when only some of them appear as asymptotic states in the energy region of interest. These problems are by no means new in Physics. For example, we would hardly derive the atomic spectrum of hydrogen considering the electromagnetic interaction of electrons with the quarks inside the proton in full QED, and even if we finally managed to get the solution we would find that the degrees of freedom related with the proton momentum give tiny corrections to the energy levels. In fact, the relevant physics governing the system can be explained by considering the electromagnetic interaction of the electron with a static (infinite mass) nucleus, i.e. the Coulomb interaction, as described by the Schrödinger theory of hydrogen-like atoms.

The two kind of difficulties mentioned above are found in the previous example: The description of compound systems from the dynamics of their fundamental constituents can be out of reach and, in addition, the detailed dynamics of some d.o.f. of the full theory may either be unimportant at the end or, in any case, could be simplified with an alternative approach. The key observation concerning the role of EFTs comes out: They should allow us to deal with the specific dynamics at some

scale in a simpler way than the fundamental theory which lies above. The price to pay is that we have to include more and more terms in the EFT to reach some degree of accuracy, typically controlled by an expansion over a characteristic parameter of a higher scale Λ. As we increase the powers of Λ in the denominator, operators of higher dimensions are introduced into the EFT and, eventually, renormalizability is lost. This is unavoidable; think for a moment that our physics problem involves light particles which interact through virtual exchange of a much heavier particle of mass M. If the characteristic energy is much lower than M, we can replace the non-local heavy-particle exchange (i.e. the propagator) by a tower of local interactions among the light particles. This set of operators is in principle infinite in number and with increasing dimension, thus requiring infinite counterterms to absorb the divergences. Fortunately, the non-renormalization of the EFT is not the end of the story, as we can recover the predictive power provided we content ourselves with a finite accuracy in our calculations. To some order in $1/\Lambda$ only a finite number of operators of the EFT expansion contribute to the physical processes and thus only a finite number of counterterms are needed.

Three main steps must be undertaken in the process of construction of the EFTs:

i/ To identify the different scales and relevant variables governing the physics problem;

ii/ To build up the terms containing the interactions among the asymptotic states which show up at these scales, satisfying analyticity, unitarity and the symmetry requirements of the underlying theory;

iii/ To restore the information kept by the d.o.f. thrown away in order to reproduce (up to some degree of accuracy) the results of the full theory.

The first step is crucial and highly non-trivial in some cases[1]. In some situations, the EFT is obtained just by eliminating a heavy particle from the theory ("integrating out" a heavy particle, using a more familiar terminology to EFT's practitioners). An example of the latter is the construction of an EFT of QCD with $N_f - 1$ light-quark flavours from QCD with N_f flavours (see [2] for a comprehensive review on this), or the Euler-Heisenberg Lagrangian describing light-by-light scattering at low energies ($E_\gamma \ll m_e$), where fermions have been integrated out. It can happen that the heavy particle does appear as an asymptotic state but only in a certain kinematic regime (as a static source or at non-relativistic velocities, for example), allowing to simplify the dynamics by integrating out the irrelevant modes. Examples of the latter are Heavy Quark Effective Theory (HQET) and Non-Relativistic QED and QCD (NRQED and NRQCD respectively). In other domains, building the EFT does not reduce to throwing out some of the d.o.f. of the underlying theory, and the nice physical picture of integrating out modes from the path integral formalism cannot be applied. This is what happens in the hadronic world at low-energies, where the

[1]Recall, for example, the difficulties found in the identification of the relevant modes in the non-relativistic versions of QED and QCD [1]

active d.o.f. are not free quarks and gluons but a large spectrum of mesons. Chiral symmetry emerges in this region, giving us a guide to write down the corresponding effective Lagrangian describing low-energy meson interactions.

Indeed symmetries represent a powerful tool to construct an EFT. Besides the desired ingredients of analyticity, unitarity, Lorentz and gauge invariance, etc, there may be some additional symmetry (fully or partly realized) in the underlying theory able to explain the main features of the dynamics at some scale. Enforcing this symmetry in the effective action guarantees that the low-energy interactions retain some knowledge of the full theory, even if the parameters are unknown. From a practical point of view, symmetries turn out to be a method to design the EFT when we lack of an analytic procedure to derive the EFT Lagrangian directly from the full one (as can be done, for example, to obtain NRQED from the QED Lagrangian performing a Foldy-Wouthuysen transformation).

By construction, the EFT inherits the right physics for the active degrees of freedom from the full theory. However, the discarded modes from the regions above the characteristic high energy scale also contribute to processes at lower scales, so their effects must be implemented correctly in the effective action. The matching procedure among the two theories translates the information from the high-energy modes to the values of the coefficients of the operators present in the EFT. The matching conditions require that the results from the full and from the effective theories agree at a given point (at the boundary of the two theories, for example), or in a certain asymptotic regime. This procedure can, in principle, determine the low-energy parameters which cannot be fixed by symmetries alone, or by the direct expansion of the full Lagrangian. Moreover, the matching allow us to relate the two theories beyond tree-level, once loop calculations within the EFT have been properly regularized. The resulting EFT is thus "tuned" to reproduce in its region of application the outcomes from the full theory through a well-defined expansion in some given scale.

Let us now show how the features just mentioned are implemented in some examples of EFT's which will be used in this work.

1.1 NRQED (NRQCD)

The Coulomb interaction governs the dynamics of a pair of charge conjugate particles when their velocity is small. The scale $|\boldsymbol{p}| \sim Mv$, characteristic of these interactions, is much lower than the mass of the fermions, and thus the evolution is clearly non-relativistic. An adequate description would come from a simplified theory that kept the relevant physics at this scale, allowing for a clear and systematic identification of leading contributions.

NRQED [3] was designed precisely for this purpose. It is an EFT of QED at low energies, applicable to fermions in non-relativistic regimes, i.e. with typical velocity $|\boldsymbol{p}|/M \sim v \ll 1$. An expansion in powers of $1/M$ can be obtained by performing a Foldy-Wouthuysen transformation of the QED Lagrangian. The procedure has the

advantage of explicitly decoupling the particle sector from the antiparticle sector to a given order in $1/M$, which do not need to be treated in an unified way in a non-relativistic system. In this way, the relativistic theory describing fermions in terms of Dirac spinors (4-component) is replaced by a non-relativistic theory with two independent Pauli spinors (2-component) for the fermion and the anti fermion.

The first terms in the NRQED Lagrangian read [3, 5]

$$\begin{aligned}\mathcal{L}_{\rm NRQED} \;=\; & \frac{1}{2}\,(\,\boldsymbol{E}^2-\boldsymbol{B}^2\,)+\;\psi^\dagger\,\Big[\,iD_t+c_2\,\frac{\boldsymbol{D}^2}{2\,M}+c_4\,\frac{\boldsymbol{D}^4}{8\,M^3}+\ldots\\ & +\frac{c_F\,e}{2\,M}\,\boldsymbol{\sigma}\cdot\boldsymbol{B}+\;\frac{c_D\,e}{8\,M^2}\,(\,\boldsymbol{D}\cdot\boldsymbol{E}-\boldsymbol{E}\cdot\boldsymbol{D}\,)+\frac{c_S\,e}{8\,M^2}\,i\,\boldsymbol{\sigma}\,(\,\boldsymbol{D}\times\boldsymbol{E}-\boldsymbol{E}\times\boldsymbol{D}\,)+\ldots\,\Big]\,\psi\\ & -\frac{d_1\,e^2}{4\,M^2}\,(\psi^\dagger\boldsymbol{\sigma}\sigma_2\chi^*)\,(\chi^T\sigma_2\boldsymbol{\sigma}\psi)-\;\frac{d_2}{M^2}\,(\psi^\dagger\sigma_2\chi^*)\,(\chi^T\sigma_2\psi)\;+\\ & +\frac{d_3\,e^2}{6\,M^4}\,\Big[\,(\psi^\dagger\boldsymbol{\sigma}\sigma_2\chi^*)\,(\chi^T\sigma_2\boldsymbol{\sigma}(-\tfrac{i}{2}\overleftrightarrow{\boldsymbol{D}})^2\psi)+\text{h.c.}\,\Big]+\ldots\end{aligned}\tag{1.1}$$

The fermion and antifermion are described by the Pauli spinors ψ and χ, respectively; D_t and $\boldsymbol{D}$ are the time and space components of the gauge covariant derivative $D_\mu=\partial_\mu+ieA_\mu$ (with e the electric charge), and $E^i=F^{0i}$, $B^i=\frac{1}{2}\epsilon^{ijk}F^{jk}$, are the electric and magnetic components of the electromagnetic field tensor. Antifermion bilinears and higher–order operators have been omitted. The first line in Eq. (1.1) is related to the kinetic term of the QED Lagrangian, with the bilinear ψ terms coming from the expansion of the fermion relativistic energy up to $\mathcal{O}(1/M^3)$. Second line terms reproduce the electromagnetic couplings of the fermions with photons of energy lower than M. The subindices F, D, S in the couplings refer to Fermi, Darwin and spin-orbit interaction terms, familiar from quantum mechanics. Four fermion operators displayed in latter lines reproduce production and annihilation of a f^+f^- pair in a S-wave singlet (d_2) or triplet (d_1 and d_3) state. The latter are processes involving energies larger than the fermion mass, and thus are simulated in the low-energy theory by contact interactions. Additional interaction terms between photon fields should be introduced to simulate fermion loops. The short-distance coefficients c_i, d_i encoding the effects of momenta of order M, must be determined following the matching procedure up to a certain order in α and v, in order to absorb infinities arising in calculations beyond tree level.

Which interactions are to be kept for a given precision (in α and $v\sim|\boldsymbol{p}|/M$) is dictated by counting rules. The presence of two dynamical scales in the theory, the fermions three-momentum $|\boldsymbol{p}|\simeq Mv$, and their kinetic energies $E_k\simeq Mv^2$, makes the NRQED counting rules more involved than in most effective field theories. While the factors of α in a specific diagram can be read off from vertex coefficients, powers of v are also generated by internal propagators and loop integrations. There has been a hard discussion during recent years on how to organize calculations within NRQED/NRQCD (the non-relativistic version of QCD) in a systematic expansion in v [1], especially in the context of dimensional regularization. The situation seems to be clarified with the new formulations proposed in Refs. [4]. In a cutoff scheme power

counting rules for the velocity had been previously derived by Labelle [5] using time ordered perturbation theory together with the Coulomb gauge to separate the "soft" photons (with energy $E_\gamma \simeq Mv$) from the "ultrasoft" ones ($E_\gamma \simeq Mv^2$). Although quite troublesome for calculations beyond next-to-next-to-leading-order (NNLO) in the velocity expansion, these rules give the order in v of diagrams containing soft photons only by simple dimensional analysis. Following these rules one proves that the latter diagrams are all we need to describe low-energy interaction between the pair of fermions up to NNLO. Moreover, soft photons have an energy independent propagator and therefore all interactions up to NNLO can be written in terms of potentials, being this a highly non-trivial result which cannot be derived in the context of full QED covariant perturbation theory[2].

A number of original results on bound state properties (hyperfine splitting, total decay width, hydrogen Lamb shift, etc) for both $\ell^+\ell^-$ ($\ell = e, \mu$) and heavy quarkonium states have been based on NRQED or NRQCD, essentially using the prescription proposed by Labelle. Another important application of this formalism in QCD has been the calculation of the total cross section of $Q\overline{Q}$ production close to threshold at NNLO in the fixed order non-relativistic expansion, which will be discussed in the case of τ leptons in Chapter 2. The technique of threshold expansion, suitable for non-relativistic loop calculations will be also covered in this chapter. For a well-founded review on the development of NRQED and NRQCD and their recent applications we refer the reader to Refs. [6, 7].

1.2 Chiral Perturbation Theory

QCD behaves quite differently in the low and high energy domains; while quarks enjoy asymptotic freedom at short distances and perturbation theory is applicable, at long distances they get confined inside hadrons and their evolution turns out to be highly non-perturbative. A rich spectrum of hadronic states floods into the phenomenology and we have to renounce the quark picture in our calculations.

Chiral symmetry then comes to our rescue. Although the roots of this symmetry lie on the Current-Algebra methods and Gell-Mann's classification of hadrons, it is nowadays understood as the symmetry of the QCD Lagrangian with N_f different massless quark flavours, $q = (u, d, \ldots)$,

$$\mathcal{L}_{\rm QCD} = -\frac{1}{4}\, G^a_{\mu\nu} G_a^{\mu\nu} + i\, \bar{q}_L \not{D}\, q_L + i\, \bar{q}_R \not{D}\, q_R\,,$$

under global $G \equiv {\rm SU}(N_f)_{\rm L} \otimes {\rm SU}(N_f)_{\rm R}$ transformations of the left- and right-handed quark fields. As masses of light quarks are small (u, d, s) chiral symmetry should be approximately realized for this sector. However, when hadrons are tried to be classified into representations of the full group we find that multiplets have no degenerate

[2] In terms of diagrams this statement means that only ladder diagrams with Coulomb-like photons and contact interactions with vertex factors contribute up to NNLO. Crossed ladder graphs vanish for soft photons.

counterpart with the opposite parity. If the vacuum is not symmetric under the action of the chiral group, the mechanism of spontaneous breaking of the symmetry yields a way out: the $\mathrm{SU(3)_L \otimes SU(3)_R}$ group is broken down to the subgroup of vector transformations $\mathrm{SU(3)_V}$ and the Goldstone's theorem predicts that an octet of pseudoscalar massless bosons should appear in the theory, as there are eight broken axial generators of the chiral group. The octet of Goldstone bosons is identified with the eight lightest hadronic states ($\pi^+,\ \pi^-,\ \pi^0,\ \eta,\ K^+,\ K^-,\ K^0$ and $\bar{K^0}$), and the simplest operator which can take a non-zero vacuum expectation value (invariant under the unbroken subgroup) is the quark bilinear operator, $\langle 0|\bar{q}q|0\rangle \neq 0$.

The identification of the asymptotic d.o.f. of low-energy QCD as Goldstone modes of a broken symmetry provides a way to construct an EFT containing their interactions. The general formalism to build effective Lagrangians with spontaneously broken symmetries was developed by Callan, Coleman, Wess and Zumino [8]. It was pointed out in Ref. [9] that the pion[3] field transformation under the action of the axial generators must be non-linear. Linear transformations were allowed, but only at the expense of introducing an extra scalar field, often denoted as σ in the literature. However, such linear σ-model has severe problems to accommodate the phenomenology, while the chiral Lagrangian built from the non-linear formalism of Callan et al. has been applied with great success to many processes of low-energy QCD.

The non-linear realization of the chiral symmetry breaking has a nice geometrical interpretation in group theory (see, for example, Ref. [10]). The Goldstone modes parametrize the vacuum manifold ($G/H = \mathrm{SU(3)_L \otimes SU(3)_R/SU(3)_V}$), and they represent fluctuations around the standard vacuum configuration $\langle\phi^a\rangle$. Different parameterizations (i.e. different choice of basis for the broken generators) must give identical results for all observables. A commonly used basis defines the elements U belonging to the coset space G/H as

$$U = \exp\left\{ i\frac{\sqrt{2}\Phi}{F} \right\},$$

with F being the pion decay constant and

$$\Phi(x) \equiv \frac{\lambda^a}{\sqrt{2}}\,\phi^a = \begin{pmatrix} \frac{1}{\sqrt{2}}\pi^0 + \frac{1}{\sqrt{6}}\eta_8 & \pi^+ & K^+ \\ \pi^- & -\frac{1}{\sqrt{2}}\pi^0 + \frac{1}{\sqrt{6}}\eta_8 & K^0 \\ K^- & \bar{K}^0 & -\frac{2}{\sqrt{6}}\eta_8 \end{pmatrix}.$$

The matrix U transforms linearly under the action of the full group,

$$U(\phi) \xrightarrow{G} g_R\, U(\phi)\, g_L^\dagger\,,$$

and it is thus straightforward to write down the low energy effective Lagrangian of QCD. Note that terms of the form $\langle UU^\dagger \ldots UU^\dagger\rangle$ are all constant. This is equivalent

[3]We can think for a moment in the simpler case of $\mathrm{SU(2)_L \otimes SU(2)_R}$ symmetry, where the 3 Goldstone bosons of the spontaneous symmetry breaking are identified with $\pi^+,\ \pi^-$ and π^0.

to consider terms with constant Goldstone boson fields, which represent a rotation of the standard vacuum by the same angle everywhere in spacetime and do not affect the dynamics. Only gradients of the Goldstone fields ϕ^a should appear in the EFT Lagrangian. The couplings of Goldstone bosons are thus proportional to their momentum, and so they interact weakly at low energy. This statement supports the idea that the theory describing the interactions among Goldstone fields at large distances can be obtained as an expansion in the number of derivatives. The lowest order contribution, $\mathcal{O}(p^2)$, is

$$\mathcal{L}_\chi^{(2)} = \frac{F^2}{4}\langle \partial_\mu U \partial^\mu U^\dagger \rangle \, .$$

Higher order terms with an increasing number of derivatives can be systematically added, and we generate an expansion of momenta over some scale Λ_χ driven by the chiral symmetry breaking, which turns out to be $\Lambda_\chi \simeq 4\pi F \sim 1$ GeV from the analysis of 1-loop amplitudes. If we now expand U in a power series in the Goldstone fields we find that $\mathcal{L}_\chi^{(2)}$ contains interaction terms among 4Φ, 6Φ,... and so on, thus relating scattering amplitudes with different number of particles, a characteristic feature of non-linear Lagrangians, and a remembrance of soft pion physics.

In addition, external fields can be accommodated in the chiral formalism to generate the couplings of the Goldstone bosons to the electroweak currents and to introduce explicit breaking of the symmetry through quark masses. The procedure will be sketched in Chapter 4. Also the discussion concerning the role of resonances in chiral theory will be postponed to the above-mentioned chapter.

Excellent reviews on the subject of chiral symmetry and on its vast number of applications and results can be found in the literature, see *e.g.* Refs. [2, 10, 14].

1.3 Large-N_C limit of QCD

The $1/N_C$ expansion [15, 16] is not an effective field theory of QCD, but rather a systematic scheme to approach the study of non-perturbative aspects of chromodynamics from a different theory which resembles QCD in some limit. One starts considering QCD with N_C colours and the SU(N_C) gauge group, and tries to solve the theory in the limit where N_C becomes very large (with the product $\alpha_s N_C$ kept fixed). In this limit, the theory is greatly simplified and very interesting results concerning meson and baryon dynamics can be extracted. An expansion of the physical amplitudes on powers of $1/N_C$ appears naturally in this framework. Going back to the $N_C = 3$ theory we hope that the qualitative and quantitative nature found in the large-N_C limit is maintained.

The main features of the $1/N_C$ expansion are deduced from the analysis of combinatoric factors in Feynman diagrams. The general statement is that the dominant diagrams for large-N_C are the planar diagrams with only a single quark loop running at the edge of the diagram. From the leading role of this specific topology many interesting properties of mesons have been proved, assuming than confinement also

exists in the large-N_C limit. Among these properties we shall highlight those relevant for our work:

i/ Mesons at $N_C = \infty$ are free, stable and do not interact among each other. Their masses have smooth limits and the spectrum of the theory has an infinite number of mesons states.

ii/ Meson physics at leading order in the $1/N_C$ expansion is given by the tree-diagrams of an effective local Lagrangian written in terms of local meson fields.

iii/ n-point functions built from quark currents are given by sums of tree-diagrams with local meson fields and local vertices; in particular, for two-point correlators only one-meson poles are found in the large-N_C limit (no multiparticle cuts), and for general n-point functions the only singularities allowed in any channel are single poles. In principle an infinite number of such mesons should be considered in the construction of the correlator.

iv/ Zweig's rule is exact at large-N_C, thus suppressing singlet-octet mixing (because diagrams that split singlets from octets involve $q\bar{q}$ annihilation). As a consequence, mesons are classified in nonets of flavour, and the QCD_∞ Lagrangian obeys the $\mathrm{U}(3)_\mathrm{R} \otimes \mathrm{U}(3)_\mathrm{L}$ symmetry.

Some results from the $1/N_C$ expansion explain crucial aspects of the observed hadron phenomenology. For example, in the large-N_C framework we understand that mesons are approximately $q\bar{q}$ states because the hadronic physics of the $q\bar{q}$ "sea" is suppressed, and the dominance of two-body final states (when kinematically allowed) in the decay of unstable mesons comes as a consequence of the N_C counting. Also theoretical arguments support the validity of the $1/N_C$ expansion and its extrapolation to the three colour theory, the most important being that, under reasonable assumptions, the $\mathrm{U}(N_f)_\mathrm{R} \otimes \mathrm{U}(N_f)_\mathrm{L}$ symmetry group of QCD in the limit $N_C \to \infty$ can be proved to be spontaneously broken down to $\mathrm{U}(N_f)_\mathrm{V}$ [17].

At a practical level, the results from the $1/N_C$ expansion are extrapolated to the three-colour world when an effective Lagrangian in terms of mesons or baryons fields is at hand. That is the case, for example, of Resonance Chiral Theory, where we can invoke the leading order results of the large-N_C limit as a convenient starting point for our calculations. In this sense, the $1/N_C$ framework yields a well-defined counting scheme to select the leading contributions in the EFT perturbative expansion. For example, the large-N_C limit tells us that in the $\pi\pi$ elastic scattering amplitude, loop diagrams with 2-meson intermediate states are suppressed with respect resonance exchange, which involves only one-particle poles, and so on.

Chapter 2

QED Box Amplitude in Heavy Fermion Production

2.1 Introduction

Heavy fermion production processes out of electron positron annihilation, $e^+e^- \to f\bar{f}$, have become a subject of thorough study in the last years. Their interest embodies multiple features and a wide energy range, from close to threshold production to high–energy colliders. LEP and LEP2 have provided the appropriate tool pushing behind this burst. In addition this is among the scattering processes with higher expected number of events at a future Linear Collider running in the $0.5\,\mathrm{TeV} - 1\,\mathrm{TeV}$ energy region like TESLA and NLC/JLC-X, or CLIC at higher energies. Their interest arises mainly from the possibility of exploring New Physics and, therefore, an accurate description within the Standard Model is necessary for the analyses of data. Projects like ZFITTER [18] and the ongoing CalcPHEP [19,20] aim to provide the relevant theoretical framework for that purpose.

QED corrections seem to be of little interest when probing the quantum effects within the Standard Model, but it is obvious that their contribution, however small, should be considered in order to disentangle New Physics effects. Besides, if a deeper understanding on the physical parameters of heavy fermions is intended, electromagnetic $\tau^+\tau^-$ and heavy quark $Q\overline{Q}$ production out of e^+e^- annihilation at threshold energies supplies the required information.

From a theoretical point of view $e^+e^- \to f\bar{f}$ cross sections close to threshold evaluated within perturbation theory are mislead due to the presence, in the physical system, of a kinematical variable of the same order than the gauge theory coupling : the velocity of the heavy fermion pair in the center of mass of the colliding system, $\beta = \sqrt{1 - 4M^2/s}$, with M the mass of the f fermion. Hence, when $\beta \sim \alpha$, care has to be taken in order to resummate terms as $(\alpha/\beta)^n$ or $(\alpha \ln \beta)^n$ that can give potentially large contributions [21]. Recently the development of non–relativistic effective field theories of QED and QCD [1, 3, 4] implements the suitable systematic procedure to follow. Facilities as the proposed Tau–Charm Factory, a high–luminosity e^+e^- collider with a center–of–mass energy near the $\tau^+\tau^-$ production threshold [22], would

provide excellent information on the mass of this lepton. Moreover an accurate determination of the mass of the top quark (difficult to get at the next hadron colliders) requires a future lepton collider at the $t\bar{t}$ threshold [23]. Consequently a thorough analysis of the non–relativistic contribution to $\sigma(e^+e^- \to f\bar{f})$ both from electromagnetic and strong interactions is mandatory.

In Ref. [24] the threshold behaviour of $\sigma(e^+e^- \to \tau^+\tau^-)$ was studied, and it was pointed out that, within the $\mathcal{O}(\alpha^2)$ electromagnetic corrections to the Born cross section, the squared amplitude of the box diagram involving two–photon $\tau^+\tau^-$ production (see Fig. 2.1) had not been considered yet. The electroweak one–loop contributions to the $e^+e^- \to f\bar{f}$ process were evaluated in Ref. [25]. Here this box contribution was already taken into account, though an explicit expression was only given for the $M = 0$ case. In this Chapter we provide the amplitude of this diagram for a final massive fermion.[1]

Once the explicit result is worked out we perform its non–relativistic expansion in terms of the β velocity and we find that the contribution of this diagram to the cross section is of $\mathcal{O}(\alpha^4\beta^3)$, that is $\mathcal{O}(\alpha^2\beta^2)$ over the Born cross section. The additional suppression driven by the velocity squared indicates that the contribution of the two–photon box diagram to the production of heavy fermions at threshold is negligible compared to the precision foreseen in the next future.

To put the box diagram evaluation in the right context we start this work giving a brief introduction on the subject of τ production close to threshold in Section 2.2. In Section 2.3 we detail the calculation of the box diagram contributing to $e^+e^- \to f\bar{f}$ in the limit when $m_e \ll M$, and we provide the full analytical result. Section 2.4 is dedicated to the study of the threshold behaviour of the box amplitude as obtained directly from our previous result. We confirm the features of this threshold amplitude by performing an alternative analysis of the integrals through the asymptotic expansion method in Section 2.5. Our conclusions are collected in Section 2.6. Finally, two Appendices contain the basic scalar integrals appearing in the article and a comment on the infrared divergent part of the box amplitude.

2.2 The $\tau^+\tau^-$ production cross section near threshold

The analysis of the $\sigma(e^+e^- \to \tau^+\tau^-)$ cross section at threshold has been addressed in full detail in Refs. [26, 24] in the framework of NRQED. It is instructive to give here a short review of the subject to understand the convenience of the effective theory description and to motivate the box amplitude evaluation.

[1] Recently Ref. [20] appeared. In this preprint a full expression for the QED box diagram amplitude is also given.

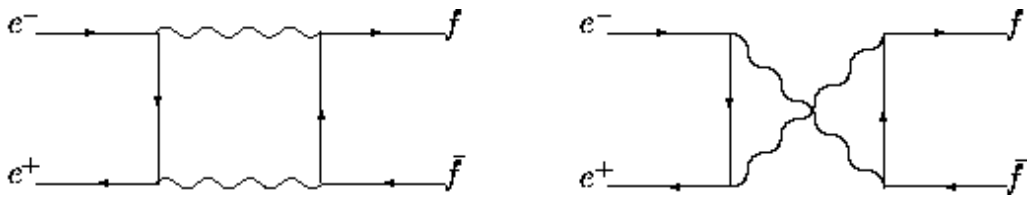

Figure 2.1: *Direct (a) and crossed (b) box diagrams for* $e^+e^- \to f\bar{f}$.

Perturbative calculation to $\mathcal{O}(\alpha^4)$

At lowest order in QED, the τ leptons are produced by one-photon exchange in the s-channel, and the total cross section formula reads

$$\sigma_B(e^+\,e^- \to \tau^+\,\tau^-) = \frac{2\pi\,\alpha^2}{3s}\,\beta_\tau\,(3-\beta_\tau^2)\,, \tag{2.1}$$

where $\beta_\tau = \sqrt{1-4m_\tau^2/s}$ is the velocity of the final τ leptons in the center-of-mass frame of the $e^+\,e^-$ pair which makes σ_B vanish when $\beta_\tau \to 0$.

Electromagnetic corrections of $\mathcal{O}(\alpha)$ arise from the interference between the tree level result and 1-loop amplitudes. A factor α/v emerges in the 1-loop final state interaction between the tau leptons, making the cross section at threshold finite. Furry's theorem guarantees that contributions to $\sigma(e^+e^- \to \tau^+\tau^-)$ coming from initial, intermediate and final state corrections completely factorize at $\mathcal{O}(\alpha^3)$, including real photon emission.

Some undesirable features appear at $\mathcal{O}(\alpha^4)$: The two-loop $\tau^+\tau^-\gamma$ vertex develops an α^2/β_τ^2 term which makes the cross section ill-defined when $\beta_\tau \to 0$, and multiple photon production of tau leptons by box-type diagrams and the non-zero interference of initial and final state radition spoil exact factorization. As it will be shown in this chapter, the squared amplitude of the $e^+e^- \to \tau^+\tau^-$ box diagram (see Fig. 2.1) is proportional to $\alpha^4\beta_\tau^2$, and so represents a N^{4}LO correction in the combined expansion in powers of α and β_τ. In addition, contributions to the total cross section from diagrams with real photons emitted from the produced taus can be shown to begin at N^{3}LO, and factorization remains at NNLO. The total cross section can thus be written as an integration over the product of separate pieces including initial, intermediate and final state corrections:

$$\sigma(s) = \int^s F(s,w)\left|\frac{1}{1+e^2\Pi_{\rm em}(w)}\right|^2 \tilde{\sigma}(w)\,dw\,. \tag{2.2}$$

The radiation function $F(s,w)$ [27] describes initial state radiation, including virtual corrections. The integration accounts for the effective energy loss due to photon emission from the $e^+\,e^-$ pair, and it includes the largest corrections coming from the emission of an arbitrary number of initial photons, which can sizeably suppress the total cross section. $\tilde{\sigma}$ collects only final-state interactions between the tau leptons, and it is usually written in terms of the tau spectral density R_τ,

$$\tilde{\sigma}(e^+e^- \to \gamma^* \to \tau^+\tau^-) = R_\tau(s)\,\sigma_{pt}\,, \tag{2.3}$$

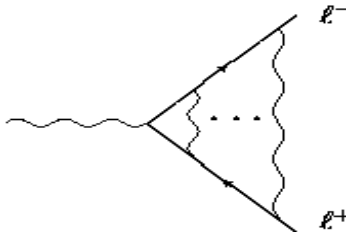

Figure 2.2: *Ladder exchange of photons between produced fermions.*

with $\sigma_{pt} = \frac{4\pi\alpha^2}{3s}$. The threshold behaviour of the total cross section is ruled by the expansion of R_τ at low velocities.

Non-Relativistic Corrections: NRQED

The aim of the effective field theory approach to threshold particle production is to achieve a given accuracy in the combined expansion in powers of α and the velocity β_τ. Such double expansion is needed at threshold due to the appearance of $(\alpha/\beta_\tau)^n$ terms in the QED perturbative expansion at the n-th loop order, which forces one to treat α and β_τ on the same footing. A non-perturbative procedure to deal with such singular terms in the limit $\beta_\tau \to 0$ is therefore mandatory.

The leading divergences (i.e. $\left(\frac{\alpha}{\beta_\tau}\right)^n$, $n > 1$), emerging from the ladder diagrams with Coulomb photons shown in Fig. 2.2, are resummed in the well-known Sommerfeld factor [28]

$$|\Psi_{\rm E}(0)|^2 \;=\; \frac{\alpha\pi/\beta_\tau}{1-\exp(-\alpha\pi/\beta_\tau)}\,, \tag{2.4}$$

multiplying the Born cross section (2.1). Next-to-leading order (NLO) entails terms proportional to $(\alpha/\beta_\tau)^n \times [\alpha, \beta_\tau]$, while NNLO accuracy stands for contributions $(\alpha/\beta_\tau)^n \times [\alpha^2, \beta_\tau^2, \alpha\,\beta_\tau]$.

A systematic way to calculate higher-order corrections in this regime is found in the framework of NRQED, the effective field theory of QED applicable to fermions in non-relativistic regimes, i.e. with typical momenta $p/M \sim \beta \ll 1$. As commented in Chapter 1, interactions contained in the NRQED Lagrangian have a definite velocity counting but propagators and loop integrations can also generate powers of β. With appropriate counting rules at hand, one can prove that all interactions between the non-relativistic pair $\tau^+\tau^-$ can be described up to NNLO in terms of time-independent potentials [5], derived from the low-energy Lagrangian. Therefore, the low-energy expression of the τ spectral density is related with the non-relativistic Green's functions [29]:

$$R_\tau^{\rm NNLO}(s) = \frac{6\,\pi}{M^2}\;{\rm Im}\Big(C_1\,G(E)\;-\frac{4E}{3M}\,G_c(E)\Big) \tag{2.5}$$

with C_1 a short distance coefficient to be determined by matching full and effective theory results and $E = m_\tau\beta^2$ the non-relativistic energy. The details of this

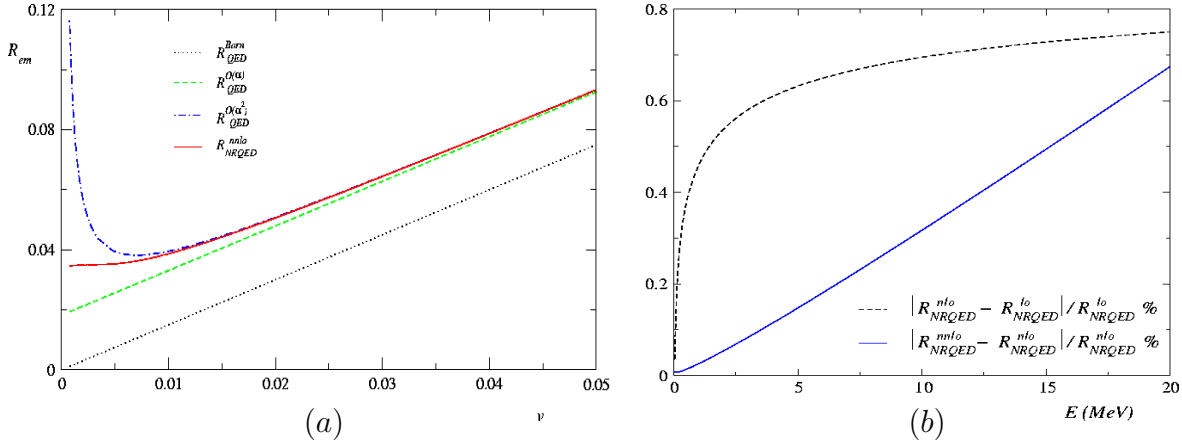

Figure 2.3: (a) The spectral density R_τ at low velocities in both QED and NRQED. (b) Relative sizes of corrections to $R_\tau(s)$ as calculated in NRQED.

derivation can be found in the Appendix B of [24]. The Green's function G obeys the Schrödinger equation corresponding to a two-body system interacting through potentials derived from $\mathcal{L}_{\rm NRQED}$ at NNLO:

$$\left(-\frac{\boldsymbol{\nabla}^2}{M}-\frac{\boldsymbol{\nabla}^4}{4M^3}+V_c(\boldsymbol{r})+V_{\rm BF}(\boldsymbol{r})+V_{\rm An}(\boldsymbol{r})-E\right)G(\boldsymbol{r},\boldsymbol{r}',E)\;=\;\delta^{(3)}(\boldsymbol{r}-\boldsymbol{r}')\,. \quad (2.6)$$

The term $-\frac{\boldsymbol{\nabla}^4}{4M^3}$ is the first relativistic correction to the kinetic energy and V_c stands for the Coulomb potential with $\mathcal{O}(\alpha^2)$ corrections. At NNLO, the heavy leptons are only produced in triplet S-wave states, so we just need to consider the corresponding projection of the Breit-Fermi potential $V_{\rm BF}$. Finally, $V_{\rm An}$ is a NNLO piece derived from a contact term in $\mathcal{L}_{\rm NRQED}$, which reproduces the QED tree level s-channel diagram for the process $\tau^+\tau^-\to\tau^+\tau^-$.

A solution of eq. (2.6) must rely on numerical or perturbative techniques. In the QED case, a significant difference between both approaches is not expected, being α such a small parameter. The perturbative approach was followed in Refs. [24, 26], using recent results [29], where NLO and NNLO corrections to the Green's function were calculated analytically, via Rayleigh-Schrödinger time-independent perturbation theory around the known LO Coulomb Green's function G_c. We refer the reader to Appendix C of Ref. [24] for complete expressions of the Green's function corrections.

Numerical analysis for $\sigma(e^+e^-\to\tau^+\tau^-)$

The need for performing resummations of the leading non-relativistic terms $(\alpha/\beta_\tau)^n \times[\beta_\tau,\beta_\tau\alpha,\beta_\tau^2,\ldots]$ is evidenced in Fig. 2.3a. The QED spectral density vanishes as $\beta_\tau\to 0$, due to the phase space velocity in formula (2.1), which is cancelled by the first β_τ^{-1} term appearing in the $\mathcal{O}(\alpha)$ correction, making the cross section at threshold finite. More singular terms near threshold, $\beta_\tau^{-2},\ldots$ arising in higher-order

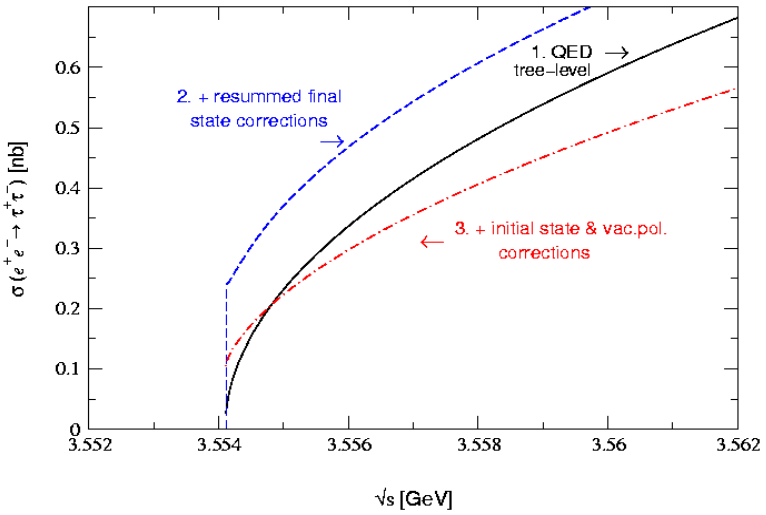

Figure 2.4: Total cross section $\sigma(e^+e^- \to \tau^+\tau^-)$ at threshold.

corrections completely spoil the expected good convergence of the QED perturbative series at low β_τ. This is no longer the case for the effective theory perturbative series, whose convergence improves as we approach the threshold point, as shown in Fig. 2.3b, and higher-order corrections reduce the perturbative uncertainty. In the whole energy range displayed in Fig. 2.3b, the differences between the NNLO, NLO and LO results are below 0.8%, which indicates that the LO result, i.e. the Sommerfeld factor, contains the relevant physics to describe the threshold region.

Adding the intermediate and initial state corrections [24] we have a complete description of the total cross section of $\tau^+\tau^-$ production, as shown in Fig. 2.4. Coulomb interaction between the produced τ's, becomes essential within few MeV's above the threshold, and its effects have to be taken into account to all orders. Initial state radiation effectively reduces the available center-of-mass energy for τ production, lowering in this way the total cross section.

To conclude this short review, we shall emphasize that NNLO corrections do not modify the predicted behaviour of the LO and NLO cross section, but are essential to guarantee that the truncated perturbative series at NLO gets small corrections from higher-order terms. It can be shown that the theoretical uncertainty of the above analysis of $\sigma(e^+e^- \to \tau^+\tau^-)$ is lower than 0.1%, much smaller than the statistical uncertainty of the most recent experiments which suffer from low statistics.

2.3 Two–photon box diagram

The contribution to the S-matrix of the process $e^-(p)e^+(p') \to f(k)\bar{f}(k')$ of the two–photon box amplitudes is depicted in Fig. 2.1 and it is defined by

$$\langle\, f\bar{f}\,|\, i\,\mathcal{T}\,|\, e^+e^-\,\rangle_{box} = (2\pi)^4\,\delta(p+p'-k-k')\,i\,\mathcal{M}_{box}\ . \tag{2.7}$$

As we are interested in heavy fermion production we will perform the evaluation for $k^2 = k'^2 = M^2$ and $p^2 = p'^2 = m^2 \ll M^2$ (we neglect the electron mass where possible). The two–photon box amplitude is gauge invariant and, consequently, we perform the calculation by taking the Feynman choice. The direct box amplitude, Fig. 2.1(a), is written down following QED Feynman rules as :

$$\mathcal{M}_a = e^4 Q_f^2 \int \frac{d^4\ell}{i(2\pi)^4} \frac{\{\bar{v}_e(p')\,\gamma^\mu\,\not{\ell}\,\gamma^\nu u_e(p)\}\,\{\bar{u}_f(k)\,\gamma_\nu\,(\not{k}-\not{p}+\not{\ell}+M)\,\gamma_\mu\,v_f(k')\}}{(\ell^2-m^2)[(\ell+k-p)^2-M^2][(\ell-p)^2-\lambda^2][(\ell+p')^2-\lambda^2]}\ , \tag{2.8}$$

where we have introduced a photon mass λ in order to regularize the infrared divergences known to be present in this amplitude. The crossed box diagram in Fig. 2.1(b) can be obtained from (2.8) by adding an overall minus sign, reversing the order of the γ_μ, γ_ν matrices in the heavy fermion bilinear, and performing the substitutions $k \to k'$ everywhere (except for the spinors) and $M \to -M$. Hence, in Eq. (2.7), $\mathcal{M}_{box} = \mathcal{M}_a + \mathcal{M}_b$. The evaluation of the integrals is slightly cumbersome but straightforward and the details are given in the Appendix A.

With the definition of the Mandelstam variables $s = (p+p')^2$ and $t = (p-k)^2$, the spinorial structure of $\mathcal{M}_{box}$ is decomposed into 4 sets of amplitudes $L_i^{\rho\kappa}$ multiplied by corresponding coefficients w_i^ρ:

$$\mathcal{M}_{box}(\kappa; s, t) = e^4 Q_f^2 \sum_{i=1}^{4} \sum_{\rho=\pm1} L_i^{\rho\kappa}\, w_i^\rho \ , \tag{2.9}$$

with the basic amplitudes

$$\begin{aligned}
L_1^{\rho\kappa} &= [\,\bar{v}_e(p')\,\gamma_\mu\,P_\kappa\,u_e(p)\,]\,[\,\bar{u}_f(k)\,\gamma^\mu\,(1+\kappa\rho\,\gamma_5)\,v_f(k')\,]\ ,\\
L_2^{\rho\kappa} &= [\,\bar{v}_e(p')\,\not{k}\,P_\kappa\,u_e(p)\,]\,[\,\bar{u}_f(k)\,\not{p}\,(1+\kappa\rho\,\gamma_5)\,v_f(k')\,]\ ,\\
L_3^{\rho\kappa} &= [\,\bar{v}_e(p')\,\not{k}\,P_\kappa\,u_e(p)\,]\,[\,\bar{u}_f(k)\,(1+\kappa\rho\,\gamma_5)\,v_f(k')\,]\ ,\\
L_4^{\rho\kappa} &= [\,\bar{v}_e(p')\,\gamma_\mu\,P_\kappa\,u_e(p)\,]\,[\,\bar{u}_f(k)\gamma^\mu\,\not{p}\,(1+\kappa\rho\,\gamma_5)\,v_f(k')\,]\ .
\end{aligned} \tag{2.10}$$

The latter have been written in terms of the initial state e^+e^- chiral projectors

$$P_\kappa = \frac{1}{2}\Big(1+\kappa\,\gamma_5\Big)\ ,\ \ \kappa = \pm 1\ , \tag{2.11}$$

which, as we are considering massless initial fermions, satisfy $P_\kappa u_e(p) = u_e(p)$, being κ the initial electron helicity; in the massless limit, positron helicity is forced to be $-\kappa$ to have a non vanishing amplitude. The dependence of $\mathcal{M}_{box}$ on the spin state of the final state fermions has not been explicitly stated.

The w_i^ρ coefficients can be written in terms of four auxiliary functions $\mathcal{F}_i$, $i = 0, 1, 2, 3$:

$$w_1^+ = \frac{1}{2}\mathcal{F}_0(s,t)\ ,$$

$$
\begin{aligned}
w_1^- &= -\frac{1}{2}\mathcal{F}_0(s,u)\ , \\
w_2^+ &= \mathcal{F}_1(s,t)+\mathcal{F}_2(s,t)\ , \\
w_2^- &= \mathcal{F}_1(s,u)+\mathcal{F}_2(s,u)\ , \\
w_3^+ &= M\Big(\mathcal{F}_1(s,u)-\mathcal{F}_1(s,t)+\mathcal{F}_3(s,u)-\mathcal{F}_3(s,t)\Big)\ , \\
w_3^- &= M\Big(\mathcal{F}_3(s,u)-\mathcal{F}_3(s,t)\Big)\ , \\
w_4^+ &= -\frac{1}{2}M\Big(\mathcal{F}_2(s,t)-\mathcal{F}_2(s,u)\Big)\ , \\
w_4^- &= \frac{1}{2}M\Big(\mathcal{F}_2(s,t)-\mathcal{F}_2(s,u)\Big)\ ,
\end{aligned}
\tag{2.12}
$$

that read

$$
\begin{aligned}
\mathcal{F}_0(s,t) \;=\; \mathcal{F}_0^{\lambda}(s,t) \;+\; \frac{M^2-t}{(M^2-t)^2+st}\Big\{ & t\ (\,sD_0\ -\ 2C_t\,) \\
& -M^2\,\frac{M^2-s-t}{M^2-t}\ \Big(\,s\overline{D}_0\ -\ 2\overline{C}_t\Big) \\
& -\ \Big(2M^2-s-2t\Big)\ (C_s+C_M)\Big\}\ ,
\end{aligned}
\tag{2.13}
$$

$$
\begin{aligned}
\mathcal{F}_1(s,t) \;=\; \frac{1}{(M^2-t)^2+st}\Big\{ & 2(B_t-B_s)+\frac{4M^2}{M^2-t}\,(B_M-B_t) \\
& +\frac{M^2-t}{(M^2-t)^2+st}\Big[\,(2M^2-s-2t) \\
& \times\Big((M^2-t)(sD_0-2C_t)+s\,C_s\,\Big) \\
& +\ \Big(\,2(M^2-t)^2+s(2t+s-4M^2)\,\Big)\,C_M\,\Big]\Big\}\ ,
\end{aligned}
\tag{2.14}
$$

$$
\begin{aligned}
\mathcal{F}_2(s,t) \;=\; \mathcal{F}_2^{\lambda}(s,t) \;-\; \frac{1}{(M^2-t)^2+st}\Big\{ & (M^2+t)\ (\,sD_0\ -\ 2C_t\,) \\
& -(s-4M^2)\,C_M\ -\ (2M^2-s-2t)\,C_s\Big\}\ ,
\end{aligned}
\tag{2.15}
$$

$$
\mathcal{F}_3(s,t) \;=\; \frac{1}{(M^2-t)^2+st}\Big\{\ \frac{2t}{M^2-t}\,(B_t-B_M)\ +\ \frac{2(M^2+t)}{4M^2-s}\,(B_s-B_M)
$$

$$
\begin{aligned}
&- \frac{(M^2-t)^2}{(M^2-t)^2+st}\Big[\,(M^2-t)\,(sD_0-2C_t)\;+\;s\,C_s\,\Big] \\
&+\frac{1}{(4M^2-s)((M^2-t)^2+st)}\,\Big[-4\,M^8\;+\;6(s+2t)\,M^6 \\
&\qquad\qquad -(s+2t)\,(s+6t)\,M^4 \\
&\qquad\qquad +2t\,(s^2+ts+2t^2)\,M^2\;+ \\
&\qquad\qquad +s^2t^2\,\Big]\,C_M\,\Big\}\;. \qquad (2.16)
\end{aligned}
$$

Full expressions for the scalar functions B_s, B_t, B_M, C_s, C_t, $\overline{C}_t$, C_M, D_0 and $\overline{D}_0$ can be found in Eqs. (A.2.5-A.2.13) of the Appendix A. It can be seen from $\mathcal{F}_1(s,t)$ and $\mathcal{F}_3(s,t)$ that the two–point functions B_t, B_s and B_M only appear in non–divergent combinations while the rest of scalar integrals in $\mathcal{F}_i(s,t)$ are UV finite. Clearly $\mathcal{M}_{box}(\kappa;s,t)$ is ultraviolet finite. Scalar integrals D_0 ($\overline{D}_0$) and C_t ($\overline{C}_t$) are infrared divergent for vanishing photon mass λ, however the combinations sD_0-2C_t and $s\overline{D}_0-2\overline{C}_t$ are divergenceless. Hence all the divergences in the $\mathcal{F}_i(s,t)$ functions are collected in $\mathcal{F}_0^\lambda(s,t)$ and $\mathcal{F}_2^\lambda(s,t)$, given by :

$$
\begin{aligned}
\mathcal{F}_0^\lambda(s,t) &= 2\,\Big(M^2-s-t\Big)\,\overline{D}_0\;, \\
\mathcal{F}_2^\lambda(s,t) &= 2\,D_0\;, \qquad (2.17)
\end{aligned}
$$

and we get for the infrared divergent part of the box amplitude :

$$
\mathcal{M}_{box}^{IR}\;=\;\frac{e^4Q_f^2}{8\pi^2\,s}\,\Big(L_1^{+\kappa}\;+\;L_1^{-\kappa}\Big)\,\ln\left(\frac{M^2-u}{M^2-t}\right)\,\ln\left(\frac{-s-i\delta}{\lambda^2}\right)\quad. \qquad (2.18)
$$

A more complete discussion on the infrared structure of the QED box diagram and the determination of $\mathcal{M}_{box}^{IR}$ is relegated to Appendix B.

Incidentally our result can be used to evaluate the similar two–gluon box contribution to the heavy quark production out of light quarks, $q(A)\bar{q}(B)\to Q(C)\overline{Q}(D)$ (between parentheses we label the colour quantum numbers). In order to get this amplitude we need to substitute the $e^4Q_f^2$ factor in Eq. (2.9) by $g_s^4(t^bt^a)_{BA}\{t^a,t^b\}_{CD}$ (a sum over repeated indices is implied). [2]

We have checked that our amplitude in Eq. (2.9), when summed over polarizations, coincides with a recent result found in Ref. [20], though these authors use a different basis of spinor operators. Moreover, from our calculation for $\mathcal{M}_{box}$, we can recover the case where the final fermions are massless. The limit $M\to 0$ can be directly applied to the $w_i^\pm$ coefficients, Eqs. (2.12), and to the scalar integrals quoted in the Appendix A. Within this limit our result agrees with the earlier calculation in Ref. [25].

[2] In this colour factor $t^i=\lambda^i/2$, where λ^i are the $SU(3)$ Gell–Mann matrices and $Tr(t^it^j)=\delta^{ij}/2$.

2.4 Heavy fermion production at threshold

Close to $f\bar{f}$ threshold, it is more convenient to expand the production amplitude in terms of the fermions velocity in the center–of–mass of the colliding system β. Hence production amplitudes are written in a combined expansion in powers of α and β, and the importance of each contribution is estimated taking $\alpha \sim \beta$. This feature spoils the perturbative expansion in QED due to the appearance of $\mathcal{O}(\alpha^n/\beta^n)$ and $\mathcal{O}(\alpha^m ln^n \beta)$ terms that diverge as $\beta \to 0$. As a consequence, a resummation of such terms is necessary to avoid a breakdown of the perturbative series, and well-known results from the familiar non-relativistic quantum mechanics are obtained. Nevertheless it is somewhat misleading to associate the appearance of these Coulomb terms to the non-relativistic motion of the fermion pair, as the scattering amplitude calculated from quantum mechanics does not show any kinematic singularity close to threshold: their ultimate origin is the inadequacy of the diagrammatic QED expansion in powers of α to account for the correct non-relativistic dynamics. Keeping this in mind, one should not discard, a priori, divergent terms in the velocity appearing in any QED diagram involving fermions with small velocities.

As it has been pointed out that the contribution at threshold of the two–photon box diagram should be analysed in a NNLO calculation of $\sigma(e^+e^- \to \tau^+\tau^-)$. In this Section we proceed to perform the expansion on $\mathcal{M}_{box}$ as given in Eq. (2.9). The leading terms in the velocity expansion of the coefficients $w_i^{\pm}$ can be obtained by taking into account the dependence of the Mandelstam invariants s, t, u on the velocity β and the angle θ between the momenta of the heavy fermion and the electron in the colliding center–of–mass system. The relation is given by :

$$s = \frac{4M^2}{1-\beta^2} \quad , \quad t = M^2 - \frac{2M^2}{1-\beta^2}(1-\beta\cos\theta) \quad , \quad u = M^2 - \frac{2M^2}{1-\beta^2}(1+\beta\cos\theta) \ . \tag{2.19}$$

Carrying these expressions to the $w_i^{\pm}$ coefficients displayed in Eq. (2.12) and neglecting $\mathcal{O}(\beta^2)$ terms we obtain :

$$\begin{aligned}
w_1^+ &= \frac{1}{384M^2\pi^2}\Big[-\pi^2 + 3\ln^2\frac{4M^2}{\lambda^2} - 3\ln^2\frac{m^2}{\lambda^2} \\
&\qquad + \left(8 - 14i\pi - 8\ln 2 + 12\ln\frac{4M^2}{\lambda^2}\right)\beta\,\cos\theta\Big] + \mathcal{O}(\beta^2) \ , \\
w_1^- &= -w_1^+(\beta \to -\beta) \ , \\
w_2^+ &= \frac{1}{384M^4\pi^2}\Big[\pi^2 - 8 + 8i\pi + 8\ln 2 - 3\ln^2\frac{4M^2}{\lambda^2} + 3\ln^2\frac{m^2}{\lambda^2} \\
&\qquad + \Big(\pi^2 - 34 + 4i\pi + 16\ln 2 + 12\ln\frac{4M^2}{\lambda^2} - 3\ln^2\frac{4M^2}{\lambda^2} \\
&\qquad\quad + 3\ln^2\frac{m^2}{\lambda^2}\Big)\beta\cos\theta\Big] + \mathcal{O}(\beta^2) \ ,
\end{aligned}$$

$$
\begin{aligned}
w_2^- &= w_2^+(\beta \to -\beta)\ , \qquad (2.20)\\
w_3^+ &= \frac{1}{240M^3\pi^2}\Big(37 + 2i\pi - 64\ln 2\Big)\,\beta\cos\theta \,+\, \mathcal{O}(\beta^2)\ ,\\
w_3^- &= \frac{-1}{480M^3\pi^2}\Big(11 + i\pi - 32\ln 2\Big)\,\beta\cos\theta \,+\, \mathcal{O}(\beta^2)\ ,\\
w_4^+ &= \frac{-1}{384M^3\pi^2}\Big(\pi^2 + 6i\pi - 48\ln 2 + 12\ln\frac{4M^2}{\lambda^2} - 3\ln^2\frac{4M^2}{\lambda^2}\\
&\qquad + 3\ln^2\frac{m^2}{\lambda^2}\Big)\,\beta\cos\theta \,+\, \mathcal{O}(\beta^2)\,,\\
w_4^- &= -w_4^+\ .
\end{aligned}
$$

The amplitudes $L_i^{\rho\kappa}$, containing fermion wave functions, must also be expanded in terms of β to fulfill the expansion of $\mathcal{M}_{box}$ at small velocities. We shall not give the full result of such expansion, but just quote their leading behaviour, which can be easily obtained by choosing an explicit representation of the gamma matrices and spinors. We thus get:

$$
L_1^{\rho\kappa} = \mathcal{O}(1)\,, \qquad L_2^{\rho\kappa} = \mathcal{O}(\beta)\,, \qquad L_3^{\rho\kappa} = \mathcal{O}(\beta)\,, \qquad L_4^{\rho\kappa} = \mathcal{O}(1)\ . \qquad (2.21)
$$

The terms quoted in Eqs. (2.20) together with the expansion in Eq. (2.21) allow us to obtain the leading near threshold contribution to the cross section of the box amplitude $\mathcal{M}_{box}$. Recall that, by virtue of Furry's theorem, the interference of the QED box amplitude with other one-loop amplitudes for the process $e^+e^- \to f\bar{f}$ vanishes and, consequently, $|\mathcal{M}_{box}|^2$ adds incoherently to the rest of $\mathcal{O}(\alpha^4)$ corrections to $\sigma(e^+e^- \to f\bar{f})$, as studied in Ref. [24]. The final result for the squared and averaged box amplitude is :

$$
\begin{aligned}
\frac{1}{4}\sum_{pol.}|\mathcal{M}_{box}|^2 = (Q_f\,\alpha)^4\Bigg\{ & \frac{16}{9}\Big(\pi^2 + (1-\ln 2)^2\Big) + \Bigg[-\frac{1}{2}L_M^4 - 4L_M^3 - 2L_M^3\ell_m \qquad (2.22)\\
& + \Big(-2\ell_m^2 - 12\ell_m + \frac{8}{3}\ln 2 + \frac{\pi^2}{3} + \frac{160}{3}\Big) L_M^2\\
& + \Big(-8\ell_m^2 + \Big(\frac{16}{3}\ln 2 + \frac{2}{3}\pi^2 + \frac{320}{3}\Big)\ell_m - 288\ln 2 + \frac{4}{3}\pi^2\\
& \quad + 32\Big) L_M\, 56\,\ell_m^2 + \Big(-288\ln 2 + \frac{4}{3}\pi^2 + 32\Big)\ell_m\\
& + \frac{3088}{9}\ln^2 2 - \frac{800}{9}\ln 2 - \frac{\pi^4}{18} - \frac{8}{9}\pi^2\ln 2 - \frac{14}{3}\pi^2 + \frac{16}{9}\Bigg]
\end{aligned}
$$

$$\times \cos^2\theta \Big\} \beta^2 \, + \, \mathcal{O}(\beta^3) \, , \tag{2.23}$$

with

$$L_M \equiv \ln \frac{4M^2}{m^2} \qquad \text{and} \qquad \ell_m \equiv \ln \frac{m^2}{\lambda^2} \quad . \tag{2.24}$$

Hence we conclude that the result in Eq. (2.23), proportional to $\alpha^4\beta^2$, represents a N^{4}LO correction with respect the LO result (the tree level $e^+e^- \to f\bar{f}$ amplitude squared, which is already of $\mathcal{O}(\alpha^2)$). In Ref. [24], box amplitudes were not included with the rest of the one-loop diagrams to complete the NNLO calculation of $\sigma(e^+e^- \to \tau^+\tau^-)$ at threshold, their behaviour with β being unknown. Our evaluation of $|\mathcal{M}_{box}|^2$ has proven that this is, indeed, β^2 suppressed with respect the NNLO contributions considered in [24].

2.5 Threshold amplitude by asymptotic expansion of integrals

The counting of powers of the velocity appearing in a defined amplitude is not straight because β is not a parameter in the Lagrangian, but rather a dynamic scale which is driven by the propagators inside loop integrals. In recent years, this issue made awkward to define a non-relativistic effective theory suitable for describing quarks and leptons at low velocities. Important progress was made after the development of the threshold expansion by Beneke and Smirnov [30]. This technique allows for an asymptotic expansion of Feynman integrals near threshold, providing a set of much simpler integrals which are manifestly homogeneous in the expansion parameter and so have a definite power counting in the velocity. The procedure should confirm that the two–photon box amplitude is not enhanced at low β, as we have found by explicit evaluation. This we discuss in the following.

The expansion method, described in Ref. [30], begins by identifying the relevant momentum regions in the loop integrals, which follow from the singularity structure of the Feynman propagators dictated by the relevant scales that appear in the problem. For on-shell scattering amplitudes of heavy fermions, three scales are identified: the heavy fermions mass, M, their relative 3-momentum, $|\boldsymbol{k}| \sim M\beta$ and their energy $k_0 \sim M\beta^2$. Accordingly, the loop four momentum near the singularities can be in any of the following regimes:

$$\begin{aligned}
hard \; : \quad & \ell_0 \sim |\boldsymbol{\ell}| \sim M \, , \\
soft \; : \quad & \ell_0 \sim |\boldsymbol{\ell}| \sim M\beta \, , \\
potential \; : \quad & \ell_0 \sim M\beta^2 \; , \; |\boldsymbol{\ell}| \sim M\beta \, , \\
ultrasoft \; : \quad & \ell_0 \sim |\boldsymbol{\ell}| \sim M\beta^2 \, .
\end{aligned} \tag{2.25}$$

The original integral is then decomposed into a set of integrals, one for every region, and a Taylor expansion in the parameters, which are small in each regime, is performed. Every integral, containing just one scale, will thus contribute only to a single power in the velocity expansion. The procedure requires the use of dimensional regularization in handling the integrals, even if they are finite, in order to assure that the result from each regime just picks up the corresponding pole contribution and vanishes outside. Following this heuristic rules, the authors of Ref. [30] reproduce the exact β expansion of some one-loop and two-loop examples. Although a formal proof of the validity of the asymptotic expansion close to threshold has not been given, the perfect agreement in the examples supports their use in general one-loop diagrams. We provide a new test by addressing the rules to the QED box amplitude with e^+e^- in the initial state, extending the use of the threshold expansion to diagrams with heavy and massless fermions in the external legs (i.e. production-like diagrams). We will keep the electron mass finite along the procedure, although much smaller than any other scale, to keep track of the logarithms of m present in the box amplitude.

Our amplitude $\mathcal{M}_{box}$ is characterized, as shown in the Appendix A, by the four point integrals $D_0, D_\mu, D_{\mu\nu}$ in (A.2.1). If present, inverse powers of the velocity in $\mathcal{M}_{box}$ can only originate from these integrals. In addition, we can focus on the behaviour of the scalar integral D_0, as the $\ell_\mu, \ell_\mu\ell_\nu$ vectors in D_μ and $D_{\mu\nu}$ will produce factors of one of the scales of the problem ($M, M\beta$ or $M\beta^2$) in the numerator of the amplitude without affecting the leading singular behaviour in β. Let us change the routing of momenta in D_0 (A.2.1) in order to make the scaling arguments more transparent:

$$D_0 = \int \frac{d^D\ell}{i(2\pi)^D} \frac{1}{[(Q/2+T/2-\ell)^2-m^2][(Q/2+R/2-\ell)^2-M^2][\ell^2-\lambda^2]} \times \frac{1}{[(Q-\ell)^2-\lambda^2]}\,, \tag{2.26}$$

where the standard $+i\delta$ prescriptions are implicitly understood in the propagators, the Q and R vectors are defined in relation with Eq. (A.2.1) and $T = p - p'$. The external four vectors Q and R scale as M and $M\beta$ respectively, while $T^2 = -s+4m^2 \sim M^2$. Using momentum T is preferred to the electron (positron) momentum p (p') because, the spatial and time components of the latter, although scale as M, cancel out in the total momentum squared $p^2 = m^2 \sim 0$. The infrared regularization of the integrals is automatically guaranteed by dimensional regularization and, therefore, we will not longer retain a fictitious mass for the photon.

In the potential region $\ell_0 \ll |\boldsymbol{\ell}| \ll M$ and, accordingly, we can expand terms in the propagators. The leading contribution is

$$D_0^p = \int \frac{d^D\ell}{i(2\pi)^D} \frac{1}{(\boldsymbol{\ell}\cdot\boldsymbol{T})\,(-\boldsymbol{\ell}^2+\boldsymbol{\ell}\cdot\boldsymbol{R}-Q_0\ell_0)\,(-\boldsymbol{\ell}^2)\,(Q_0^2)}\,, \tag{2.27}$$

where we have also dropped the term $-\boldsymbol{\ell}^2$ in the electron propagator to be compared to $\boldsymbol{\ell}\cdot\boldsymbol{T} \sim M^2\beta$. The overall scaling of the potential integration is easily estimated

to be of order $M^4\beta^5/M^8\beta^5 \sim 1/M^4$, so no velocity enhancement is this region is expected. In fact, the integral above is zero because, closing the ℓ_0 integration contour in the lower half-plane, the pole at $\ell_0 = (\boldsymbol{\ell}\cdot\boldsymbol{R}-\boldsymbol{\ell}^2)/Q_0 + i\delta$ lies outside [3]. Similarly, subleading terms in the expansion of propagators in this region are vanishing, as they share the same pole structure.

When the loop momentum ℓ is soft or ultrasoft, the assumption $\ell_0 \sim |\boldsymbol{\ell}| \ll M$ leads to the same expansion of the propagators in D_0:

$$D_0^{s,us} = \int \frac{d^D\ell}{i(2\pi)^D} \frac{1}{(\boldsymbol{\ell}\cdot\boldsymbol{T} - Q_0\ell_0)\,(-Q_0\ell_0)\,(\ell_0^2-\boldsymbol{\ell}^2)\,(Q_0^2)} \ . \tag{2.28}$$

It scales as $1/M^4$ in both the soft and ultrasoft regimes and, indeed, vanishes in dimensional regularization because, after picking up the residue in the lower plane, $\ell_0 = |\boldsymbol{\ell}| - i\delta$, the remaining $D-1$ dimension integral is scaleless:

$$\begin{aligned} D_0^{s,us} &= \frac{1}{2Q_0^3}\int \frac{d^{D-1}\ell}{(2\pi)^{D-1}} \frac{1}{|\boldsymbol{\ell}|^2} \frac{1}{(Q_0|\boldsymbol{\ell}| - \boldsymbol{T}\cdot\boldsymbol{\ell})} \\ &= \frac{1}{2Q_0^3}\int \frac{d\Omega_{D-1}}{(2\pi)^{D-1}} \frac{1}{(Q_0 - |\boldsymbol{T}|\cos\varphi)} \int d|\boldsymbol{\ell}||\boldsymbol{\ell}|^{D-2} \frac{1}{|\boldsymbol{\ell}|^3} \ = \ 0 \ , \end{aligned} \tag{2.29}$$

with φ the angle between the vectors $\boldsymbol{T}$ and $\boldsymbol{\ell}$. The same argument holds for subleading terms in this region.

Finally, the integral in the hard region is obtained by dropping out terms involving non-relativistic fermion three-momenta from propagators. Hence, the only scale which remains is the hard parameter M, and so there is no additional velocity dependence in the denominators. More explicitly, the expanded integral in the hard regime, at leading order in β, is

$$D_0^{h,\mathcal{O}(1)} = \int \frac{d^D\ell}{i(2\pi)^D} \frac{1}{(\ell^2 - \ell\cdot T - Q\cdot\ell)\,(\ell^2 - Q\cdot\ell)\,\ell^2\,(Q-\ell)^2} \ , \tag{2.30}$$

and there is no need to separate time from spatial components in the integration. The above integral trivially scales a $1/M^4$, and its explicit calculation in $D = 4-2\epsilon$ dimensions has been performed following Ref. [31]:

$$D_0^{h,\mathcal{O}(1)} \ = \ \frac{\mu^{-2\epsilon}}{8\pi s^2} \ \ln\frac{s}{m^2} \ \left[\frac{1}{\epsilon} - \ln\left(\frac{-s-i\delta}{\mu^2}\right) + \ln(4\pi) - \gamma_E\right] \ , \tag{2.31}$$

where γ_E is the Euler-Mascheroni constant. Terms proportional to the electron mass m have been dropped. The pole in Eq. (2.31) is of infrared origin, and it

[3] Notice that the ℓ_0–integration in D_0^p does not vanish in the outer semicircle. Rigorously we should keep the ℓ_0^2 term in the heavy fermion propagator, so D_0^p is well defined. Poles would then be located at $\ell_0^\pm = \frac{1}{2}\Big(Q_0 \pm \sqrt{Q_0^2 - 4(\boldsymbol{\ell}\cdot\boldsymbol{R}-\boldsymbol{\ell}^2) - i\delta}\Big)$. The root ℓ_0^+ scales as M and is taken into account in the hard region while $\ell_0^- = (\boldsymbol{\ell}\cdot\boldsymbol{R}-\boldsymbol{\ell}^2)/Q_0 + i\delta$ once we consider that $|\boldsymbol{\ell}| \ll M$ in the potential region, and we recover the above result.

is the analogous to the $\ln\lambda^2$ term in the full result of D_0, Eq. (A.2.5). Indeed, Eq. (2.31) reproduces the leading term in the velocity expansion of D_0, after the usual replacement $\ln\lambda^2 \to (4\pi)^\epsilon/\Gamma(1-\epsilon)/\epsilon$.

The following order in the expansion within the hard region would have a $\ell\cdot R = -\boldsymbol{\ell}\cdot\boldsymbol{R}$ term in the numerator, and it would behave as β/M^4:

$$\begin{aligned} D_0^{h,\,\mathcal{O}(\beta)} &= \int \frac{d^D\ell}{i(2\pi)^D}\,\frac{\ell\cdot R}{(\ell^2-\ell\cdot T-Q\cdot\ell)\,(\ell^2-Q\cdot\ell)^2\,\ell^2\,(Q-\ell)^2} \\ &= \frac{R\cdot T}{T^2}\left(D_0^h - \int \frac{d^D\ell}{i(2\pi)^D}\,\frac{1}{(\ell^2-Q\cdot\ell)^2\,\ell^2\,(Q-\ell)^2}\right) \\ &= \frac{\beta\cos\theta}{8\pi^2 s^2}\,\mu^{-2\epsilon}\left(\ln\frac{s}{m^2}-2\right)\left[\frac{1}{\epsilon}-\ln\left(\frac{-s-i\delta}{\mu^2}\right)+\ln(4\pi)-\gamma_E\right] \end{aligned} \tag{2.32}$$

which agrees with the second term in the velocity expansion of D_0. The series expansion in β of the scalar function D_0 is thus reproduced by that of D_0^h, while the rest of integration regions does not contribute at all.

Therefore we have seen, by asymptotic expanding the integral before its computation, that the box amplitude receives no contributions from the regions of potential, soft and ultrasoft loop momentum, and it is then preserved from Coulomb type singularities, as it was shown by explicit calculation. This fact reveals that, as expected, the box production graph is a process dominated by the high scale, as it involves annihilating photons which carry energies of the order of the mass of the non-relativistic fermions.

Let us finally note that, although we have reproduced the (logarithmic) electron mass dependence of D_0 through the threshold expansion technique, we could, a priori, need to consider new regions to successfully obtain the subleading terms $\mathcal{O}(m^2/M^2)$, $\mathcal{O}(m^2/(q^2-4M^2))$, etc. This is what happens, for example, if one considers the 1-loop two-point scalar function with one heavy mass M and one light mass m at values of $q^2 \gtrsim M^2$: Keeping m finite but smaller than any other scale present (i.e. $m \ll (q^2-M^2)/M \ll \sqrt{q^2-M^2} \ll M$), the integration region where $\ell^2 \sim m^2$ gives a non-vanishing contribution proportional to $m^2/(q^2-M^2)$. A new pattern of integration regimes should then be considered to make each integral homogeneous also in the m^2 scale.

2.6 Conclusions

The interest in the study of electron positron annihilation into heavy fermions has been ushered by the multiple features foreseen both in high–energy colliders and production at threshold. These include all–important aspects of the phenomenology like an accurate measurement of the heavy fermion masses (like τ or t) and, the possibility, of exploring New Physics beyond the Standard Model. This goal requires the computation and implementation of complete perturbative orders within the Standard Model.

We have evaluated the QED two–photon box diagrams of Fig. 2.1 contributing to $\sigma(e^+e^- \to f\bar{f})$ with massive final fermions ($m_e \ll M$), and we have provided a full analytical expression for the amplitude. Its contribution at the production threshold has also been studied and we have found that it is negligible because of the high velocity suppression. This non–relativistic analysis complements the one carried out in Ref. [24] and shows that the conclusions reached in that reference are not modified by the QED box amplitude.

Finally we have analysed this low velocity behaviour using the strategy of regions to expand the Feynman integrals near threshold, confirming that such expansion can also be applied to diagrams involving heavy and light fermions. This feature allows to identify and evaluate, at a fixed order in the heavy fermion velocity, contributions to heavy fermion production or annihilation diagrams triggered by light fermions.

The box evaluation presented in this chapter has been published in Ref. [32].

Appendices

A Integrals in the box amplitude

In this Appendix we outline several features of the integration procedure, followed to evaluate the QED box diagrams, and we collect the explicit expressions for the relevant scalar integrals that appear in our results.

The general structure of the two–photon box amplitude in Fig. 2.1(a), $\mathcal{M}_a$ takes the form $\mathcal{M}_a = a_0 D_0 + a^\mu D_\mu + a^{\mu\nu} D_{\mu\nu}$, where $a_0, a_\mu, a_{\mu\nu}$ contain Dirac algebra γ's and spinors, and $D_0, D_\mu, D_{\mu\nu}$ are the integrals over the loop momentum ℓ :

$$D_0; D_\mu; D_{\mu\nu} = \int \frac{d^4\ell}{i(2\pi)^4} \frac{1;\, \ell_\mu;\, \ell_\mu\ell_\nu}{(\ell^2-m^2)[(\ell+k-p)^2-M^2][(\ell-p)^2-\lambda^2][(\ell+p')^2-\lambda^2]} \,, \tag{A.2.1}$$

which depend on three independent four-vectors and where $+i\delta$ prescriptions are understood in the propagators . Let us define our basis as $P = p - k$, $Q = p + p'$ and $R = k - k'$, with scalar products

$$P^2 = t \quad , \quad Q^2 = s \quad , \quad R^2 = 4M^2 - s \,,$$

$$P\cdot Q = 0 \quad , \quad P\cdot R = m^2 - M^2 - t \quad , \quad Q\cdot R = 0 \ .$$

The integrals in Eq. (A.2.1) are invariant under the interchange $\{p\,;k\} \leftrightarrow \{-p'\,;-k'\}$. Under the same transformation $P \to P$, $Q \to -Q$ and $R \to R$, and thus the tensor integrals $D_\mu, D_{\mu\nu}$ do not contain terms linear in Q, justifying our choice of basis. Tensor decomposition of $D_\mu, D_{\mu\nu}$ then reads

$$D_\mu = D_P\, P_\mu + D_R\, R_\mu \tag{A.2.2}$$

$$D_{\mu\nu} = D_{PP}\, P_\mu P_\nu + D_{PR}\Big(P_\mu R_\nu + R_\mu P_\nu\Big) + D_{RR}\, R_\mu R_\nu + D_{QQ}\, Q_\mu Q_\nu + s\, D_{00}\, g_{\mu\nu} \ . \tag{A.2.3}$$

Further reduction of the coefficient functions appearing in Eqs. (A.2.2,A.2.3) has been performed with the help of *FeynCalc* [33]. These coefficients are thus expressed as a linear combination of a set of scalar integrals: D_0, C_s, C_t, C_M, B_s, B_t and B_M, with four (D_0), three (C_a, $a = s,t,M$) and two (B_a, $a = s,t$) propagators that we collect next.

The relevant scalar integrals have been evaluated following the method described in [34], except for the rather cumbersome 4-point function D_0. In the latter case we have first calculated its imaginary part in the s-channel, following the optical theorem, and then the real part has been reconstructed through the t–fixed unsubtracted dispersion relation that satisfies D_0 :

$$\mathrm{Re}D_0(s,t) \,=\, \frac{1}{\pi} \fint_{4\lambda^2}^{\infty} dx\, \frac{\mathrm{Im}D_0(x,t)}{x-s} \ , \tag{A.2.4}$$

where the Principal Value of the integral is understood. We have performed its calculation in the $\lambda \ll m \ll M$ limit and, therefore, we have neglected photon

masses when possible. As emphasized in Ref. [35], the limit $\lambda \to 0$ is not trivial for the occurrence of terms like $\lambda^2/(x-4\lambda^2)$, which diverge for finite λ as $x \to 4\lambda^2$ but vanish for $\lambda \to 0$ at fixed $x \neq 4\lambda^2$. As a consequence the photon mass should be kept finite until the final stages.

The scalar integrals that appear in the two–photon box amplitude result in Eq. (2.9) through the $\mathcal{F}_i$ functions of Eqs. (2.13-2.16) have been evaluated in the limit where $\lambda \ll m \ll M$ and for the specific cases $p^2 = p'^2 = m^2$, $k^2 = k'^2 = M^2$, $(p+p')^2 = (k+k')^2 = s$, $(p-k)^2 = t$. They read :

$$\begin{aligned} D_0 &= \int \frac{d^4\ell}{i(2\pi)^4} \frac{1}{[\ell^2-\lambda^2]\,[(\ell+p)^2-m^2)]\,[(\ell+p+p')^2-\lambda^2]\,[(\ell+k)^2-M^2]} \\ &= \frac{-1}{8\pi^2 s\,(M^2-t)}\,\ln\frac{M^2-t}{mM}\,\ln\frac{-s-i\delta}{\lambda^2}\;, \end{aligned} \tag{A.2.5}$$

$$\overline{D}_0 = D_0\,(t \to u)\;, \tag{A.2.6}$$

$$\begin{aligned} C_s &= \int \frac{d^4\ell}{i(2\pi)^4} \frac{1}{[\ell^2-\lambda^2]\,[(\ell+p)^2-m^2]\,[(\ell+p+p')^2-\lambda^2]} \\ &= \frac{1}{32\pi^2 s}\left[\ln^2\left(\frac{-s-i\delta}{m^2}\right)+\frac{\pi^2}{3}\right]\;, \end{aligned} \tag{A.2.7}$$

$$\begin{aligned} C_t &= \int \frac{d^4\ell}{i(2\pi)^4} \frac{1}{[\ell^2-M^2]\,[(\ell-k)^2-\lambda^2]\,[(\ell+p-k)^2-m^2]} \\ &= \frac{-1}{16\pi^2(M^2-t)}\left[\mathrm{Li}_2\left(\frac{t}{M^2}\right)+\ln^2\left(\frac{M^2-t}{Mm}\right)+\ln\left(\frac{M^2-t}{Mm}\right)\ln\left(\frac{m^2}{\lambda^2}\right)\right]\;, \end{aligned} \tag{A.2.8}$$

$$\overline{C}_t = C_t\,(t \to u)\;, \tag{A.2.9}$$

$$\begin{aligned} C_M &= \int \frac{d^4\ell}{i(2\pi)^4} \frac{1}{[\ell^2-\lambda^2]\,[(\ell+k)^2-M^2]\,[(\ell+k+k')^2-\lambda^2]} \\ &= \frac{1}{16\pi^2 s\,\beta}\Big[-2\,\mathrm{Li}_2(1-\beta)+2\,\mathrm{Li}_2\left(\frac{1-\beta}{1+\beta}\right)+\frac{1}{2}\ln^2\left(\frac{1-\beta}{1+\beta}\right)-2\,\mathrm{Li}_2(-\beta) \\ &\qquad -2\ln\beta\,\ln(1+\beta)+i\pi\,\ln\frac{1-\beta}{1+\beta}\Big]\;, \end{aligned} \tag{A.2.10}$$

$$B_s = \int \frac{d^D\ell}{i(2\pi)^D} \frac{1}{[\ell^2-\lambda^2]\,[(\ell+p+p')^2-\lambda^2]}$$
$$= \frac{-1}{16\pi^2}\left(\Delta + \ln\frac{-s-i\delta}{\mu^2} - 2\right) , \qquad \text{(A.2.11)}$$

$$B_t = \int \frac{d^D\ell}{i(2\pi)^D} \frac{1}{[\ell^2-M^2]\,[(\ell+p-k)^2-m^2]}$$
$$= \frac{-1}{16\pi^2}\left(\Delta + \ln\frac{-t}{\mu^2} + \ln\left(1-\frac{M^2}{t}\right) - \frac{M^2}{t}\,\ln\frac{M^2-t}{M^2} - 2\right) \qquad \text{(A.2.12)}$$

$$B_M = \int \frac{d^D\ell}{i(2\pi)^D} \frac{1}{[\ell^2-\lambda^2]\,[(\ell+k)^2-M^2]}$$
$$= \frac{-1}{16\pi^2}\left(\Delta + \ln\frac{M^2}{\mu^2} - 2\right) , \qquad \text{(A.2.13)}$$

where $\mathrm{Li}_2(x)$ is the dilogarithm function. The two–point functions have been regularized within dimensional regularization in D dimensions and $\Delta = 2\mu^{D-4}/(D-4) + \gamma_E - \ln(4\pi)$, with μ the renormalization scale. From the full expressions above we see that only the integrals C_t, $\overline{C}_t$, D_0 and $\overline{D}_0$ are infrared divergent for vanishing photon mass ($\lambda \to 0$). However, as remarked in the main text, the combinations $sD_0 - 2C_t$ (or $s\overline{D}_0 - 2\overline{C}_t$) are infrared finite; accordingly all the infrared divergent contribution is provided by D_0 and $\overline{D}_0$ in Eq. (2.17) that carry a $\ln\lambda^2$ factor.

B Infrared divergence of the QED box diagram

There are several well-known facts on the structure of infrared divergences in QED that are relevant for our discussion [36] :

- Virtual photon radiative corrections between the external legs of a divergenceless root diagram generate an infrared divergent contribution that follows a specific pattern in the perturbative expansion. Such a structure provides a factorization of the resummation of the divergences at all orders.

- All the infrared divergence in virtual photon radiative corrections commented above, arises from the eikonal approach in the propagator of the radiating external legs. For spin 1/2, for example, with k the outgoing soft photon momentum of $\varepsilon_\mu(k)$ polarization and p the ingoing external momentum, the

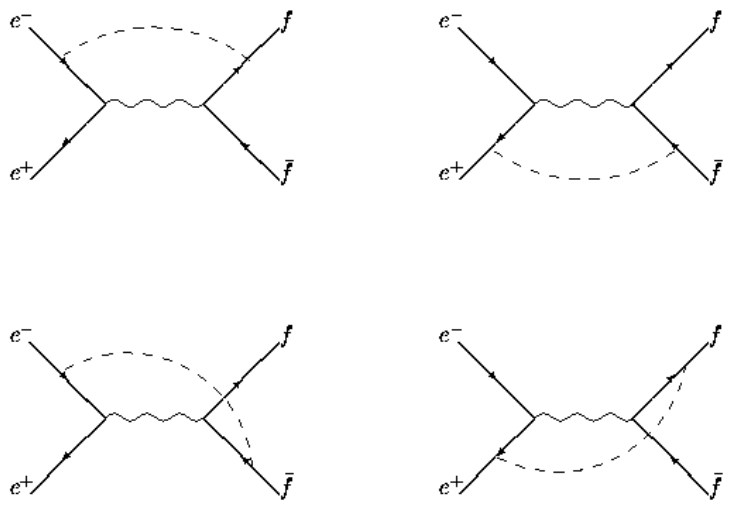

Figure 2.5: *Diagrams contributing to the infrared divergence of the QED box diagram. The wavy line corresponds to a hard photon and the dashed line to a soft photon. As explained in the text the infrared divergence factorizes and the spinor structure is the one of the hard diagram (without radiative corrections).*

modification of the fermion wave function reads :

$$u(p) \xrightarrow{photon} \frac{1}{\not p - \not k - m + i\,\delta}\, \not\varepsilon\, u(p) = \frac{(2p-k)\cdot\varepsilon - \frac{1}{2}\,[\not k\,, \not\varepsilon\,]}{k^2 - 2k\cdot p + i\delta}\, u(p)\,, \tag{B.2.1}$$

that, in the eikonal approximation reduces to

$$u(p) \xrightarrow[photon]{soft} \frac{2p\cdot\varepsilon}{k^2 - 2k\cdot p + i\delta}\, u(p)\,, \tag{B.2.2}$$

neglecting, essentially, the spin of the radiating field.

Hence to extract the infrared divergent part of the QED box diagram in Fig. 2.1 we need to implement the eikonal approximation into the amplitude $\mathcal{M}_a$ in Eq. (2.8) and the crossed $\mathcal{M}_b$. This corresponds to evaluate the four diagrams in Fig. 2.5. These are built from the tree–level diagram for $e^+e^- \to f\bar f$ through one photon annihilation, by attaching a soft photon between an ingoing and an outgoing external leg in all possible ways. Their evaluation gives :

$$\mathcal{M}^{IR}_{box} = \overline{v}_e(p')\,\gamma_\mu\, u_e(p)\,\frac{e^2Q_f}{s}\,\overline{u}_f(k)\,\gamma^\mu\, v_f(k')\,\left[\frac{e^2Q_f}{4\pi^2}\,\ln\left(\frac{M^2-u}{M^2-t}\right)\,\ln\left(\frac{m^2}{\lambda^2}\right)\right]\,, \tag{B.2.3}$$

where infrared finite terms have not been written. In fact this result has been obtained by integrating over the full range of momentum of a massive photon. Rigorously we should define the infrared contribution by imposing an upper limit on

its momentum $|\boldsymbol{q_\gamma}| < \Lambda$, and m^2 would then be replaced by Λ^2 in the logarithm of $\mathcal{M}^{IR}_{box}$. In Eq. (B.2.3) we have explicitly stated the factorization between the hard gluon exchange, on the left, and the soft photon exchange inside the square brackets.

Alternatively we can evaluate $\mathcal{M}^{IR}_{box}$ from our result in Eq. (2.9) and we obtain :

$$\mathcal{M}^{IR}_{box} = \frac{e^4 Q_f^2}{8\pi^2\, s}\left\{ \frac{(M^2-t)L_1^{-\kappa} + 2\,L_2^{+\kappa} - M\left(L_4^{+\kappa} - L_4^{-\kappa}\right)}{M^2-t}\,\ln\left(\frac{M^2-t}{Mm}\right) \right.$$
$$\left. - \frac{(M^2-u)L_1^{+\kappa} - 2\,L_2^{-\kappa} - M\left(L_4^{+\kappa} - L_4^{-\kappa}\right)}{M^2-u}\,\ln\left(\frac{M^2-u}{Mm}\right)\right\}$$
$$\times\,\ln\left(\frac{\lambda^2}{-s-i\delta}\right)\,, \tag{B.2.4}$$

where the spinor operators $L_i^{\rho\kappa}$ have been defined in Eq. (2.10). Then, using the following relations : [4]

$$\begin{aligned}(M^2-t)\,L_1^{+\kappa} &= 2\,L_2^{+\kappa} - M\left(L_4^{+\kappa} - L_4^{-\kappa}\right)\,,\\ (M^2-u)\,L_1^{-\kappa} &= -2\,L_2^{-\kappa} - M\left(L_4^{+\kappa} - L_4^{-\kappa}\right)\,,\end{aligned} \tag{B.2.5}$$

we finally get :

$$\mathcal{M}^{IR}_{box} = \frac{e^2 Q_f}{2\,s}\left(L_1^{+\kappa} + L_1^{-\kappa}\right)\left[\frac{e^2 Q_f}{4\pi^2}\,\ln\left(\frac{M^2-u}{M^2-t}\right)\ln\left(\frac{-s-i\delta}{\lambda^2}\right)\right]\,, \tag{B.2.6}$$

whose infrared logarithm coincides with our previous result in Eq. (B.2.3), since $P_\kappa u_e(p) = u_e(p)$ in $L_1^{\pm\kappa}$, being κ the massless electron helicity.

We conclude that the infrared divergence of the QED box diagram satisfies the expected features [36] and hence its cancellation should take place when real soft photon radiation contributions, at a fixed α perturbative order, are taken into account.

[4] Relations between spinor operators like these can be obtained by explicit evaluation in a particular reference frame or transforming the operators into traces in the spinor basis, hence working with Lorentz invariant expressions.

Chapter 3

New Contributions to Heavy Quark Sum Rules

3.1 Introduction

Sum rules analyses have extensively exploited the relation between the correlator of the quark electromagnetic currents and the cross section of $e^+e^- \to hadrons$ under the assumption of quark-hadron duality, to extract fundamental information of hadron systems. The two-point function containing the QCD dynamics of the produced quarks is built from the sum of the electromagnetic vector currents associated to each flavour:

$$\begin{aligned} \Pi^{\mu\nu}_{had}(p) &= i \int d^4x\, e^{ipx} \sum_{q,q'} e_q\, e_{q'} \,\langle\, 0 \,|\, T\, (\, \overline{q}(x)\, \gamma^\mu\, q(x)\,)\, (\, \overline{q'}(0)\, \gamma^\nu\, q'(0)\,)\,|\, 0\,\rangle \\ &= (\, -g^{\mu\nu}\, p^2 \,+\, p^\mu\, p^\nu\,)\, \Pi_{had}(p^2)\ , \end{aligned} \tag{3.1}$$

where q and q' stand for heavy or light quarks, indistinctly, with electric charges e_q and $e_{q'}$. Here we find two types of correlators: the symmetric ones, both electromagnetic currents corresponding to the same flavour, and non-symmetric correlators, where $q \neq q'$. Strictly, the latter are needed to fully describe the electromagnetic production of hadrons, even in the case where a definite flavour type of hadrons is isolated in the final state. Sum rules analyses applied to heavy quark production are written down in terms of the symmetric correlator built from the vector current $j^\mu_Q(x) = e_Q\, \overline{Q}(x)\, \gamma^\mu\, Q(x)$ of the heavy quark Q, and the effects of the non-symmetric correlators are never considered. The reason is that they begin to contribute beyond $\mathcal{O}(\alpha_s^2)$ in QCD perturbation theory (see Fig. 3.1(a)), which means one order beyond the actual knowledge of the (symmetric) heavy quark correlator $\Pi_{Q\overline{Q}}$. The study of such new effects in $Q\overline{Q}$ production will be mandatory if $\mathcal{O}(\alpha_s^3)$ accuracy is reached in the future. However, already at $\mathcal{O}(\alpha_s^2)$ the production of heavy quarks $Q\overline{Q}$ receives contributions which have neither been accounted for in the theoretical input of heavy quark sum rules. These arise from heavy quark discontinuities of symmetric correlators built from quarks such that $m_q < m_Q$, as the cut shown in Fig. 3.1(b), representing the production of heavy hadrons radiated off a pair of lighter quarks.

Figure 3.1: *Examples of perturbative non–heavy quark current correlators at* $\mathcal{O}(\alpha_s^3)$ *(a) and* $\mathcal{O}(\alpha_s^2)$ *(b) that contribute to the production of* $Q\overline{Q}$ *states.*

Finally, Groote and Pivovarov have recently pointed out [37,38] that, at $\mathcal{O}(\alpha_s^3)$, a three–gluon intermediate state (see Fig. 3.2) contributes to the $\Pi_{Q\overline{Q}}$ correlator. As these authors have shown, this massless intermediate state invalidates the usual definition of the moments $\mathcal{M}_n$,

$$\mathcal{M}_n \;=\; \frac{1}{n!}\left(\frac{d}{dp^2}\right)^n \Pi_{Q\overline{Q}}(p^2)\,\Big|_{p^2=0} \;, \tag{3.2}$$

for $n \geq 4$, when they become singular. Consequently the use of heavy quark sum rules at $\mathcal{O}(\alpha_s^3)$ is debatable.

All the features we have just quoted arise as a consequence of the interplay between the implementation of quark–hadron duality and the proper definition of the observables in the case of heavy quarks QCD sum rules. The correlation between the perturbative input and the observable information on the experimental side requires a careful matching that cannot be fully achieved. Accordingly the introduced incertitudes should be estimated and included in the errors of the parameters determined through this method.

Here we discuss the aspects pointed out above and their consequences in the methodology of extracting information from QCD sum rules. The aim of this work is to provide a consistent procedure to implement the perturbative input in the theoretical side of the heavy quark sum rules. Our proposal relies in a careful application of the general theory of singularities of perturbation theory. The crucial point will be to isolate all the cuts related to $Q\overline{Q}$ production from the general vector two–point function (3.1) in order to construct a modified correlator containing only contributions to heavy quark production.

In section 3.2 we recall the theory of singularities of perturbative amplitudes. The relation between the phenomenological and the theoretical input in the QCD sum rules is discussed in section 3.3. Hence sections 3.4 and 3.5 collect the implementation of our proposal to include heavy quark radiation off light quarks and to exclude massless singularities, respectively. We will comment on the uncertainties related with our method too. In section 3.6 we emphasize our conclusions.

3.2 Analyticity of $\Pi_{had}(s)$

As it is well known two–point functions are analytic except for singularities at simple poles or branch cuts, the latter being originated by normal thresholds of production of internal on–shell states. Assuming that the absorptive part of $\Pi_{had}(p^2)$ starts at some point s_0, vanishing below this point, the correlator satisfies the dispersion relation [39] [1] :

$$\widehat{\Pi}_{had}(p^2) \doteq \Pi_{had}(p^2) - \Pi_{had}(0) = \frac{p^2}{\pi}\int_{s_0}^{\infty}\frac{ds}{s}\,\frac{\mathrm{Im}\,\Pi_{had}(s)}{s-p^2-i\epsilon} \quad . \tag{3.3}$$

The absorptive part $\mathrm{Im}\,\Pi_{had}(s)$ is a physical observable, as it is proportional to the total hadron production cross section by a vector current $J^\mu = \sum_q j_q^\mu$. Being QCD the underlying theory of strong interactions, the quark–hadron duality hypothesis allows us to identify, inclusively, the states in terms of observable hadrons with the partonic intermediate states. Hence the optical theorem tells us that the total absorptive part is the sum of the absorptive parts corresponding to different intermediate partonic states:

$$\mathrm{Im}\,\Pi_{had}(s) = -\frac{1}{6s}\int\sum_n dR_n\,\langle\,0\,|\,J^\mu\,|\,n\,\rangle\,\langle\,n\,|\,J_\mu^\dagger\,|\,0\,\rangle = \sum_n \mathrm{Im}\,\Pi_n(s) \quad , \tag{3.4}$$

where the phase space integration has been explicitly stated [2]. A similar separation between contributions of different final hadron states in the perturbative evaluation of the two-point correlator, Eq. (3.1), would allow us to keep only the desired heavy quark cuts in the symmetric and non-symmetric correlators. Although Cutkosky rules provide a method to isolate cuts corresponding to different intermediate states at the perturbative level, some care is needed in their application.

The study of analytic properties of perturbation theory amplitudes shows that their singularities are isolated and, therefore, we can discuss each singularity of a perturbative amplitude by itself [40]. As a consequence, any one–variable dependent amplitude $F(z)$ satisfies a dispersion relation from Cauchy's theorem given by [3] :

$$F(z) = \frac{1}{2\pi i}\oint dz'\frac{F(z')}{z'-z} = \sum_n\int_{z_n}^{\infty}\frac{dz'}{2\pi i}\,\frac{[\,F(z')\,]_n}{z'-z} \quad , \tag{3.5}$$

where $[\,F(z)\,]_n$ is the discontinuity across a branch cut which starts at the point z_n and it is associated to a definite intermediate state. For the general two-point

[1] Sometimes the Adler function defined as $\partial\Pi(p^2)/\partial\ln p^2$, to get rid of the subtraction constant, is used. The choice of the regularization prescription is not relevant for our discussion here.

[2] We use $dR_n = (2\pi)^4\,\delta^4(q-\sum_{i=1}^n p_i)\,\prod_{i=1}^n dp_i$, where q is the current four–momentum and $dp_i = \frac{d^3p_i}{(2\pi)^3 2E_i}$. The $-1/(6s)$ factor in Eq. (3.4) originates from $\Pi_{had} = -g_{\mu\nu}\,\Pi_{had}^{\mu\nu}/(3s)$ and the $(1/2)$ factor from the unitarity relation.

[3] This expression also gives the residue R_i of a pole at $z = z_i$ if we interpret the discontinuity as $[\,F(z)\,]_n = 2\pi i R_i\delta(z-z_i)$.

function in Eq. (3.1), which depends on the total momentum squared p^2, we would have

$$\widehat{\Pi}_{had}(p^2) \,=\, \sum_n \, \frac{p^2}{2\pi i} \int_{s_n}^{\infty} \frac{ds}{s} \, \frac{[\,\Pi(s)\,]_n}{s \,-\, p^2 \,-\, i\epsilon} \quad , \tag{3.6}$$

where now $[\Pi(s)]_n$ provides the sum of all the cut diagrams associated to a definite intermediate state labeled n, ($n = q\bar{q}, q'\bar{q}', ggg, q\bar{q}q'\bar{q}', \ldots$). In the perturbative calculation, every discontinuity contributing to $[\Pi(s)]_n$ can be associated to a "reduced" Feynman diagram obtained by contracting internal off–shell propagators to a point and leaving internal on–shell lines untouched. Its contribution is written down following the Cutkosky rules for the graph. However the discontinuity across a specified cut in a single diagram needs not to be a pure real function in the physical region. Hence the separation between the imaginary parts coming from different final states, as stated in Eq. (3.4), does not seem to apply for individual diagrams. But from Eqs. (3.4) and (3.6) we can conclude that $[\,\Pi(s)\,]_n = 2i\,\mathrm{Im}\,\Pi_n(s)$, meaning that only the sum of all cuts corresponding to a defined intermediate state provides the physical observable, i.e. $\mathrm{Im}\,\Pi_n(s)$. Evidently, this holds at any perturbative order in α_s, and gives a prescription to isolate contributions to different quark intermediate states in the hadron two–point function. This assertion might seem obvious but it is not : A $Q\overline{Q}$ cut on the right–hand fermion loop in Fig. 3.2(a) does not provide, by itself, a pure real contribution. Only when both $Q\overline{Q}$ cuts, on the left–hand and right–hand fermion loops of Fig. 3.2(a), are added we get a term contributing to the physical observable $\mathrm{Im}\,\Pi_{n=Q\overline{Q}}$.

This last example also shows that some subsets of discontinuities of the same intermediate state give already real functions prior to the summation of all contributions at a fixed perturbative order. This is the case for the set of cuts coming from a symmetric correlator, and for the set arising from a non–symmetric correlator with currents j_q^μ, $j_{q'}^\mu$ together with its conjugate. This is easily seen if we rewrite the absorptive part corresponding to the state n, $\mathrm{Im}\,\Pi_n$, as a sum of terms arising from symmetric and from non–symmetric correlators:

$$\begin{aligned}\mathrm{Im}\,\Pi_n(s) = -\frac{1}{6s} \int dR_n \Bigg[\sum_q \langle\, 0 \,|\, j_q^\mu \,|\, n \,\rangle \, \langle\, n \,|\, j_{q,\mu}^\dagger \,|\, 0 \,\rangle \\ + \sum_{m_q < m_{q'}} \Big(\langle\, 0 \,|\, j_q^\mu \,|\, n \,\rangle \, \langle\, n \,|\, j_{q',\mu}^\dagger \,|\, 0 \,\rangle \,+\, \langle\, 0 \,|\, j_{q'}^\mu \,|\, n \,\rangle \, \langle\, n \,|\, j_{q,\mu}^\dagger \,|\, 0 \,\rangle \Big) \Bigg] .\end{aligned} \tag{3.7}$$

The first term in the r.h.s. of Eq. (3.7) represents the absorptive contribution from symmetric correlators, and the perturbative expansion of each one, following Cutkosky rules, is clearly real. In the case of interest, $n \equiv [Q\overline{Q}]$ [4], this term contains the usual heavy quark spectral density built from heavy quark currents, $\Pi_{Q\overline{Q}}$, and $[Q\overline{Q}]$ production through light quark currents correlators. The second and third terms in Eq. (3.7) are conjugate to each other, so their sum also gives a pure real

[4]Brackets $[Q\overline{Q}]$ are short for any hadron state containing at least a $Q\overline{Q}$ pair and, possibly, light quarks and gluons too.

number. In terms of diagrams, this means that to extract the desired absorptive part from non-symmetric correlators we need to add to the cut of a diagram the corresponding one in the conjugated diagram (see Fig. 3.1(a); the discontinuity obtained from the same diagram with quark q and quark Q lines interchanged should be added up to get a real contribution).

3.3 Phenomenology vs theoretical input in heavy quark sum rules

The analysis above shows that a clear control can be enforced on the perturbative side of the sum rules in order to include or exclude specific contributions. However while there is no doubt about the observable that provides $\mathrm{Im}\,\Pi_{had} \propto \sigma(e^+e^- \to hadrons)$ when an exclusive hadron sector (like, for example, heavy quark production) is specified, it is clear that the matching between the perturbative and the phenomenological side includes incertitudes related with the content and definition of the final state.

Heavy quark sum rules [41] have been successful in providing information on the heavy quark parameters. In short they make use of global quark–hadron duality that translates into the ansatz on the vector correlator $\Pi_{[Q\overline{Q}]}(s)$:

$$\int_{s_0}^{\infty} ds\, \frac{\mathrm{Im}\,\Pi^{phen}_{[Q\overline{Q}]}(s)}{s^n} \;\simeq\; \int_{4M^2}^{\infty} ds\, \frac{\mathrm{Im}\,\Pi^{pert}_{[Q\overline{Q}]}(s)}{s^n} \;+\; \ldots\,, \tag{3.8}$$

where $\mathrm{Im}\,\Pi^{phen}_{[Q\overline{Q}]}(s)$ on the l.h.s. gives the phenomenological information on heavy quark production and it is related with the cross–section of vector current production of hadrons containing Q–flavoured states. On the r.h.s. $\mathrm{Im}\,\Pi^{pert}_{[Q\overline{Q}]}(s)$ is the QCD perturbative contribution to the correlator, and in the lower limit of integration M is usually taken as the pole mass of the heavy quark. Finally the dots on the r.h.s. are short for non–perturbative (the gluon condensate essentially) contributions and possible Coulomb–like bound states coming from non–relativistic resummations in $\Pi^{pert}_{[Q\overline{Q}]}$ below threshold. These last two features are not relevant for the discussion here and have to be implemented on our results without modification.

To a definite perturbative order in α_s, $\mathrm{Im}\,\Pi^{pert}_{[Q\overline{Q}]}(s)$ includes all the absorptive contributions to the correlator that provide $[Q\overline{Q}]$ production. Notice that this is not the same that the absorptive $Q\overline{Q}$ contribution of the heavy–quark current correlator $\Pi_{Q\overline{Q}}$, as it is usually assumed. The total experimental cross section $\sigma(e^+e^- \to hadrons)$ can be split into two disjoint quantities : the cross section for producing hadrons with Q–flavoured states, and the production of hadrons with no Q–flavoured components. If the experimental set up was accurate enough to classify events into one of these two clusters, the first class would be the required ingredient for the phenomenological part of the heavy quark sum rule. However this separation, implemented in the theoretical side within perturbative QCD, is rather involved.

Up to $\mathcal{O}(\alpha_s^2)$ there has not been any doubt, in the literature, that contributions to this side arise wholly from $Q\overline{Q}$ cuts in the heavy quark correlator $\Pi_{Q\overline{Q}}$. The physical picture behind this assertion relies in the assumption of factorization between hard and soft regions in the quark production process and subsequent hadronization. The hard region described with perturbative QCD entails the production of the pair of heavy quarks, and the soft part of the interaction is responsible for the observed final hadron content. Although possible, annihilation of the partonic state $Q\overline{Q}$ due to the later interaction is very unlikely, as jets arising from the short distance interaction fly apart before long–distance effects become essential. Consequently, each jet hadronizes to a content of Q–flavoured states with unit probability. As local duality is implicitly invoked, this picture is assumed to hold at sufficient high energies; hence perturbative corrections to the hard part are successively included through the heavy quark currents correlator. We claim, though, that similar $Q\overline{Q}$ cuts are present in non–symmetric correlators, starting at $\mathcal{O}(\alpha_s^3)$, as the one shown in Fig. 3.1(a), where the left hand part of the cut diagram is a genuine production of $Q\overline{Q}$ states triggered by virtual light quarks. If the use of heavy quark sum rules up to this order is considered, the inclusion of these terms of the correlator of a heavy and a light quark currents should be taken into account. According to our conclusion in the last section, once the discontinuity provided by Fig. 3.1(a) is known, it has to be added to $\mathrm{Im}\,\Pi^{pert}_{[Q\overline{Q}]}(s)$.

Other extra $Q\overline{Q}$ cuts, i.e. not contained in $\Pi_{Q\overline{Q}}$, arise even at $\mathcal{O}(\alpha_s^2)$ as the diagram of Fig. 3.1(b). In this case the $Q\overline{Q}$ pair is produced through the splitting of a hard gluon radiated off a pair of light quarks. Whether this cut should be accounted for or not in the theoretical side depends crucially on which is the content and the configuration of the reconstructed final state in the experimental data, as the physical picture outlined above for pure $Q\overline{Q}$ cuts does not apply so clearly for $Q\overline{Q}q\overline{q}$ discontinuities. We will come back to this point at the end of section 3.4. In addition a discussion about other possible contributing cuts should arise. The case of the three–gluon discontinuity is postponed to section 3.5.

In the following we will discuss, in turn, the inclusion of heavy quark radiation by light quarks and the infrared massless discontinuities noticed by Groote and Pivovarov. We will provide specific solutions along the lines put forward in sections 3.2 and 3.3.

3.4 Heavy quark radiation

Starting at $\mathcal{O}(\alpha_s^2)$, symmetric correlators built from light quark currents include four fermion cuts with a heavy quark pair radiated off the light quarks as shown in Fig. 3.1(b) (two additional diagrams, one with the two gluons attached to the lower light fermion line, and the other with one gluon attached to each light fermion line, should be considered too). The sum of all these four fermion absorptive parts in the three-loop diagrams with massless light quarks currents has been calculated in

Ref. [42], and can be cast into the following form [5] :

$$12\pi\,\mathrm{Im}\,\Pi_{q\bar{q}Q\overline{Q}}(s) \;=\; R_{q\bar{q}Q\overline{Q}} \;\equiv\; N_c\,(\sum_{i=u,d,s} Q_i^2)\,C_8\left(\frac{\alpha_s}{\pi}\right)^2 \int_{4M^2}^{s} \frac{ds'}{s'}\,R(s')\,F(s'/s) \quad , \tag{3.9}$$

with

$$\begin{aligned} F(x) \;&=\; \frac{1}{6}\Big\{(1+x)^2\ln^2 x + (3+4x+3x^2)\ln x + 5(1-x^2) \\ &\qquad -4(1+x)^2\left[\mathrm{Li}_2(-x) + \ln(1+x)\ln x + \frac{\pi^2}{12}\right]\Big\} \quad . \end{aligned} \tag{3.10}$$

The function $F(s'/s)$ gives the rate for the decay of a vector boson of mass $\sqrt{s}$ into a vector boson of mass $\sqrt{s'}$ plus a pair of massless fermions ($q\overline{q}$). The spectral density $R(s) = \beta(3-\beta^2)/2$ (at lowest order) is the normalized cross section for the production of a pair of fermions with unit charge through a vector boson; here $\beta = \sqrt{1-4M^2/s}$ is the velocity of the produced heavy quarks. The integral can be solved analytically in this case and the result is found in Ref. [42]. Note that the heavy quark pair is created in a colour octet state, and the factor

$$C_8 = \frac{1}{N_c}\,\mathrm{Tr}\Big(\frac{\lambda^a}{2}\frac{\lambda^b}{2}\Big)\,\mathrm{Tr}\Big(\frac{\lambda^a}{2}\frac{\lambda^b}{2}\Big) \;=\; \frac{2}{3}$$

retains this colour structure. It is interesting to compare the contribution from $R_{q\bar{q}Q\overline{Q}}$ with the $\mathcal{O}(\alpha_s^2)$ contributions to $R_{Q\overline{Q}}$ (i.e. to the spectral density of the heavy quark correlator). Note that in the high energy limit there is no difference between the diagram shown in Fig. 3.1(b) and the same one with Q and q lines interchanged or with $q = Q$, both of them being included in $\Pi_{Q\bar{Q}}$. Differences arise because the heavy quark currents correlator, $\Pi_{Q\overline{Q}}$, also accounts for two heavy quark cuts where the internal (light or heavy) quark loop represents a virtual correction to the electromagnetic current.

We have written Eq. (3.9) in terms of a general $R(s)$ function in the integrand because it allow us to introduce in a straightforward way final state interactions between the heavy quark pair. In particular, we know that close to threshold the Coulomb interaction between the heavy quark pair dominates the dynamics. Resummation of leading terms $\sim (\alpha_s/\beta)^n$ becomes mandatory, and gives rise to the well known Sommerfeld factor multiplying the cross section:

$$R^{thr}(s) = R(s) \times \frac{C\pi\alpha_s/\beta}{1-\exp(-C\pi\alpha_s/\beta)} \quad . \tag{3.11}$$

The colour factor C appears in the Coulomb QCD potential and its value depends on the relative colour state of the quark pair. For singlet states $C = C_F$, and the potential is attractive, increasing the cross section at threshold. This is the case of

[5] Notice that our definition of $R_{q\bar{q}Q\overline{Q}}$ differs from the one in Ref. [42].

heavy quark production in e^+e^- collisions. However, in our case the heavy quark pair is produced through the splitting of a gluon. The Coulomb potential becomes repulsive between quarks in a colour octet state, $C = C_F - C_A/2 = -1/(2N_c)$, and the Sommerfeld factor at low velocities then reads

$$\frac{-\pi\alpha_s/6\beta}{1-\exp(\pi\alpha_s/6\beta)} \stackrel{\beta\to 0}{\Longrightarrow} \frac{\pi\alpha_s}{6\beta}\, e^{-\frac{\pi\alpha_s}{6\beta}} \quad ,$$

causing the cross section to decrease near threshold even faster than β, the phase-space velocity in $R(s)$. The production of heavy quarks radiated off massless quarks through a virtual gluon is then very much suppressed in the threshold region. However, as mentioned above, high energy quark lines can be considered massless and the contribution from this diagram is numerically equal to the same one with Q and q lines interchanged.

The inclusion in $\mathrm{Im}\Pi^{pert}_{[Q\overline{Q}]}(s)$ of four–fermion cuts coming from light–quark correlators is possible because we have shown in section 3.2 how to discern and extract these pieces. As discussed before, the procedure depends crucially on the definition of the observable information input in the sum rule, and consistence between the theoretical and phenomenological parts is required. Let us come back to the discussion of section 3.3. There it was argued why perturbative $Q\overline{Q}$ cuts are thought to reproduce the phenomenology of two jet events. Notice that, in heavy quark radiation from light quarks, the signature of the event is likely to be a 3–jet configuration where one of the jets is generated from a gluon. If heavy flavour components are to be found in this jet, the diagram of Fig. 3.1(b) would certainly be needed to account for these events in the theoretical side. However the heavy partons in this jet are not as energetic as in a pure $Q\overline{Q}$ production and, consequently, the proposed factorization between long and short distance effects may not longer apply, allowing for an interference between both regimes. In this case we cannot argue that these kind of cut diagrams would result in a final state with Q–flavoured hadrons with unit probability, although we may impose kinematical constraints to reduce uncertainties in both the experimental reconstruction of data and theoretical cross section of these $Q\overline{Q}q\overline{q}$ states. This issue is the source of a recent discussion in the literature related with the secondary production of $b\bar{b}$ through gluon splitting [42, 43].

3.5 Massless contribution to heavy quark sum rules

Until present the evaluation of the perturbative two–point correlation function $\Pi^{pert}(q^2)$ (in this section we will denote the heavy quark currents correlator by $\Pi(q^2)$) has only been carried out completely, with massive quarks, up to $\mathcal{O}(\alpha_s^2)$ [44] and the sum rules procedure, given by Eq. (3.8), has been termed consistent and effective in its task because the first branch point is set at the massive two–particle threshold. However Groote and Pivovarov have pointed out [37] that at $\mathcal{O}(\alpha_s^3)$ there is a contribution to the correlator which contains a three–gluon massless intermediate state (see Fig. 3.2(a)). Its absorptive part starts at zero energy and, therefore,

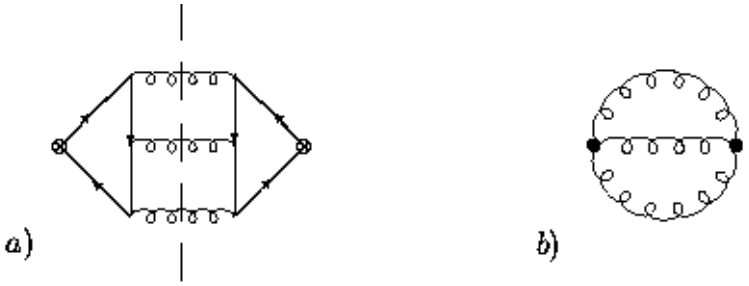

Figure 3.2: *(a) $\mathcal{O}(\alpha_s^3)$ diagram contributing to the vacuum polarization function of the heavy quark current (the vertical dashed line indicates the massless cut). (b) "Effective" diagram obtained by integrating out the fermion loops. It also has the topological structure of the "reduced" diagram that determines the massless cut singularity.*

Eq. (3.8) is no longer correct because on the r.h.s. there is a discontinuity starting at $s = 0$. Moreover those authors have also warned about the fact that, at this perturbative order, the massless intermediate state invalidates the definition of the moments $\mathcal{M}_n$ for $n \geq 4$ because they become singular. Let us collect their reasoning.

The perturbative contribution given by the diagram in Fig. 3.2(a) has been calculated at small q^2 ($q^2 \ll M^2$) in Ref. [37]. In this limit the quark triangle loop can be integrated out and it ends up in the diagram in Fig. 3.2(b) generated by an induced effective current describing the interaction of the vector current with three gluons,

$$J^\mu \,=\, -\frac{\pi}{180 M^4}\left(\frac{\alpha_s}{\pi}\right)^{\frac{3}{2}}\,(5\,\partial_\nu \mathcal{O}_1^{\mu\nu} \,+\, 14\,\partial_\nu \mathcal{O}_2^{\mu\nu})\;, \tag{3.12}$$

with

$$\begin{aligned} \mathcal{O}_1^{\mu\nu} &= d_{abc}\, G_a^{\mu\nu} G_b^{\alpha\beta} G_{\alpha\beta}^c \;\;, \\ \mathcal{O}_2^{\mu\nu} &= d_{abc}\, G_a^{\mu\alpha} G_{\alpha\beta}^b G_c^{\beta\nu} \;\;, \end{aligned} \tag{3.13}$$

where $G_a^{\mu\nu}$ is the gluon strength field tensor. The effective current in the QED case ($G_a^{\mu\nu} \to F^{\mu\nu}, \alpha_s \to \alpha_{em}, d_{abc} \to 1$) can be easily identified from the lowest order Euler-Heisenberg Lagrangian (see Ref. [38]).

The correlator of the induced current (3.12) is then evaluated in the configuration space giving :

$$\langle 0|T\, J_\mu(x)\; J_\nu^\dagger(0)\,|0\rangle \,=\, -\frac{34}{2025\pi^4 M^8}\left(\frac{\alpha_s}{\pi}\right)^3 d_{abc}d_{abc}\,\left(\partial_\mu\partial_\nu - g_{\mu\nu}\partial^2\right)\frac{1}{x^{12}}\,. \tag{3.14}$$

In momentum space we need to perform the Fourier transform of Eq. (3.14). Following the differential regularization procedure [45], which works directly in configuration space, the result for the vacuum polarization contribution of the diagram in

Fig. 3.2(b) at small q^2 reads

$$\Pi_{\mu\nu}(q) \;=\; \frac{17}{2916000\pi^2}\, d_{abc}d_{abc} \left(\frac{\alpha_s}{\pi}\right)^3 (q_\mu q_\nu - q^2 g_{\mu\nu}) \left(\frac{q^2}{4M^2}\right)^4 \ln\left(\frac{\mu^2}{-q^2}\right) + \mathcal{O}\Big[\Big(\frac{q^2}{M^2}\Big)^5\Big] , \tag{3.15}$$

with μ the renormalization point in this scheme, and $d_{abc}d_{abc} = 40/3$.

As noticed by Groote and Pivovarov [37], moments associated to the diagram in Fig. 3.2(b) are not defined if $n \geq 4$. Indeed differentiating Eq. (3.15) four times, at $q^2 \approx 0$, we get:

$$\frac{1}{4!}\left(\frac{d}{dq^2}\right)^4 \Pi(q^2)|_{q^2\approx 0} = \frac{17}{218700\pi^2}\left(\frac{\alpha_s}{\pi}\right)^3 \left(\frac{1}{4M^2}\right)^4 \left[\ln\left(\frac{\mu^2}{-q^2}\right) - \frac{25}{12}\right] + \mathcal{O}\Big[\frac{q^2}{M^{10}}\Big] \;\; , \tag{3.16}$$

whose real part clearly diverges if we set $q^2 = 0$. Larger n moments are also infrared divergent, and so the authors of Ref. [37] conclude that the standard sum rule analysis must limit the accuracy of theoretical calculations for the $n \geq 4$ moments to the $\mathcal{O}(\alpha_s^2)$ order of perturbation theory. This is, essentially, the conclusion of Ref. [37].

An infrared safe redefinition of the moments, to cure the latter problem, has been provided in Ref. [38]; it consists in evaluating the moments at an Euclidean point $q^2 = -s_E$, $s_E > 0$, thus avoiding the singular behaviour. This solution, as explained by the authors of that reference, is rather ill–conditioned from the phenomenological side though. Nevertheless the fault in Eq. (3.8) due to the massless threshold still represents a problem because even if, up to $\mathcal{O}(\alpha_s^3)$, we substitute the dispersion relation by

$$\widehat{\Pi}^{pert}(q^2) \;=\; \frac{q^2}{\pi}\int_{4M^2}^{\infty} \frac{ds}{s}\, \frac{\mathrm{Im}\,\Pi^{pert}_{Q\overline{Q}}(s)}{s - q^2 - i\epsilon} \;+\; \frac{q^2}{\pi}\int_0^{\infty} \frac{ds}{s}\, \frac{\mathrm{Im}\,\Pi_{3g}(s)}{s - q^2 - i\epsilon} \quad , \tag{3.17}$$

(where $\mathrm{Im}\,\Pi^{pert}_{Q\overline{Q}}(s)$ includes discontinuities starting at $s = 4M^2$), the spectral function $\mathrm{Im}\,\Pi_{3g}(s)$ associated to the cut in Fig. 3.2(a) would hardly be implemented phenomenologically as gluons hadronize to both heavy and light quark pairs. We wish to provide a bypass to recover the balance between the right-hand and left-hand parts of Eq. (3.17). We will now see that if one does not insist in using full vacuum polarization for the sum rule analysis there is a way to overcome this infrared problem.

In the heavy quark correlator the discontinuity across the three–gluon cut gives a contribution to the spectral function that is unequivocally real :

$$\frac{1}{2i}\,[\,\Pi(s)\,]_{3g} \;=\; \mathrm{Im}\,\Pi_{3g}(s) \;=\; -\,\frac{1}{6s}\int dR_{3g}\,\langle\,0\,|\,j^\mu\,|\,3\,g\,\rangle\,\langle\,3\,g\,|\,j^\dagger_\mu\,|\,0\,\rangle \;\; , \tag{3.18}$$

from which the dispersive part can be evaluated independently of the $Q\overline{Q}$ cuts. Accordingly we conclude that we can identify and isolate the troublesome massless cut contribution to the two–point function. Indeed Eqs. (3.6) and (3.18) justify our previous Eq. (3.17).

Let us go back then to Eq. (3.17). All the difficulty with the phenomenological application of the sum rules is now the fact that the contribution from the three–gluon cut is contained in both sides of the equality. This intermediate state hadronizes completely into hadrons with a content of light and/or heavy quarks indistinctly. It is conspicuous that if we could disentangle the heavy quark hadronization, $3g \to Q\overline{Q}$, we should include only this piece into the sum rule. Then the singularity at $q^2 = 0$ would disappear because heavy quarks are produced starting at $q^2 = 4M^2$. However there is no way to sort out light and heavy quark production off three gluons and, therefore, if we extract this contribution from the heavy quark sum rules we are introducing an incertitude in the procedure because we make sure that there is no light quark hadronization but we miss the heavy quark production. It is easy to see that the induced error is small, due to the fact that three gluons hadronize mostly to light hadrons. On one side, in the very high energy region and following perturbative QCD with $N_F = 4$, we have only a $1/4 = 25\,\%$ probability of finding a specified pair of heavy quarks produced. And this is a generous upper limit because when we go down in energy, phase space restrictions severely reduce the counting of heavy quarks. Hence we estimate that excluding the three–gluon cut we introduce a tiny very few percent error in the sum rules procedure.

Thus we propose an *infrared safe* definition of the moments by the trivial subtraction :

$$\widetilde{\Pi}^{pert}(q^2) \;\doteq\; \widehat{\Pi}^{pert}(q^2) - \frac{q^2}{\pi}\int_0^\infty \frac{ds}{s}\,\frac{\mathrm{Im}\,\Pi_{3g}(s)}{s-q^2-i\epsilon} \;=\; \frac{q^2}{\pi}\int_{4M^2}^\infty \frac{ds}{s}\,\frac{\mathrm{Im}\,\Pi^{pert}_{Q\overline{Q}}(s)}{s-q^2-i\epsilon}\;, \tag{3.19}$$

$$\widetilde{\mathcal{M}}_n \;\doteq\; \mathcal{M}_n - \frac{1}{\pi}\int_0^\infty ds\,\frac{\mathrm{Im}\,\Pi_{3g}(s)}{s^{n+1}}\;. \tag{3.20}$$

Once we had identified $\mathrm{Im}\,\Pi_{3g}$, we could plug it in the dispersion integral of the right–hand side of Eq. (3.20) and perform such integration. Divergences contained in both this integral and $\mathcal{M}_n$ as $q^2 \to 0$ will cancel with each other if the same infrared regularization is employed in the two quantities. The intuitive choice would be a low-energy cutoff $s_0 > 0$, and Eq. (3.20) would be more precisely written as:

$$\widetilde{\mathcal{M}}_n \;\equiv\; \lim_{s_0\to 0^+}\left[\frac{1}{n!}\left(\frac{d}{dq^2}\right)^n \Pi^{pert}(q^2)|_{q^2=-s_0} \;-\; \frac{1}{\pi}\int_0^\infty \frac{ds}{s}\,\frac{\mathrm{Im}\,\Pi_{3g}(s)}{(s+s_0)^n}\right]\;, \tag{3.21}$$

where a vanishing term in the $s_0 \to 0^+$ limit has been omitted.

The evaluation of the $\mathcal{M}_n$ moments at $q^2 = 0 < 4M^2$ made sense because, up to $\mathcal{O}(\alpha_s^2)$, this point, being far away of the heavy quark production threshold, is unphysical and the moments are well defined through an analytic continuation from the high–energy region. However note that the absorptive three–gluon contribution starts at $q^2 = 0$ and perturbative QCD becomes unreliable. This introduces a further new difficulty in evaluating $\mathcal{M}_n$ moments at $q^2 = 0$, as we reach the physical

non–perturbative region. Our definition of the moments, $\widetilde{\mathcal{M}}_n$ in Eq. (3.20), skips this problem by fully eliminating the massless terms and, therefore, the final heavy quark sum rule will only involve physics at $q^2 > 4M^2$, apart from possible bound states.

Of course Eqs. (3.19) and (3.20) are meaningless unless we give a precise prescription about how to subtract the contribution of the massless cuts represented by $\mathrm{Im}\,\Pi_{3g}$. Note that even if the full $\mathcal{O}(\alpha_s^3)$ $\Pi^{pert}(s)$ was calculated we could only extract the three gluon imaginary part which starts at $s = 0$ (accompanied thus by a $\theta(s)$ function) for $s < 4M^2$. Above the heavy quark threshold, $\mathrm{Im}\,\Pi_{3g}$ and $\mathrm{Im}\,\Pi^{pert}_{Q\overline{Q}}$ would not be easy to distinguish, as mixed $\theta(s)\cdot\theta(s-4M^2)$ terms appear in the imaginary part of the vacuum polarization function. We would then encourage the strong loop practitioners to calculate first the desired absorptive parts of the two-point function and afterwards reconstruct their associated real parts, thus throwing away the massless contributions from the very beginning.

Lacking of a procedure to extract the massless absorptive part from the full result of $\Pi(q^2)$ calculated at a definite order, we should however bear in mind that beyond $\mathcal{O}(\alpha_s^2)$ complete analytical results for the heavy quark correlator will probably be out of reach and only numerical approaches may be at hand. In this sense, it would be convenient to have a method to calculate $\mathrm{Im}\,\Pi^{pert}_{Q\overline{Q}}$ only based on Feynman graphs. We have already sketched such a method in the discussion following Eq. (3.6) : we just need to sum up all the massless cut graphs to get $\mathrm{Im}\,\Pi_{3g}$, and then proceed with the dispersion integration that gives the associated dispersive part. For example, at $\mathcal{O}(\alpha_s^3)$, the only massless absorptive part comes from the three–gluon cut in the diagram of Fig. 3.2(a); let us call $\mathcal{M}^{\mu}_{3g}$ the amplitude producing three gluons from the heavy quark current at lowest order (i.e. through the quark triangle loop in Fig. 3.3). The massless contribution to the absorptive part of the correlator is then:

$$\mathrm{Im}\,\Pi_{3g}(s) = -\frac{1}{6s}\int dR_{3g}\ \mathcal{M}^{\mu}_{3g}\cdot\mathcal{M}^{*}_{3g\,\mu}\ \ , \tag{3.22}$$

with the three–gluon phase space integral defined as

$$\int dR_{3g} \equiv \frac{1}{3!}\frac{1}{(2\pi)^5}\frac{\pi^2}{4s}\int_0^s ds_1\int_0^{s-s_1} ds_2\ \ , \tag{3.23}$$

in terms of the invariants $s_1 \equiv (k_1+k_2)^2 = (q-k_3)^2$ and $s_2 \equiv (k_2+k_3)^2 = (q-k_1)^2$, and k_i being the momenta of the gluons. The real part would be obtained by integrating Eq. (3.22) :

$$\frac{s_0}{\pi}\int_0^{\infty}\frac{ds}{s}\,\frac{\mathrm{Im}\,\Pi_{3g}(s)}{s+s_0} = \frac{-s_0}{288(2\pi)^4}\int_0^{\infty}\frac{ds}{s^3(s+s_0)}\int_0^s ds_1\int_0^{s-s_1} ds_2\ \mathcal{M}^{\mu}_{3g}\cdot\mathcal{M}^{*}_{3g\,\mu}\,, \tag{3.24}$$

which, in principle, could be performed also numerically. The nth-derivative of relation (3.24) respect to s_0, in the limit $s_0 \to 0^+$, would give the infrared divergent contribution that should be subtracted from the full moments, as dictated by Eq. (3.21).

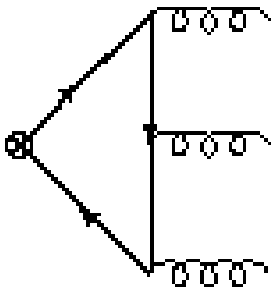

Figure 3.3: *Feynman diagram for the production of three gluons at* $\mathcal{O}(\alpha_s^3)$.

Finally, we would like to mention that using the non–relativistic expansion of the heavy quark correlator in sum rules analyses does not avoid this infrared problem, at least formally. The $\mathcal{O}(\alpha_s^3)$ diagram of Fig. 3.2 will be highly suppressed in the velocity expansion, following the non–relativistic effective field theory approach, and therefore it is not relevant in the corresponding heavy quark currents correlator. However such two–point function cannot describe the $Q\overline{Q}$ spectrum for energies far from threshold and even when higher n–moments, which strongly enhance the threshold, are used, perturbative QCD is needed in order to implement the remaining high–energy region; the diagram of Fig. 3.2 has to be accounted for to include properly this input, and its discontinuity at $s = 0$ cannot be obviated. This point is more clearly seen by noticing that, besides the resummations in (α_s/β) performed in the non–relativistic correlator, one could improve such expansion by adding the terms needed to reproduce the exact $\mathcal{O}(\alpha_s^3)$ result $\Pi(q^2)$.

3.6 Conclusions

Heavy quark sum rules, relying in global quark–hadron duality, are a compelling procedure to extract information on the theory from phenomenology. However, as higher perturbative order analyses are performed, the consistency of the method demands the inclusion of novel features. While at $\mathcal{O}(\alpha_s)$ the correlator of two heavy quark currents gives the full perturbative information, at $\mathcal{O}(\alpha_s^2)$ we have noticed that a heavy quark $Q\overline{Q}$ pair radiated from light quarks in a correlator of light quark currents should be considered. At $\mathcal{O}(\alpha_s^3)$ the complexities grow with the essential role of non–symmetric correlators. Closely related with this situation is the feature recently pointed out by Groote and Pivovarov on the uneasy problem arising from a massless three–gluon discontinuity in the heavy quark current correlator at $\mathcal{O}(\alpha_s^3)$.

We have shown that rigorous results of the general theory of singularities of perturbation theory provide all–important tools to analyse the new contributions. The inclusion or exclusion of specific discontinuities in the perturbative side is shown to be feasible and the decision involves a clear definition of the observable input on

the phenomenological side of the sum rules.

A solution for the problem pointed out by Groote and Pivovarov at $\mathcal{O}(\alpha_s^3)$ has been given. We conclude that the appropriate procedure to obtain information about the heavy quark parameters should make use of the infrared safe corrected moments, defined in Eq. (3.21), that now indeed satisfy the modified sum rule :

$$\widetilde{\mathcal{M}}_n \;=\; \frac{1}{\pi}\int_{4M^2}^{\infty} ds\, \frac{\mathrm{Im}\,\Pi^{phen}_{[Q\overline{Q}]}(s)}{s^{n+1}} \quad , \tag{3.25}$$

where the right–hand side can be extracted from the heavy quark production cross section $\sigma(e^+e^- \to [Q\overline{Q}])$. The incertitude associated to heavy quark hadronization of the three–gluon should be taken into account but it is shown to be tiny.

The analysis we have carried out is completely general, relying in the theory of singularities of perturbative theory amplitudes only, and provides a sharp tool for the future analysis of heavy quark sum rules.

The contents of this work have been published in Refs. [46, 47].

Chapter 4

Odd–intrinsic–parity Processes within R$_\chi$T

4.1 Introduction

Effective field theories of QCD have provided efficient ways to explore hadron dynamics in those regimes where we are not able to solve the full theory. Built from the same principles and symmetries which govern QCD, the effective actions put at our disposal a model-independent framework to generate the interactions between the active degrees of freedom. In the very low-energy domain, chiral perturbation theory [11, 12, 13] has achieved a remarkable success in describing the strong interactions among pseudoscalar mesons. Moving up to the 1 GeV region has been proved more difficult, as the effects of vector resonances become dominant and must be accommodated in the theory. Several works [12, 8, 48] have provided a sound procedure to include resonance states within the chiral framework, later christened Resonance Chiral Theory. This approach, however, leaves the couplings entering the effective Lagrangian unknown, as they are not fixed by the symmetry alone. One should then rely on the phenomenology or, alternatively, construct theoretical tools that could provide a meaningful way to compare the results of the effective theory with those of QCD. The pioneering work of Ref. [49] indicated that the analysis of Green's functions and form factors of QCD currents yields valuable information on the resonance sector and, at the same time, clarifies the ambiguities related to the choice of the Lorentz group representation for the resonance fields.

Recently, several authors have pushed forward this direction, either by using a Lagrangian with explicit resonance degrees of freedom [50], or within the framework of the lowest meson dominance (LMD) approximation to the large number of colours (N_C) limit of QCD [50,51,52,53,54]. In particular, the authors of Ref. [50] undertook a systematic study of several QCD three-point functions which share the property of being zero in absence of spontaneous chiral symmetry breaking for massless quarks. This common feature means that these Green's functions are free of perturbative contributions from QCD at short distances. Therefore, their OPE expansion, although formally applicable in the high-energy region, should be more reliable when

descending to energies close to the resonance region, thus supporting the idea that a smooth matching between QCD and the effective description involving resonances may exist for these functions. Under this hypothesis, it was shown in Ref. [50] that while the ansatz derived from the LMD approach automatically incorporates the right short-distance behaviour of QCD by construction, the same Green's functions as calculated with a resonance Lagrangian, in the vector-field representation, are incompatible with the OPE outcome. Thus, the $\mathcal{O}(p^6)$ low-energy constants they extract from the resonance Lagrangian differ from the estimates of the LMD ansatz. Moreover the authors put forward that these discrepancies cannot be repaired just by introducing local counterterms from the chiral Lagrangian $\mathcal{L}_\chi^{(6)}$, as it was done at $\mathcal{O}(p^4)$ in Ref. [49]. New terms with resonance fields and higher-order derivatives need to be added, at least in the vector-field representation, but the general procedure remains unknown.

The result above severely questions the usefulness of the resonance effective theory beyond the initial work of Ref. [49], that relies not only on the QCD global symmetries but also on the fact that its large–N_C limit resembles, at least qualitatively, the three colour theory [15, 16]. In addition one of the basic tenets, after the conclusions of Ref. [16], is that meson physics in the large–N_C limit is described by the tree diagrams of an effective local Lagrangian, with local vertices and local meson fields. Hence after the qualm put forward by Ref. [50] we think that this issue deserves further investigation. With this aim, we have reanalysed one of the Green's function studied in this last reference, the vector-vector-pseudoscalar three-point function, this time with the vector mesons described in terms of antisymmetric tensor fields.

The latter study requires the introduction of an odd-intrinsic-parity effective Lagrangian in the formulation of Ref. [48] containing all allowed interactions between two vector objects (currents or resonances) and one pseudoscalar meson. After a brief introduction on chiral theory, Section 4.2 of this Chapter is devoted to this subject. In Section 4.3 we evaluate the vector-vector-pseudoscalar three-point function $\langle \mathrm{VVP} \rangle$ within our effective theory at leading order in the $1/N_C$ expansion. We recall its short-distance properties, as obtained from the OPE calculation, and then we demand that the $\langle \mathrm{VVP} \rangle$ Green's function built with the effective action with unknown parameters matches the same behaviour. The set of relations among couplings derived is then tested in several intrinsic-parity-violating decays in Section 4.4. Finally, we give our conclusions.

4.2 Resonance Chiral Theory and the odd-intrinsic-parity sector

The low-energy behaviour of QCD for the light quark sector (u, d, s) is known to be ruled by the spontaneous breaking of chiral symmetry giving rise to the lightest hadron degrees of freedom, identified with the octet of pseudoscalar mesons. The corresponding effective realization of QCD describing the interaction between

the Goldstone fields is called chiral perturbation theory [11, 12, 13]. The effective Lagrangian to lowest order in derivatives, $\mathcal{O}(p^2)$, is given by :

$$\mathcal{L}_\chi^{(2)} = \frac{F^2}{4}\langle u_\mu u^\mu + \chi_+\rangle \ , \tag{4.1}$$

where

$$\begin{aligned} u_\mu &= i[u^\dagger(\partial_\mu - ir_\mu)u - u(\partial_\mu - i\ell_\mu)u^\dagger] \ , \\ \chi_\pm &= u^\dagger\chi u^\dagger \pm u\chi^\dagger u \quad , \quad \chi = 2B_0(s+ip) \ . \end{aligned} \tag{4.2}$$

The unitary matrix in flavour space

$$u(\phi) = \exp\left\{i\frac{\Phi}{\sqrt{2}\,F}\right\} \quad , \tag{4.3}$$

is a (non-linear) parameterization of the Goldstone octet of fields :

$$\Phi(x) \equiv \frac{\vec{\lambda}}{\sqrt{2}}\,\vec{\phi} = \begin{pmatrix} \frac{1}{\sqrt{2}}\pi^0 + \frac{1}{\sqrt{6}}\eta_8 & \pi^+ & K^+ \\ \pi^- & -\frac{1}{\sqrt{2}}\pi^0 + \frac{1}{\sqrt{6}}\eta_8 & K^0 \\ K^- & \bar{K}^0 & -\frac{2}{\sqrt{6}}\eta_8 \end{pmatrix} . \tag{4.4}$$

The external hermitian matrix fields r_μ, ℓ_μ, s and p promote the global $\mathrm{SU(3)_R}\times\mathrm{SU(3)_L}$ symmetry of the Lagrangian to a local one, and generate Green functions of quark currents by taking appropriate functional derivatives. Interactions with electroweak bosons can be accommodated through the vector $v_\mu = (r_\mu + \ell_\mu)/2$ and axial-vector $a_\mu = (r_\mu - \ell_\mu)/2$ fields, while the scalar field s provides a very convenient way of incorporating explicit chiral symmetry breaking through the quark masses

$$s = \mathcal{M} + \ldots \quad , \quad \mathcal{M} = diag(m_u, m_d, m_s) \ .$$

The generating functional $Z[v, a, s, p]$ calculated in terms of the external sources is manifestly chiral invariant, but the physically interesting Green functions (with broken chiral symmetry) are obtained by taking a particular direction in flavour space through functional differentiation. Finally, the $\mathcal{L}_\chi^{(2)}$ Lagrangian is settled by fixing the unknown F and B_0 parameters from the phenomenology : $F \simeq F_\pi \simeq 92.4\,\mathrm{MeV}$ is the decay constant of the charged pion and $B_0F^2 = -\langle 0|\bar{\psi}\psi|0\rangle_0$ in the chiral limit.

Spectroscopy reveals the existence of vector meson resonances as we approach the 1 GeV energy region. These can be classified in $\mathrm{SU(3)_V}$ octets and must be included as explicit degrees of freedom in order to describe hadron dynamics [8]. At the lowest order in derivatives, the chiral invariant Lagrangian for the vector mesons and their interaction with Goldstone fields reads [48], in the antisymmetric tensor formulation,

$$\mathcal{L}_\mathrm{V} \ = \ \mathcal{L}_\mathrm{Kin}(V) + \mathcal{L}_2(V)\,, \tag{4.5}$$

with kinetic terms

$$\mathcal{L}_{\rm Kin}(V) = -\frac{1}{2}\,\langle \nabla^\lambda V_{\lambda\mu}\nabla_\nu V^{\nu\mu} - \frac{M_V^2}{2}\,V_{\mu\nu}V^{\mu\nu}\rangle\,, \tag{4.6}$$

where M_V is the mass of the lowest octet of vector resonances under $\mathrm{SU(3)_V}$, and the covariant derivative

$$\nabla_\mu V = \partial_\mu V + [\Gamma_\mu, V] \quad , \quad \Gamma_\mu = \frac{1}{2}\{u^\dagger(\partial_\mu - ir_\mu)u + u(\partial_\mu - i\ell_\mu)u^\dagger\}\,,$$

is defined in such a way that $\nabla_\mu V$ also transforms as an octet under the action of the group. For the interaction Lagrangian $\mathcal{L}_2(V)$ we have

$$\mathcal{L}_2(V) = \frac{F_V}{2\sqrt{2}}\,\langle V_{\mu\nu} f_+^{\mu\nu}\rangle + \frac{iG_V}{\sqrt{2}}\,\langle V_{\mu\nu}u^\mu u^\nu\rangle\,, \tag{4.7}$$

$$f_\pm^{\mu\nu} = uF_L^{\mu\nu}u^\dagger \pm u^\dagger F_R^{\mu\nu}u\,,$$

with $F_{L,R}^{\mu\nu}$ the field strength tensors of the left and right external sources ℓ_μ and r_μ, and F_V, G_V are real couplings. The octet fields are written in the usual matrix notation

$$V_{\mu\nu} = \frac{\vec{\lambda}}{\sqrt{2}}\,\vec{V}_{\mu\nu} = \begin{pmatrix} \frac{1}{\sqrt{2}}\rho^0 + \frac{1}{\sqrt{6}}\omega_8 & \rho^+ & K^{*+} \\ \rho^- & -\frac{1}{\sqrt{2}}\rho^0 + \frac{1}{\sqrt{6}}\omega_8 & K^{*0} \\ K^{*-} & \bar{K}^{*0} & -\frac{2}{\sqrt{6}}\omega_8 \end{pmatrix}_{\mu\nu}\,. \tag{4.8}$$

The chiral couplings contained in $\mathcal{L}_2(V)$ only concern the even–intrinsic–parity sector. In Ref. [49] it was shown that, up to $\mathcal{O}(p^4)$ in the chiral counting, the effective Lagrangian $\mathcal{L}_{\chi V} \equiv \mathcal{L}_\chi^{(2)} + \mathcal{L}_{\rm V}$ is enough to satisfy the short-distance QCD constraints where vector resonances play a significant role. For the odd–intrinsic–parity sector, three different sources might be considered : (i) the Wess-Zumino action [55], which is $\mathcal{O}(p^4)$ and fulfills the chiral anomaly, (ii) chiral invariant $\epsilon_{\mu\nu\rho\sigma}$ terms involving vector mesons which, upon integration, will start to contribute at $\mathcal{O}(p^6)$ in the antisymmetric formulation, and (iii) the relevant operators in the $\mathcal{O}(p^6)$ Goldstone chiral Lagrangian [56, 57]. All of them may contribute to the $\langle$VVP$\rangle$ Green's function.

The chiral anomaly is driven by the Wess-Zumino action $Z_{\rm WZ}[v,a]$. We do not recall its functional here and address the reader to Ref. [58] for the explicit expression. On the other side effective odd-intrinsic-parity Lagrangians with vector resonances have been previously considered in the literature in order to study the equivalence of different vector resonance models to reproduce the one-loop divergences of the Wess-Zumino action [59], in the context of the extended Nambu-Jona-Lasinio model [60], or to estimate the low-energy constants of the $\mathcal{O}(p^6)$ Goldstone chiral Lagrangian [50]. Within the antisymmetric formalism, we shall build an independent set of odd-intrinsic-parity operators which comprise all possible vertices involving two vector resonances and one pseudoscalar (VVP), and vertices with one vector resonance and one external vector source plus one pseudoscalar (VJP).

The building blocks for these terms are the ones defined above, which share the right properties under chiral transformations. Besides, the terms must satisfy Lorentz, P and C invariance. Other useful relations to reduce the number of independent terms and construct the basis are detailed in the Appendix. Our basis reads [1]:

VJP terms

$$\begin{aligned}
\mathcal{O}^1_{\rm VJP} &= \epsilon_{\mu\nu\rho\sigma}\,\langle\,\{V^{\mu\nu},f_+^{\rho\alpha}\}\nabla_\alpha u^\sigma\,\rangle\ , \\
\mathcal{O}^2_{\rm VJP} &= \epsilon_{\mu\nu\rho\sigma}\,\langle\,\{V^{\mu\alpha},f_+^{\rho\sigma}\}\nabla_\alpha u^\nu\,\rangle\ , \\
\mathcal{O}^3_{\rm VJP} &= i\,\epsilon_{\mu\nu\rho\sigma}\,\langle\,\{V^{\mu\nu},f_+^{\rho\sigma}\}\,\chi_-\,\rangle\ , \\
\mathcal{O}^4_{\rm VJP} &= i\,\epsilon_{\mu\nu\rho\sigma}\,\langle\,V^{\mu\nu}\,[\,f_-^{\rho\sigma},\chi_+]\,\rangle\ , \\
\mathcal{O}^5_{\rm VJP} &= \epsilon_{\mu\nu\rho\sigma}\,\langle\,\{\nabla_\alpha V^{\mu\nu},f_+^{\rho\alpha}\}u^\sigma\,\rangle\ , \\
\mathcal{O}^6_{\rm VJP} &= \epsilon_{\mu\nu\rho\sigma}\,\langle\,\{\nabla_\alpha V^{\mu\alpha},f_+^{\rho\sigma}\}u^\nu\,\rangle\ , \\
\mathcal{O}^7_{\rm VJP} &= \epsilon_{\mu\nu\rho\sigma}\,\langle\,\{\nabla^\sigma V^{\mu\nu},f_+^{\rho\alpha}\}u_\alpha\,\rangle\ , \qquad (4.9)
\end{aligned}$$

VVP terms

$$\begin{aligned}
\mathcal{O}^1_{\rm VVP} &= \epsilon_{\mu\nu\rho\sigma}\,\langle\,\{V^{\mu\nu},V^{\rho\alpha}\}\nabla_\alpha u^\sigma\,\rangle\ , \\
\mathcal{O}^2_{\rm VVP} &= i\,\epsilon_{\mu\nu\rho\sigma}\,\langle\,\{V^{\mu\nu},V^{\rho\sigma}\}\,\chi_-\,\rangle\ , \\
\mathcal{O}^3_{\rm VVP} &= \epsilon_{\mu\nu\rho\sigma}\,\langle\,\{\nabla_\alpha V^{\mu\nu},V^{\rho\alpha}\}u^\sigma\,\rangle\ , \\
\mathcal{O}^4_{\rm VVP} &= \epsilon_{\mu\nu\rho\sigma}\,\langle\,\{\nabla^\sigma V^{\mu\nu},V^{\rho\alpha}\}u_\alpha\,\rangle\ . \qquad (4.10)
\end{aligned}$$

The operators with $\chi_\pm$ break SU(3)$_{\rm V}$ symmetry when distinct quark masses are introduced through the external scalar field $s=\mathcal{M}+\ldots$. However, only the pseudoscalar source p in $\mathcal{O}^3_{\rm VJP}$ and $\mathcal{O}^2_{\rm VVP}$ will enter our calculation of the Green's function, while $\mathcal{O}^4_{\rm VJP}$ will not contribute at all and has just been included in the VJP basis for completeness.

The authors of Ref. [59] also built the VVP operators in the tensor-field representation and further constrained the number of independent operators to three by applying the equation of motion of the pseudoscalar field at lowest order; some care is needed in our case, as particles inside Green's functions are not on their mass shell. The resonance Lagrangian for the odd–intrinsic–parity sector will thus be defined as

$$\mathcal{L}_V^{\rm odd} = \mathcal{L}_{\rm VJP}+\mathcal{L}_{\rm VVP}\ ,$$

$$\mathcal{L}_{\rm VJP}=\sum_{a=1}^{7}\frac{c_a}{M_V}\,\mathcal{O}^a_{\rm VJP}\ ,\qquad \mathcal{L}_{\rm VVP}=\sum_{a=1}^{4}d_a\,\mathcal{O}^a_{\rm VVP}\ . \qquad (4.11)$$

[1] We use the convention $\epsilon_{0123}=+1$ for the Levi-Civita tensor $\epsilon_{\mu\nu\rho\sigma}$ throughout this work

The octet mass M_V has been introduced in $\mathcal{L}_{\rm VJP}$ to define dimensionless c_a couplings. We stress that the set defined above is a complete basis for constructing vertices with only one-pseudoscalar; for a larger number of pseudoscalars additional operators may emerge.

Finally we have to pay attention to the $\mathcal{O}(p^6)$ Goldstone chiral Lagrangian. Two operators may contribute at leading order in the $1/N_C$ expansion to the $\langle {\rm VVP}\rangle$ Green's function :

$$\mathcal{L}^{(6)}_{\rm odd} \,=\, i\,\epsilon_{\mu\nu\alpha\beta}\Big\{\, t_1\,\langle\,\chi_-\,f_+^{\mu\nu}\,f_+^{\alpha\beta}\,\rangle - i\,t_2\,\langle\nabla_\lambda\,f_+^{\lambda\mu}\{f_+^{\alpha\beta},u^\nu\}\,\rangle\,\Big\}\quad . \tag{4.12}$$

The t_i couplings are in principle unknown [2]. These operators belong both to the effective theory where resonances are still active degrees of freedom and to the theory where those have been integrated out. Hence in the latter case the couplings can be split as $t_i = t_i^R + \hat{t}_i$ where t_i^R is generated by the integration of resonances and $\hat{t}_i$ is a remainder that may survive in the effective theory where resonances are still active. Vector and pseudoscalar resonances can contribute, in principle, to t_1^R, though the latter are suppressed because of their higher masses. Therefore we will consider that $t_1^R \simeq t_1^V$. Meanwhile t_2 has only vector resonance contributions and then $t_2^R = t_2^V$. Indeed by integrating out the vector mesons in $\mathcal{L}_{\rm V} + \mathcal{L}^{\rm odd}_{\rm V}$ we obtain :

$$\begin{aligned} t_1^V &= -\frac{F_V}{4\sqrt{2}M_V^3}\,[c_1+c_2+8c_3-c_5] + \frac{F_V^2}{8M_V^4}\,[\,d_1+8d_2-d_3\,]\;,\\ t_2^V &= -\frac{F_V}{\sqrt{2}M_V^3}\,(c_5-c_6) + \frac{F_V^2}{2M_V^4}\,d_3\,. \end{aligned} \tag{4.13}$$

On the other side the successful resonance saturation of the chiral Lagrangian couplings at $\mathcal{O}(p^4)$ [48] might translate naturally to $\mathcal{O}(p^6)$ couplings too, implying that $\hat{t}_i$ could be neglected. We will attach to this point and will assume that the t_i couplings are generated completely through integration of vector resonances. Accordingly we should not include $\mathcal{L}^{(6)}_{\rm odd}$ in our evaluation of the Green's function in order not to double count degrees of freedom. We shall come back to this discussion in the next Section.

In summary we will proceed in the following by considering the relevant effective resonance theory (ERT) given by :

$$Z_{\rm ERT}[v,a,s,p] \;=\; Z_{\rm WZ}[v,a] \;+\; Z^{\rm odd}_{\rm V\chi}[v,a,s,p]\quad , \tag{4.14}$$

where $Z^{\rm odd}_{\rm V\chi}[v,a,s,p]$ is generated by $\mathcal{L}^{(2)}_\chi$ in Eq. (4.1), $\mathcal{L}_{\rm V}$ in Eq. (4.5) and $\mathcal{L}^{\rm odd}_V$ in Eq. (4.11).

[2] In the notation of Ref. [57] $t_1 = C_7^W$ and $t_2 = -C_{22}^W$.

4.3 Short-distance information on the odd-intrinsic-parity couplings

The construction of an effective field theory that satisfies the symmetry requirements of QCD is a model-independent procedure to accomplish the low-energy properties of the theory without missing essential dynamics. The price to pay for the universality of such approach is an increasing number of (a priori) unknown low-energy constants as we tend to improve the accuracy of our calculations, which eventually reflects in a loss of predictive power. Comparison with data has been a fruitful way to extract the values of most of the chiral couplings up to $\mathcal{O}(p^4)$, as well as some of the resonance parameters for the lightest vector octet and, to a small extent, for the axial–vector, scalar and pseudoscalar resonances.

Jointly with the experimental determination, alternative ways to infer the values of the resonance couplings have been explored. Thus the QCD ruled short–distance behaviour of the vector and axial form factors in the large-N_C limit (approximated with only one octet of vector resonances) constrains the couplings of $\mathcal{L}_2(V)$ in Eq. (4.7), that must satisfy [49] :

$$1 - \frac{F_V\, G_V}{F^2} \;=\; 0 \quad , \tag{4.15}$$

$$2F_V\, G_V - F_V^2 \;=\; 0 \quad , \tag{4.16}$$

and predict $F_V = \sqrt{2}\, F$ and $G_V = F/\sqrt{2}$, in excellent agreement with the phenomenology. The strict large-N_C limit would demand that the full spectrum of infinite zero–width vector resonances should be included in the evaluation of the form factors above. However the agreement with data suggests that the approximation of the lightest vector multiplet resembles the limit. This is the basic assumption of the LMD approach.

In addition, the study of the short-distance properties of Green's functions and the comparison with the same objects built from the effective action with explicit resonance degrees of freedom can yield relevant information on the resonance couplings, as explored in previous works [52, 53, 50, 51, 54]. We now follow this method to impose restrictions on the new couplings introduced in the odd-intrinsic-parity sector.

The relevant Green's function for this purpose is the vector-vector-pseudoscalar QCD three-point function $\langle \mathrm{VVP} \rangle$,

$$(\Pi_{\mathrm{VVP}})^{(abc)}_{\mu\nu}(p,q) = \int d^4x \int d^4y\, e^{i(p\cdot x + q\cdot y)} \langle 0|\, T\,[\, V^a_\mu(x)\, V^b_\nu(y)\, P^c(0)\,]\,|0\rangle \ , \tag{4.17}$$

which requires the octet vector current,

$$V^a_\mu(x) = \Big(\bar\psi \gamma_\mu \frac{\lambda^a}{2} \psi\Big)(x)\,, \tag{4.18}$$

and the octet pseudoscalar density

$$P^a(x) = \Big(\bar\psi i\gamma_5 \frac{\lambda^a}{2} \psi\Big)(x)\,. \tag{4.19}$$

The invariances of QCD under parity and time-reversal transformations allow us to extract the group and tensor structure of $\langle \mathrm{VVP} \rangle$ in the $\mathrm{SU(3)_V}$ limit,

$$(\Pi_{\mathrm{VVP}})^{(abc)}_{\mu\nu} = \epsilon_{\mu\nu\alpha\beta}\, p^\alpha q^\beta d^{abc}\, \Pi_{\mathrm{VVP}}(p^2, q^2, r^2)\,, \tag{4.20}$$

with the four-vector $r = -(p+q)$. The first situation concerning the short–distance behaviour of the $\langle \mathrm{VVP} \rangle$ Green's function that we can analyse is the case when both momenta p, q in Π_{VVP} become simultaneously large. The QCD calculation within the OPE framework gives, in the chiral limit and up to corrections of $\mathcal{O}(\alpha_s)$, [52]:

$$\lim_{\lambda\to\infty} \Pi_{\mathrm{VVP}}((\lambda p)^2, (\lambda q)^2, (\lambda p + \lambda q)^2) = -\frac{\langle \bar\psi\psi\rangle_0}{2\lambda^4}\, \frac{p^2+q^2+r^2}{p^2 q^2 r^2} + \mathcal{O}\left(\frac{1}{\lambda^6}\right)\,, \tag{4.21}$$

where $\langle \bar\psi\psi\rangle_0$ is the single flavour bilinear quark condensate. $(\Pi_{\mathrm{VVP}})^{(abc)}_{\mu\nu}$ is an order parameter of the spontaneous breaking of chiral symmetry. Hence, in the chiral limit, it does not receive contributions from perturbative QCD at large momentum transfers. This non-perturbative feature is in fact desirable to guarantee that the OPE domain of applicability can be enlarged down to the 1-2 GeV energy region.

In position space, Eq. (4.21) corresponds to the limit where the space-time arguments of the three operators in $\langle \mathrm{VVP} \rangle$ approach the same point at equal rates. We can also demand that only the argument of two of the three operators converge towards the same point [50]. In this case two situations arise: either the two vector currents are taken at the same point, or one of the vector currents and the pseudoscalar density are evaluated at the same argument. The first situation was exploited in the analysis of the decay of pseudoscalars into lepton pairs of Ref. [54].

We shall now build the $\langle \mathrm{VVP} \rangle$ Green's function with the effective resonance theory given by $Z_{\mathrm{ERT}}[v, a, s, p]$, and impose that the short-distance constraint in Eq. (4.21) is fulfilled.

At leading order in the $1/N_C$ expansion of QCD, the three-point correlator is evaluated from the tree-level diagrams shown in Fig. 4.1. In this limit, an infinite spectrum of zero-width vector resonances should be considered in each channel. Fortunately, the LMD approximation to large-N_C, which assumes that a single resonance in each channel saturates the requirements of QCD, can be invoked as a first test of the short-distance behaviour of our Green's function. Indeed, we shall prove that this approximation is sufficient to satisfy the short–distance QCD constraints commented above.

The couplings of the resonances among themselves and to the external sources have been detailed in Eq. (4.14), and the chiral limit is implied throughout. Our result reads

$$\Pi^{\mathrm{res}}_{\mathrm{VVP}}(p^2, q^2, r^2) = -\frac{\langle \bar\psi\psi\rangle_0}{F^2}\left\{ 4\, F_V^2\, \frac{(d_1 - d_3)\, r^2 + d_3(p^2+q^2)}{(M_V^2 - p^2)\,(M_V^2 - q^2)\, r^2}\right.$$

$$\left. -2\sqrt{2}\, \frac{F_V}{M_V}\, \frac{r^2(c_1 + c_2 - c_5) + p^2(-c_1 + c_2 + c_5 - 2c_6) + q^2(c_1 - c_2 + c_5)}{(M_V^2 - p^2)\, r^2}\right.$$

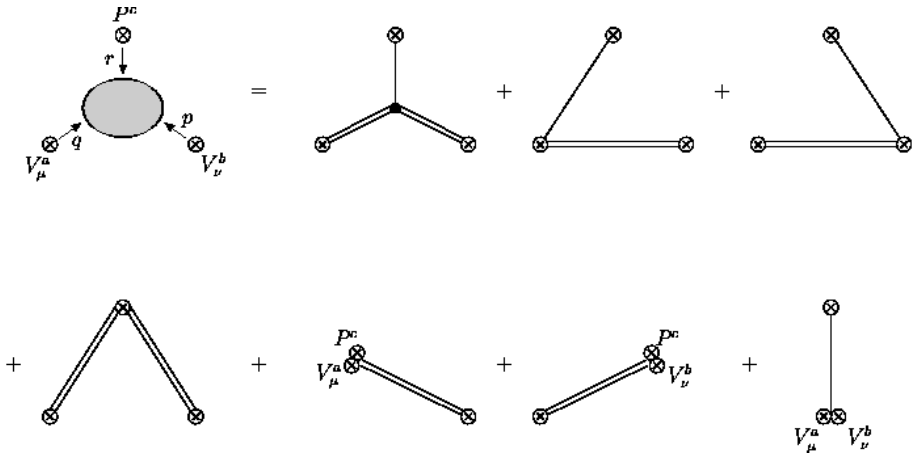

Figure 4.1: Diagrams entering the calculation of the VVP 3-point function with the ERT action. Double lines represent vector resonances, single lines are short for pseudoscalar mesons.

$$-2\sqrt{2}\,\frac{F_V}{M_V}\,\frac{r^2(c_1+c_2-c_5)+q^2(-c_1+c_2+c_5-2c_6)+p^2(c_1-c_2+c_5)}{(M_V^2-q^2)\,r^2}$$

$$+\frac{32F_V^2\,d_2}{(M_V^2-p^2)\,(M_V^2-q^2)}\;-\;\frac{16\sqrt{2}F_V c_3}{M_V(M_V^2-p^2)}\;-\;\frac{16\sqrt{2}F_V c_3}{M_V(M_V^2-q^2)}\;-\;\frac{N_C}{8\pi^2 r^2}\Bigg\}\,. \tag{4.22}$$

The contributions in Eq. (4.22) have been written following the same ordering of Fig. 4.1 (left to right, top to bottom). The last term originates from the piece of the Wess-Zumino action $Z_{\rm WZ}[v,a]$ responsible of the pseudoscalar meson decays into two photons,

$$\mathcal{L}^{(4)}_{\rm WZ} = -\frac{\sqrt{2}\,N_C}{8\pi^2\,F}\;\epsilon_{\mu\nu\alpha\beta}\,\langle\,\Phi\,\partial^\mu v^\nu\,\partial^\alpha v^\beta\,\rangle\,. \tag{4.23}$$

If we now take the limit of two momenta becoming simultaneously large in $\Pi^{\rm res}_{\rm VVP}$, we find compatibility with the QCD short-distance constraint up to order $1/\lambda^4$, Eq. (4.21), provided the following conditions among the $\mathcal{L}_V^{\rm odd}$ couplings hold:

$$\begin{aligned}
4\,c_3 + c_1 &= 0 \quad , \\
c_1 - c_2 + c_5 &= 0 \quad , \\
c_5 - c_6 &= \frac{N_C}{64\pi^2}\,\frac{M_V}{\sqrt{2}F_V} \quad , \\
d_1 + 8\,d_2 &= -\frac{N_C}{64\pi^2}\,\frac{M_V^2}{F_V^2} + \frac{F^2}{4F_V^2} \quad ,
\end{aligned}$$

$$d_3 \;=\; -\frac{N_C}{64\pi^2}\frac{M_V^2}{F_V^2} + \frac{F^2}{8F_V^2}\,. \qquad (4.24)$$

These relations have been obtained within the chiral limit. However the couplings of the Effective Lagrangian do not depend on the masses of the Goldstone fields and, consequently, the constraints in Eq. (4.24) apply for non–zero pseudoscalar masses too.

Actually our $\langle \mathrm{VVP}\rangle$ three-point function fully reproduces the LMD ansatz suggested in Ref. [52] :

$$\Pi^{\mathrm{res}}_{\mathrm{VVP}}(p^2,q^2,(p+q)^2) = -\frac{\langle\bar{\psi}\psi\rangle_0}{2}\;\cdot\;\frac{(p^2+q^2+r^2)-\frac{N_C}{4\pi^2}\frac{M_V^4}{F^2}}{(p^2-M_V^2)(q^2-M_V^2)r^2}\,. \qquad (4.25)$$

As a consequence both the short–distance behaviour in Eq. (4.21) and those conditions where two vector currents or one vector current and the pseudoscalar density meet at the same point, mentioned above, are thoroughly satisfied.

The ansatz (4.25) implies that we recover the LMD estimates for the low-energy constants derived in Ref. [50]. The authors of this reference found that the same agreement with the short and long-distance QCD behaviour could not be reached working with the resonance Lagrangian in the vector representation, not even at the expense of introducing local contributions from the $\mathcal{O}(p^6)$ chiral Lagrangian. They then suggested that the problem may be inherent to the effective Lagrangian approach and unlikely to be fixed just by using other representations for the resonance fields; our result, derived in the antisymmetric tensor-field formulation with an odd-intrinsic-parity sector, contradicts this assertion, at least in what concerns the $\langle \mathrm{VVP}\rangle$ Green's function.

Finally it is worth to comment the situation that would arise if local $\mathcal{O}(p^6)$ operators of the chiral Lagrangian in Eq. (4.12) were introduced in this analysis. We argued in Section 2 that the couplings of those operators, t_i, could be completely saturated by vector resonances and, accordingly, $t_i \simeq t_i^V$ and $\hat{t}_i \simeq 0$. If we include a non–vanishing $\hat{t}_i$ in the evaluation of the Green's function carried above it is easy to see that the high energy behaviour is spoiled unless higher–derivative couplings with resonances are considered. If we stay within our $Z_{\mathrm{ERT}}[v,a,s,p]$ action, that satisfies by itself the matching with the QCD result, the OPE imposes $\hat{t}_i = 0$, $i = 1, 2$.

It is also interesting to notice that the combinations of odd–intrinsic couplings which appear in the expressions of t_i^V, Eq. (4.13) are predicted from the QCD conditions above. We obtain :

$$\begin{aligned} t_1^{\mathrm{V}} &= \frac{F^2}{64\,M_V^4}\;, \\ t_2^{\mathrm{V}} &= -\frac{N_C}{64\,\pi^2\,M_V^2}\left[1-\frac{4\,\pi^2}{N_C}\frac{F^2}{M_V^2}\right]\;, \end{aligned} \qquad (4.26)$$

which coincide [3] with the predictions made for these parameters in [52]. This fact is not surprising, since the relations (4.26) were derived in [52] by expanding the

[3] There is a minus sign difference in the definitions of t_1 and t_2 in [52] because the convention used there for the Levi-Civita tensor is the opposite to ours.

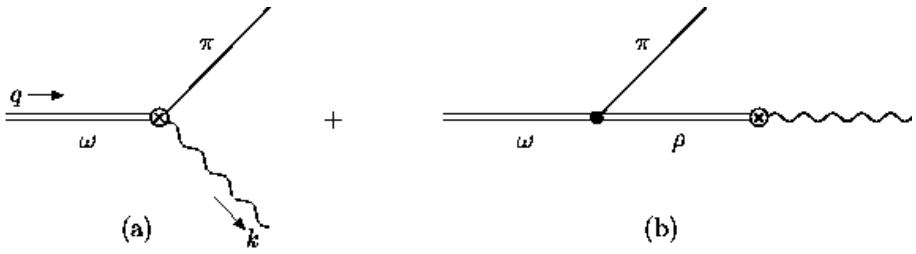

Figure 4.2: Lowest order diagrams for the process $\omega \to \pi\gamma$.

$\langle \mathrm{VVP} \rangle$ ansatz, Eq. (4.25), at low-momenta and comparing it with the $\langle \mathrm{VVP} \rangle$ expression obtained from the $\mathcal{L}^{(6)}_{\mathrm{odd}}$ Lagrangian. The success in reproducing the same representation for Π_{VVP} within the resonance effective Lagrangian has automatically generated identical values for the chiral parameters [4].

4.4 Phenomenology of intrinsic-parity violating processes

Odd–intrinsic–parity processes have been widely studied within chiral perturbation theory where resonances are integrated out [61]. In order to gain more insight on the odd-intrinsic-parity sector of the resonance Lagrangian and, to make some test on the validity of the short-distance conditions obtained above, we study in this section the processes $\omega \to \pi\gamma$, $\rho \to \pi\gamma$, $\omega \to 3\pi$ and $\pi \to 2\gamma$.

4.4.1 $\omega \to \pi\gamma$

At tree-level, the intrinsic-parity violating transition $\omega \to \pi\gamma$ receives contributions from both the VJP and VVP terms of $\mathcal{L}^{\mathrm{odd}}_V$. The corresponding diagrams are displayed in Fig. 4.2. The physical ω resonance is a superposition of an octet component, ω_8, and a singlet one, ω_1, which can be added as a diagonal matrix $\omega_1/\sqrt{3}$ to the octet, Eq. (4.8); if ideal mixing is assumed then the states of defined mass are

$$|\,\omega\,\rangle = \sqrt{\frac{2}{3}}\,|\,\omega_1\rangle + \sqrt{\frac{1}{3}}\,|\,\omega_8\rangle \quad ,$$

and

$$|\,\phi\,\rangle = -\sqrt{\frac{1}{3}}\,|\,\omega_1\rangle + \sqrt{\frac{2}{3}}\,|\,\omega_8\rangle \, .$$

[4] The author of [52] extended the results for t^V_1 and t^V_2 above by including an additional pole-contribution in the VVP ansatz from a pseudoscalar $\pi(1300)$ resonance.

The amplitudes for the direct and ρ-mediated diagrams, Figs. 4.2a and 4.2b respectively, read

$$i\,\mathcal{M}^{direct}_{\omega\to\pi\gamma} = i\,\epsilon_{\alpha\beta\rho\sigma}\,\epsilon^{\alpha}_{\omega}\epsilon^{\beta}_{\gamma}q^{\rho}k^{\sigma}\,2\sqrt{2}\,\frac{e}{M_\omega M_V F}\Big[\,(c_2-c_1+c_5-2c_6)\,M_\omega^2 + (c_1+c_2+8c_3-c_5)\,m_\pi^2\,\Big]\,,$$

$$i\,\mathcal{M}^{\rho}_{\omega\to\pi\gamma} = -i\,\epsilon_{\alpha\beta\rho\sigma}\,\epsilon^{\alpha}_{\omega}\epsilon^{\beta}_{\gamma}q^{\rho}k^{\sigma}\,\frac{4\,e}{M_V^2 M_\omega}\,\frac{F_V}{F}\Big[\,d_3\,M_\omega^2 + (d_1+8d_2-d_3)m_\pi^2\,\Big]\,, \quad (4.27)$$

where we have kept the generic mass M_V of the meson octet in the ρ propagator, in consistency with the procedure followed in the analysis of Section 4.3; distinction is made between M_V and M_ω when the latter is of kinematic origin. Quite remarkably, if we now plug in the QCD constraints, Eq. (4.24), obtained from the analysis of the short-distance behaviour of the $\langle VVP\rangle$ Green's function, we find a full prediction for this process :

$$i\,\mathcal{M}_{\omega\to\pi\gamma} = i\,\epsilon_{\alpha\beta\rho\sigma}\,\epsilon^{\alpha}_{\omega}\epsilon^{\beta}_{\gamma}q^{\rho}k^{\sigma}\,\frac{e}{F_V}\,\Big[\,\frac{N_C}{8\pi^2}\,\frac{M_\omega}{F}\,-\frac{F}{2}\,\frac{M_\omega}{M_V^2}\,\Big(1+\frac{m_\pi^2}{M_\omega^2}\Big)\,\Big]\,. \quad (4.28)$$

We notice that the direct (Fig. 4.2a) and the ρ exchange diagrams (Fig.4.2b) almost contribute to similar extent to this process. This means that contrary to what we would expect from vector meson dominance, the $\omega\rho\pi$ coupling does not saturate the decay $\omega\to\pi\gamma$. The actual value of this coupling in our formalism [5], d_3, is less than half of the one that would arise from VMD, where only the diagram Fig. 4.2b contributes. This has immediate consequences to other decay channels, as we shall see in the next subsection.

Finally, the width is easily obtained, giving

$$\Gamma(\omega\to\pi\gamma) = \frac{\alpha}{192}\,M_\omega\Big(1-\frac{m_\pi^2}{M_\omega^2}\Big)^3\,\Big[\,\frac{N_C}{4\pi^2}\,\frac{M_\omega^2}{F^2}\,-\frac{M_\omega^2}{M_V^2}\,\Big(1+\frac{m_\pi^2}{M_\omega^2}\Big)\,\Big]^2\,. \quad (4.29)$$

The relation $F_V=\sqrt{2}\,F$, consequence of conditions (4.15) and (4.16), has been employed in deriving the result in Eq. (4.29). Varying the parameter F from the bare value $F_0\simeq 87$ MeV to the dressed one (i.e. the pion decay constant), $F_\pi\simeq 92.4$ MeV [62], we get that our prediction for $\Gamma(\omega\to\pi\gamma)$ ranges from 0.703 MeV to 0.524 MeV, with the choices $M_V=M_\rho=771.1$ MeV and $M_\omega=782.6$ MeV [62]. This 5–30% deviation from the experimental value, $\Gamma(\omega\to\pi\gamma)|_{\rm exp}=(0.734\pm 0.035)\,$MeV, is in accordance with the expected size of next-to-leading $1/N_C$ corrections. Also the $\rho\to\pi\gamma$ decays, related with $\omega\to\pi\gamma$ by a $SU(3)_V$-symmetry factor, can be compared with the phenomenology. We obtain

$$\Gamma(\rho^\pm\to\pi^\pm\gamma)=\Gamma(\rho^0\to\pi^0\gamma)=\frac{1}{9}\,\Gamma(\omega\to\pi\gamma)=78.1-58.2\ \text{keV}\,,$$

[5] The tiny contribution coming from the pion mass contribution in $\mathcal{M}^{\rho}_{\omega\to\pi\gamma}$ can be obviated in this discussion.

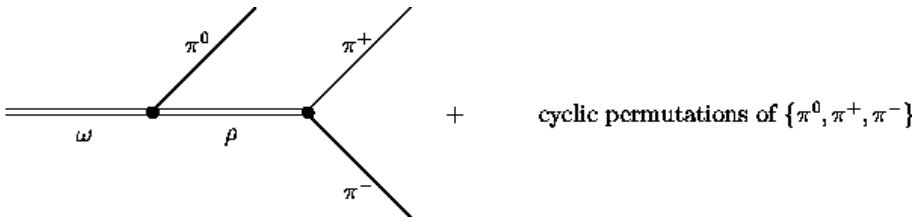

Figure 4.3: The $\omega \to \pi^+\pi^-\pi^0$ decay amplitude via an intermediate ρ exchange.

depending on the value of the parameter F, to be compared with the experimental measurements, $\Gamma(\rho^\pm \to \pi^\pm\gamma)|_{\rm exp} = (67 \pm 7)$ keV and $\Gamma(\rho^0 \to \pi^0\gamma)|_{\rm exp} = (120 \pm 30)$ keV. It is interesting to note that our predictions are rather close to the ones derived from the extended Nambu-Jona-Lasinio model [60].

Our result for $\Gamma(\omega \to \pi\gamma)$ is quite significant being a pure prediction of the matching procedure of the resonance effective theory with the OPE expansion given by QCD. The extension of our analysis to other decay channels (e.g. $K^* \to K\gamma$, $\phi \to \eta\gamma$) requires that exact SU(3)$_{\rm V}$ symmetry is left aside in order not to lose the predictive power shown in $\omega \to \pi\gamma$. This study would require to consider the OPE expansion in the asymptotic regime keeping distinct masses for each quark flavour, a rather non trivial task.

4.4.2 $\omega \to \pi^+\pi^-\pi^0$

The odd-intrinsic parity sector included in the resonance Lagrangian can also account for the ρ-mediated mechanism of decay of the ω meson to the $\pi^+\pi^-\pi^0$ final state, Fig. 4.3. If we label as k_1, k_2, k_3 the momenta of the π^+, π^- and π^0 respectively, the amplitude associated to the diagram of Fig. 4.3, including cyclic permutations among k_1, k_2 and k_3, reads

$$i\,\mathcal{M}_{\omega\to 3\pi} = i\,\epsilon_{\alpha\beta\rho\sigma}\,k_1^\alpha k_2^\beta k_3^\rho \epsilon_\omega^\sigma \frac{8\,G_V}{M_\omega F^3}\left[\frac{m_\pi^2(d_1+8d_2-d_3)+(M_\omega^2+s_{12})\,d_3}{M_V^2-s_{12}} + \{s_{12}\to s_{13}\}+\{s_{12}\to s_{23}\}\right]. \qquad (4.30)$$

The kinematic invariants are defined as usual, i.e. $s_{ij} = (k_i + k_j)^2$. The VMD hypothesis for this decay predicts that the amplitude above is the dominant one. Then the corresponding width would be calculated as

$$\Gamma(\omega \to \pi^+\pi^-\pi^0) = \frac{G_V^2}{4\,\pi^3\,M_\omega^5\,F^6}\int_{4m_\pi^2}^{(M_\omega-m_\pi)^2} ds_{13}\int_{s_{23}^{min}}^{s_{23}^{max}} ds_{23}\,\mathcal{P}(s_{13},s_{23})\,\times \qquad (4.31)$$

$$\times\left[\frac{m_\pi^2(d_1+8d_2-d_3)+(M_\omega^2+s_{12})\,d_3}{M_V^2-s_{12}} + \{s_{12}\to s_{13}\} + \{s_{12}\to s_{23}\}\right]^2,$$

where the function $\mathcal{P}$ is the polarization average of the tensor structure of $\mathcal{M}_{\omega\to 3\pi}$,

$$\mathcal{P}(s_{13},s_{23}) = \frac{1}{12}\left\{-m_\pi^2(m_\pi^2-M_\omega^2)^2 - s_{13}s_{23}^2 + (3m_\pi^2+M_\omega^2-s_{13})s_{13}s_{23}\right\} . \quad (4.32)$$

With $G_V = F/\sqrt{2}$ and the relations obtained by the short-distance matching, we find that the width above works out $\Gamma(\omega\to\pi^+\pi^-\pi^0) \simeq 1.4\,\text{MeV}$, quite far from the experimental result [62], $\Gamma(\omega\to\pi^+\pi^-\pi^0)|_{\text{exp}} = (7.52\pm 0.06)\,\text{MeV}$. Clearly, the contribution from a direct $\omega\to 3\pi$ amplitude must be larger than expected from VMD. Such deviation can be traced back to the result obtained in the previous section for $\omega\to\pi\gamma$. There we found that the d_3 parameter was less than half the value one should expect from a dominant role of the $\rho\omega\pi$ coupling. The $\omega\to 3\pi$ width calculated above, Eq. (4.31), is essentially (neglecting the tiny piece driven by the pion mass squared) proportional to d_3^2; therefore, there is roughly a factor of ~ 4 between our calculation of $\Gamma(\omega\to\pi\rho\to 3\pi)$ and the result obtained under VMD by fixing the $\rho\omega\pi$ coupling from the $\omega\to\pi\gamma$ width (see for example Ref. [63]). This factor would raise the result of (4.31) to $\sim 5.6\,\text{MeV}$, i.e. reaching the level of accuracy of leading large-N_C calculations.

According to the precedent discussion, the intermediate meson exchange does not account entirely for the ω decay into three pions, and the direct terms must be considered [6]. In fact both contributions appear at the same order in the large–N_C expansion and the ρ resonance, being far off–shell in this process, does not resonate. Consequently, there is no reason that justifies neglecting the direct vertex. Indeed, it was pointed out in Ref. [63] that VMD alone predicts a too large $\rho\omega\pi$ coupling with respect to what suggests naive chiral counting. The QCD–enforced appearance of a direct term in our approach, which has reduced the $\rho\omega\pi$ coupling to the half, casts some light on the issue.

4.4.3 $\pi\to\gamma\gamma$

In the chiral limit, the amplitude for the $\pi\to\gamma\gamma$ process is non-vanishing and exactly predicted by the ABJ anomaly [64], Eq. (4.23). Away from this limit, the amplitude receives small contributions from different sources, including isospin-breaking effects, as well as electromagnetic and higher-order chiral corrections. As the loop contribution vanishes [65], the latter corrections start with the $\mathcal{O}(p^6)$ Goldstone chiral Lagrangian. The odd-intrinsic-parity interactions among vector resonances introduced in Section 4.2 also generate chiral corrections to this process proportional to m_π^2. Let us first study the numerical size of these corrections, fixed by virtue of the short-distance constraints.

The amplitudes for the decay via intermediate meson exchange, depicted in Fig. 4.4, give as a result

$$i\,\mathcal{M}^{(a)}_{\pi\to\gamma\gamma} \;=\; -i\,\epsilon_{\alpha\beta\rho\sigma}\,\epsilon_1^\alpha\epsilon_2^\beta k_1^\rho k_2^\sigma\;\frac{8\sqrt{2}}{3}\,\frac{e^2}{M_V}\,\frac{F_V}{F}\,\frac{m_\pi^2}{M_V^2}\left(c_1+c_2+8c_3-c_5\right)$$

[6] In our effective theory, these terms would be obtained by writing down the operators which give rise to local contributions to $\omega\to 3\pi$.

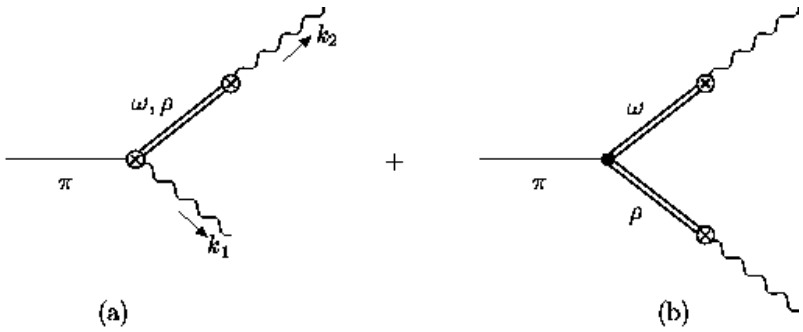

Figure 4.4: Feynman diagrams with vector mesons giving $\mathcal{O}(m_\pi^2)$ corrections to $\pi \to \gamma\gamma$ decay. The diagrams with interchanged photon momenta must be added.

$$= \quad 0 \quad ,$$

$$\begin{aligned} i\,\mathcal{M}^{(b)}_{\pi\to\gamma\gamma} &= i\,\epsilon_{\alpha\beta\rho\sigma}\,\epsilon_1^\alpha \epsilon_2^\beta k_1^\rho k_2^\sigma\ \frac{8\,e^2}{3\,F}\,\frac{F_V^2}{M_V^2}\,\frac{m_\pi^2}{M_V^2}\left(d_1+8d_2-d_3\right) \\ &= i\,\epsilon_{\alpha\beta\rho\sigma}\,\epsilon_1^\alpha \epsilon_2^\beta k_1^\rho k_2^\sigma\,\frac{e^2\,F}{3M_V^2}\,\frac{m_\pi^2}{M_V^2}\ . \end{aligned} \tag{4.33}$$

The diagram with a VJP vertex vanishes after the short-distance conditions are applied, and the remaining contribution gets completely fixed. The correction induced into the $\pi \to \gamma\gamma$ width, by our result above gives :

$$\Gamma(\pi\to\gamma\gamma) = \frac{\alpha^2}{64\,\pi^3\,F^2} m_\pi^3\,[\,1\,-\,\Delta\,]^2 \quad , \tag{4.34}$$

where

$$\Delta \;=\; \frac{4\pi^2}{3}\,\frac{F^2}{M_V^2}\,\frac{m_\pi^2}{M_V^2} \;\simeq\; 0.006 \quad . \tag{4.35}$$

This result provides a tiny 1% correction to the width, and it is perfectly compatible with the experimental uncertainty, $\Gamma(\pi \to \gamma\gamma)|_{\rm exp} = (7.7 \pm 0.6)$ eV.

This evaluation of the amplitude for the $\pi \to \gamma\gamma$ process could also have been carried out within the chiral Lagrangian $\mathcal{L}^{(6)}_{\rm odd}$ of Eq. (4.12), where only the operator with t_1 contributes [7]. With $t_1 \simeq t_1^V$ and using the value given in Eq. (4.26) we obtain the result above. The exercise carried out in this Subsection, evaluating the diagrams in Fig. 4.4, shows explicitly that only the two–resonance driven amplitude gives contribution to this process in the antisymmetric formulation.

4.4.4 $\pi \to \gamma\gamma^*$

The same diagrams depicted in Fig. 4.4, when one of the photons is taken off-shell, contribute to the $\pi \to \gamma\gamma^*$ amplitude. The later process is usually written as

[7] The operator with the t_2 coupling only contributes if one of the photons is off–shell.

a slope parameter α which modifies the on-shell behaviour:

$$\mathcal{M}_{\pi\to\gamma\gamma^*} \,=\, \mathcal{M}_{\pi\to\gamma\gamma}\left(1+\alpha\, k^{*2}\right)\,, \tag{4.36}$$

where k^* is the off-shell photon momentum. The interactions contained in $\mathcal{L}_V^{\rm odd}$ yield a contribution to the parameter α that amounts

$$\alpha^{\rm odd} \,=\, \frac{1}{M_V^2}\left[1-\frac{4\pi^2F^2}{N_C M_V^2}\right] \,\simeq\, 1.36\ {\rm GeV}^{-2}\,, \tag{4.37}$$

which is smaller than the VMD estimate, $\alpha^{\rm VMD}=1/M_V^2\simeq 1.68\ {\rm GeV}^{-2}$. The chiral loops contributions to this slope,

$$\alpha^{\chi} = -\frac{1}{16\pi\, F^2}\frac{1}{3}\left(2+\ln\frac{m_\pi^2 m_K^2}{\mu^4}\right) \,\simeq\, 0.26\ {\rm GeV}^{-2}\,, \tag{4.38}$$

with the renormalization scale $\mu\simeq M_\rho$, were calculated in Ref. [66]. We can add both contributions, Eqs. (4.37) and (4.38) to get $m_\pi^2\alpha\simeq 0.029$, to be compared with the averaged value $m_\pi^2\alpha|_{\rm exp}=0.032\pm 0.004$ in the PDG [62]. The result for $\alpha^{\rm odd}$ above, has been extended beyond the LMD approximation by the inclusion of a second vector resonance into the $\langle$VVP$\rangle$ ansatz, Eq. (4.25), in Ref. [50]. The latter is in fact needed to have the right $1/k^{*2}$ behaviour for large k^* [67, 68] in the form factor $\mathcal{F}_{\pi\gamma\gamma^*}(k^*)$ that describes the transition between a pion, one off-shell and one on-shell photon. The $1/k^{*2}$ fall-off of this form factor has been observed experimentally [69].

4.5 Conclusions

Effective theories of QCD carry all–important features of the underlying theory to describe the relevant hadron dynamics in the non–perturbative regime. The odd–intrinsic–parity sector has been studied within chiral perturbation theory but its extension to the energy region of the resonances requires a proper implementation of the active degrees of freedom and to generate the effective theory through a procedure able to enforce the relevant dynamics on the coupling constants. This task has been addressed in this Chapter. After considering the operators of the Lagrangian, that rely on the global symmetries of QCD, we proceed to drive the information, from the underlying theory onto the couplings, through a matching with the leading OPE of the Green's function in the chiral limit.

Let us highlight the main results that can be extracted from the previous sections.

- The lowest order Lagrangian involving interactions among one Goldstone mode and two vector particles has been introduced in the Resonance Chiral Theory with the vector resonances described in terms of antisymmetric tensor fields.

- The vector-vector-pseudoscalar three-point-function $\langle$VVP$\rangle$ has been calculated at tree level with the new sector added to the resonance Lagrangian.

Assuming that a matching procedure between the result obtained from the effective action and from QCD in terms of massless quarks is reliable at large momenta, we have derived a set of relations among the parameters of the odd-intrinsic-parity sector.

- In contrast to the result of Ref. [50], where vector resonances were described in the Proca formalism, the expression for the $\langle \mathrm{VVP} \rangle$ Green's function obtained from the Lagrangian with antisymmetric tensor fields is fully compatible with the short–distance QCD constraints, which reduce it to the ansatz suggested by LMD in the large-N_C limit of QCD, successfully tested in previous works [52, 54].

- On the way, we have found that the same combinations of couplings which appears in the short-distance QCD constraints, show up in the $\omega \to \pi\gamma$ and $\rho \to \pi\gamma$ amplitudes calculated with the resonance Lagrangian, thus allowing us to give a full prediction for these decays. The agreement with the experimental values is remarkable.

- The $\omega \to \pi\gamma$ calculation above shows an important feature: the contribution from a direct $\omega\pi\gamma$ vertex is larger than expected from VMD. Indeed, it amounts to more than 50% of the total result for this amplitude. This agrees with the expectations from the $1/N_C$ counting, as both mechanisms contribute to the same order.

- The last point has an important consequence for other channels where VMD alone was thought to be the relevant mechanism of decay. To serve as an example, we have shown that the intermediate meson exchange $\omega \to \rho\pi \to 3\pi$ cannot dominate the $\omega \to 3\pi$ process in our framework, and the local contribution thus becomes essential.

Our study has shown that the use of effective theories of QCD in the intermediate energy region, populated by resonances, endows the basic information to provide both qualitative and quantitative descriptions of the hadron phenomenology in a model–independent way. Consequently it provides a compelling framework to work with.

Appendix

A Construction of the odd-intrinsic-parity sector

Within the antisymmetric formulation, the integration of a vector meson gives a contribution which starts at $\mathcal{O}(p^4)$ in the chiral counting. Interaction terms with a Levi-Civita tensor start to contribute [8] at $\mathcal{O}(p^6)$, as terms with one vector meson and an $\mathcal{O}(p^2)$ chiral tensor are not charge conjugation or parity invariant, and a possible term with two resonance fields, $\epsilon_{\mu\nu\rho\sigma}\langle V^{\mu\nu}V^{\rho\sigma}\rangle$, is forbidden by parity conservation. Besides, terms of odd order, i.e. $\mathcal{O}(p^3)$ or $\mathcal{O}(p^5)$, cannot be written down in the presence of an $\epsilon_{\mu\nu\rho\sigma}$ tensor. Either a chiral tensor of $\mathcal{O}(p^4)$ together with a vector meson is needed, giving rise to the VJP terms, or two vector resonances and a chiral tensor of $\mathcal{O}(p^2)$ (VVP terms).

The available chiral tensors have already been introduced in Section 4.2: $\chi_\pm$, $f_\pm^{\mu\nu}$ are $\mathcal{O}(p^2)$, while the covariant derivative ∇_α and u_α count as $\mathcal{O}(p)$. These tensors have defined transformation properties under chiral rotations and thus allow us to write down chiral invariant objects in a straightforward way.

Let us first give some clues about the construction of the VVP basis. Aside from the two vector mesons, we should consider all possible tensors giving one pseudoscalar. Therefore, we can have:

- One covariant derivative ∇_μ and one u_ν tensor, with the covariant derivative acting on either the resonance fields or the pseudoscalar u_ν. In the latter case $\nabla_\mu u_\nu$ is symmetric in its indices for the linear term of the expansion of u_ν in terms of Goldstone fields:

$$u_\nu = -\frac{\sqrt{2}}{F}\,\partial_\nu\Phi + \text{terms with 3 pseudoscalar fields} + \dots \quad .$$

- A χ_- external field, whose expansion in terms of the pseudoscalar octet of fields starts with one particle states. A χ_+ external field together with the two vector mesons is however not allowed by parity conservation.

In addition, the Schouten identity,

$$g_{\rho\sigma}\epsilon_{\alpha\beta\mu\nu} + g_{\rho\alpha}\epsilon_{\beta\mu\nu\sigma} + g_{\rho\beta}\epsilon_{\mu\nu\sigma\alpha} + g_{\rho\mu}\epsilon_{\nu\sigma\alpha\beta} + g_{\rho\nu}\epsilon_{\sigma\alpha\beta\mu} = 0\,, \tag{A.4.1}$$

reduces the number of independent operators because it may establish relations among those with different ordering of the Lorentz indices. As an example, consider the two following VVP terms:

$$\begin{aligned}
\mathcal{O}^1 &= \epsilon_{\mu\nu\rho\sigma}\,\langle\,\{V^{\mu\nu},V^{\rho\alpha}\}\nabla_\alpha u^\sigma\,\rangle = g_{\alpha\lambda}\,\epsilon_{\mu\nu\rho\sigma}\,\langle\,\{V^{\mu\nu},V^{\rho\lambda}\}\nabla^\alpha u^\sigma\,\rangle\,,\\
\mathcal{O}^2 &= \epsilon_{\mu\nu\rho\sigma}\,\langle\,\{V^{\mu\nu},V^{\rho\sigma}\}\nabla_\alpha u^\alpha\,\rangle = g_{\alpha\sigma}\,\epsilon_{\mu\nu\rho\lambda}\,\langle\,\{V^{\mu\nu},V^{\rho\lambda}\}\nabla^\alpha u^\sigma\,\rangle\,.
\end{aligned}$$

[8] For terms involving vector resonances, this counting should be understood as the one obtained after integrating out the resonances, i.e. the order of the chiral operator induced by vector exchange.

With the identity (A.4.1) we find that the second operator is proportional to the first one:

$$\mathcal{O}^2 = 4\,\mathcal{O}^1\,.$$

Similarly, the Schouten identity must be applied to operators with the ∇_μ acting on the resonance fields and to operators from the VJP sector to further reduce the basis.

To close with the analysis of the VVP interactions, recall that a term $\sim \langle V^{\mu\nu} V^{\rho\sigma} f_-^{\alpha\beta}\rangle$ would include an external vector (or axial-vector) source in addition to the wanted pseudoscalar. Clearly, these terms do not belong to our VVP sector.

For the VJP interactions, basically the same considerations made above hold, and the substitution of one of the resonance fields $V^{\mu\nu}$ by and external vector field $f_+^{\mu\nu}$, which has the same properties under P and C transformations, gives the allowed VJP structures. Note that for each VVP term two VJP operators emerge with this procedure (except for the term with χ_-), as the vector tensors are not equal now. We have chosen that ∇^α acts on the vector meson or on the pseudoscalar field to define the final set of independent VJP operators. As quoted in the main text, the term $\mathcal{O}^4_{\rm VJP}$, where the pseudoscalar now comes up from the $f_+^{\mu\nu}$ tensor, is a SU(3)$_{\rm V}$-breaking operator. Indeed its lower order expansion in terms of Goldstone fields is proportional to $m_K^2 - m_\pi^2$.

Chapter 5

The Hadronic Cross Section in the 1-2 GeV Energy Region

5.1 Introduction

The hadronic spectrum from e^+e^- annihilation in the energy range between 1 and 2 GeV exhibits a rather rich and complex structure. Theoretically, the region, being far away from the chiral domain ($E \ll M_\rho$, with M_ρ the mass of the $\rho(770)$ resonance), is poorly known due to the intricate non-perturbative dynamics of QCD. The conventional approach to extract the hadronic matrix elements of the relevant QCD currents has mainly relied on the available experimental information, such as $e^+e^- \to$ hadrons or semileptonic decays. From these data, the hadronic observables have been obtained either by direct integration of the data or by *ad hoc* parameterizations lousily inspired by QCD. Both approaches have an obvious drawback: they do not tell us much about the physics which lies behind. Even when we can obviate the physical interpretation, we shall keep in mind that fitting (or integrating) procedures inherit all the uncertainties associated to the experimental data, making it very difficult to define the accuracy of the results. An estimation of the theoretical errors introduced by the above techniques is always a matter of discussion. Recall, for example, the running of the QED fine structure constant $\alpha(s)$ and the anomalous magnetic moment of the muon. These are observables whose theoretical predictions are limited by loop effects from hadronic vacuum polarization. Both magnitudes are related via dispersion relations to the hadronic production rate in e^+e^- annihilation, which can be evaluated using e^+e data and hadronic τ decays. It is clear that the apparent discrepancy between the measured value for the anomalous magnetic moment of the muon [70] and the Standard Model prediction [71] requires a careful review of the theoretical uncertainties associated to the hadronic contribution to accurately determine the size of this deviation. An analysis of these observables in a model-independent way could clarify the issue.

Attempts based on effective actions of QCD have achieved a remarkable success in describing the data for energies up to 1 GeV, and indeed suggest that this approach may be continued to higher energies. The pion vector form factor at very low

energies has been calculated in chiral perturbation theory, allowing to describe the $e^+e^- \to \pi^+\pi^-$ data in this region very accurately with the known values of the chiral parameters [72, 73]. Concerning the muon anomalous magnetic moment, the use of the chiral expansion for the two-pion contribution at $E \leq 0.5$ GeV has dramatically decreased its error as compared to previous estimations directly obtained from the raw data. At higher energies ($E \sim M_\rho$), the appropriate framework to implement QCD information is Resonance Chiral Theory (RχT). This scheme has been the starting point of several works devoted to the study of the pion form factor in the region close to the $\rho(770)$ mass [74, 75, 76], which have also implemented features provided by the $1/N_C$ expansion, resummation techniques and other important constraints such as analyticity and unitarity. Our goal is to derive an expression for the vector-vector current correlator in the resonance driven 1-2 GeV region, following similar methods to those used in the works just mentioned. With this aim, we outline in this chapter the general strategy to follow, mainly focusing in the technical part of the analysis. As we shall see, the practical implementation of our results shall require further investigations. Among other interesting applications, this project could cast some light on the aove mentioned issue of the anomalous magnetic moment of the muon, for which about 90% of the total hadronic contribution comes from the enery region $E \leq 2$ GeV.

To extend the validity of the resonance chiral theory above 1 GeV, we should take into account the contributions from higher resonance states. This is accomplished by considering RχT with N different multiplets, as shown in Section 5.3. In addition, the appearance of meson final states with higher multiplicities must be correctly reproduced in the absorptive contents of the correlator. In Section 5.2 we explain how the intermediate states of 4π and $K\overline{K}\pi$ can be accounted for by the 1-loop diagrams which arise from the odd–intrinsic–parity sector introduced in Chapter 4. The extension of the above sector to several multiplets, undertaken in Section 5.3, introduces new unknown couplings in the theory. Section 5.4 presents the calculation of the 1-loop diagrams, while their regularization is postponed to Section 5.5. In Section 5.6 we explain how to perform a resummation of the 1-loop topologies for the simpler case of only one resonance multiplet and give the final expressions for the vector-vector correlator and for the pion form factor which shall be used in future works. Some missing contributions in our framework are briefly discussed in Section 5.7. Lastly, we give some final comments and suggest the lines to follow in the next steps of this project. Among others, analysis as the one performed for the $\langle$VVP$\rangle$ three-point function in the last chapter should be pushed forward in the future to gain information about the new parameters from QCD, either by going beyond the LMD approximation or by considering additional Green's functions.

The appendices collect the formulas from the 1-loop calculations and a generalization of the resummation procedure to the case of N multiplets.

5.2 Phenomenology of the resonance region

The $e^+e^- \to hadrons$ cross section is determined in the energy range between 0.5 and 2 GeV by the presence there of vector resonances which are classified in multiplets of the $SU(3)_V$ symmetry ($U(3)_V$ in the large-N_C limit). According to the PDG [62] three nonets of vector resonances may be identified in this region, with the $\rho(770)$, $\rho(1450)$ and $\rho(1700)$ resonances corresponding to the $I = 1$ component of each multiplet, and ($\omega(782)$, $\phi(1020)$), ($\omega(1420)$, $\phi(1680)$) and $\omega(1650)$ the $I = 0$ vector fields experimentally observed. The light isoscalar mesons $\omega(782)$ and $\phi(1020)$, belonging to the first nonet, have small widths and the narrow width approximation is enough to obtain a good description of the data close to their masses[1]. The isovector resonances, $\rho(770)$, $\rho(1450)$ and $\rho(1700)$ have larger widths and thus give sizeable contributions far from the on-shell energies. To a large extent, they are responsible for the main features of the observed spectrum and therefore we shall concentrate our efforts in describing the $I = 1$ channel

As we move up in energies the multiplicity of the final states is increased. Within the effective theory approach the opening of new channels must be accounted for perturbatively in the absorptive content of the vector-vector correlator. Beyond the two-pseudoscalar states ($\pi^+\pi^-$, K^+K^- and $K^0\bar{K}^0$ in the I=1 channel), already accounted for in previous works [74, 75, 76], the next relevant intermediate states to consider are the 4π and the $K\overline{K}\pi$ contributions.

Within perturbation theory, the $I = 1$ photon in e^+e^- annihilation is connected to ρ-like resonances which eventually decay into a defined hadronic state. Under the vector meson dominance (VMD) hypothesis [77], the $\rho^0 \to 4\pi$ amplitude is dominated in the 1 GeV region by the ω exchange diagram for the $2\pi^0\pi^+\pi^-$ channel, and by the axial a_1 exchange contribution for the $2\pi^+2\pi^-$ channel, as the 3π final state is the dominant decay mode for both the ω and a_1 resonances. A recent theoretical study on the $e^+e^- \to 4\pi$ cross section within chiral theory [63] has validated this assumption for the two charge configurations. The important role of such $\rho\omega\pi$ coupling in describing the 4π absorptive contribution is accounted for in our approach by the VVP vertices contained in the odd-intrinsic-parity sector introduced in Section 4.2. Recall that these operators also produce ρK^*K couplings and, as K^*-resonances decay almost at 100% to $K\pi$, the relevant channel $K\overline{K}\pi$ would also be encoded in our framework. For consistency, the $j_{ext}\,\omega\pi$ couplings are also introduced with the VJP vertices, Eq. (4.9), at the same chiral order. Similarly, we could include the axial-vector interactions in the effective resonance Lagrangian to reproduce the $a_1\rho\pi$ interaction, relevant to account for the $2\pi^+2\pi^-$ channel. We should then introduce the (even–intrinsic–parity) AVP and AJP terms in the correlator following identical lines to those of Section 5.3. This would not pose any technical difficulties in our analysis, although it would decrease the predictive power of our so-built correlator. Also note that the absorptive part of the $a_1\pi$ loops starts to contribute at higher energies ($\sim$ 1.5 Gev) than the $\omega\pi$ loop, due to phase space

[1] We are aware that the widths of the $I = 0$ resonances from the second and third multiplets are not so narrow; still they are smaller than the ones from their $I = 1$ partners.

availability[2]. With this argument in mind, we shall expect that the VVP and VJP operators are enough to provide a phenomenological description of the 4π channel with an adequate choice of the parameters.

5.3 Resonance Chiral Theory with several multiplets

The framework to build up an expression for the vector-vector current correlator in the resonance region is Resonance Chiral Theory, as it has been introduced in Section 4.2. As we tend to explore the $I = 1$ resonance region from 1 to 2 GeV, we need to extend the resonance Lagrangian defined in Eqs. (4.5) and (4.11) by including several vector multiplets $V = V_1, \ldots V_N$:

$$\mathcal{L}_{\rm R} \;=\; \sum_{V=V_1,\ldots V_N} \{\mathcal{L}_{\rm Kin}(V) + \mathcal{L}_2(V)\} + \mathcal{L}_R^{\rm odd}\,, \tag{5.1}$$

The kinetic terms $\mathcal{L}_{\rm Kin}(V)$ and the interaction Lagrangian $\mathcal{L}_2(V)$ have already been defined in Eqs. (4.6) and (4.7) respectively, and we shall consider different masses M_{V_i} and coupling constants F_{V_i}, G_{V_i} for each multiplet of vector resonances. The usual matrix notation will be employed for these fields:

$$V_1^{\mu\nu} = \frac{\vec{\lambda}}{\sqrt{2}}\,\vec{V}_1^{\mu\nu} = \begin{pmatrix} \frac{1}{\sqrt{2}}\rho^0 + \frac{1}{\sqrt{2}}\omega & \rho^+ & K^{*+} \\ \rho^- & -\frac{1}{\sqrt{2}}\rho^0 + \frac{1}{\sqrt{2}}\omega & K^{*0} \\ K^{*-} & \bar{K}^{*0} & -\phi \end{pmatrix}^{\mu\nu}\,, \tag{5.2}$$

and similarly for the other nonets ($\rho(1450)$ and $\rho(1700)$ belonging to multiplets 2 and 3 respectively, and so on). We have written Eq. (5.2) in terms of the physical states ω and ϕ, assuming ideal mixing between the singlet ω_1 and the octet ω_8 components.

The odd-intrinsic-parity Lagrangian,

$$\mathcal{L}_R^{\rm odd} = \mathcal{L}_{\rm VJP} + \mathcal{L}_{\rm VVP}\,, \tag{5.3}$$

is included to account for the 4π channel in the absorptive content of the vector-vector correlator, as commented in Section 5.2.

The extension of the even–intrinsic–parity interactions contained in $\mathcal{L}_2(V)$ to several multiplets is trivial. For the odd–intrinsic–parity sector, the linear terms which comprise interactions among one vector, one external vector source and one pseudoscalar ($\mathcal{L}_{\rm VJP}$, in Eq. (4.11)), can also be easily generalized to N distinct multiplets V_i by writing N sets of $\mathcal{O}^a_{\rm V_iJP}$ operators with different couplings $c_a^{(i)}$ $i = 1, \ldots N$ for each set:

$$\mathcal{L}_{\rm VJP} = \sum_i^N \sum_{a=1}^7 \frac{c_a^{(i)}}{M_{V_i}}\,\mathcal{O}^a_{\rm V_iJP}\,. \tag{5.4}$$

[2]This is strictly true only if the a_1 width is set to zero. This is far from being a good approximation [78], and we should introduce a q^2-dependent width in the a_1 propagator to account for its off-shell behaviour.

For the vector–vector–pseudoscalar sector $\mathcal{L}_{\rm VVP}$, the allowance of interactions among resonances of different multiplets enlarges the initial set defined in Eq. (4.10), which now reads:

VVP terms

$$\begin{aligned}
\mathcal{O}^1_{\rm VWP} &= \frac{1}{2}\Big(\epsilon_{\mu\nu\rho\sigma}\,\langle\,\{V^{\mu\nu},W^{\rho\alpha}\}\nabla_\alpha u^\sigma\,\rangle\,+\,\langle\,V\leftrightarrow W\,\rangle\Big)\,,\\
\mathcal{O}^2_{\rm VWP} &= i\,\epsilon_{\mu\nu\rho\sigma}\,\langle\,\{V^{\mu\nu},W^{\rho\sigma}\}\,\chi_-\,\rangle\,,\\
\mathcal{O}^3_{\rm VWP} &= \frac{1}{2}\Big(\epsilon_{\mu\nu\rho\sigma}\,\langle\,\{\nabla_\alpha V^{\mu\nu},W^{\rho\alpha}\}u^\sigma\,\rangle\,+\,\langle\,V\leftrightarrow W\,\rangle\Big)\,,\\
\mathcal{O}^4_{\rm VWP} &= \frac{1}{2}\Big(\epsilon_{\mu\nu\rho\sigma}\,\langle\,\{\nabla^\sigma V^{\mu\nu},W^{\rho\alpha}\}u_\alpha\,\rangle\,+\,\langle\,V\leftrightarrow W\,\rangle\Big)\,,\\
\mathcal{O}^5_{\rm VWP} &= \epsilon_{\mu\nu\rho\sigma}\,\langle\,\{V^{\mu\alpha},W^{\rho\sigma}\}\nabla_\alpha u^\nu\,\rangle\,-\,\langle\,V\leftrightarrow W\,\rangle\,,\\
\mathcal{O}^6_{\rm VWP} &= \epsilon_{\mu\nu\rho\sigma}\,\langle\,\{\nabla_\alpha V^{\mu\alpha},W^{\rho\sigma}\}u^\nu\,\rangle\,-\,\langle\,V\leftrightarrow W\,\rangle\,,
\end{aligned}\tag{5.5}$$

where V and W do not need to correspond to the same nonet. The operators $\mathcal{O}_{\rm VWP}$ have been written in a symmetric form to derive a master formula for the loop amplitudes from which results for the different resonance configurations can be obtained straightforwardly. For interactions among resonances of the same multiplet ($W\equiv V$) $\mathcal{O}^5_{\rm VVP}=0$ and $\mathcal{O}^6_{\rm VVP}=0$, thus reducing the number of independent VVP terms to four, and the basis of Eq. (4.10) is recovered. The VVP Lagrangian would be then defined as:

$$\mathcal{L}_{\rm VVP}=\sum_i^N\sum_{a=1}^4 d_a^{(i)}\,\mathcal{O}^a_{\rm V_iV_iP}+\sum_{i<j}^N\sum_{a=1}^6 d_a^{(ij)}\,\mathcal{O}^a_{\rm V_iV_jP}\,,\tag{5.6}$$

with the indices $i,j=1,\ldots N$ identifying the corresponding vector multiplets.

Keeping the three observed multiplets in the 1-2 GeV energy region, the number of operators introduced for the odd–intrinsic–parity–sector is 51; if we work just with the lowest-lying nonet only 11 remain. Moreover, in the later case the conditions among the odd-intrinsic-parity couplings of the first multiplet obtained in Section 4.3 by matching the short-distance behaviour of the vector-vector-pseudoscalar Green's function built from $\mathcal{L}_R^{\rm odd}$ with the OPE result further reduce the number of unknown constants for the lowest octet. Again, the set of operators that make up $\mathcal{L}_R^{\rm odd}$ is a complete basis for constructing vertices with only one pseudoscalar; for a larger number of pseudoscalars additional operators may emerge.

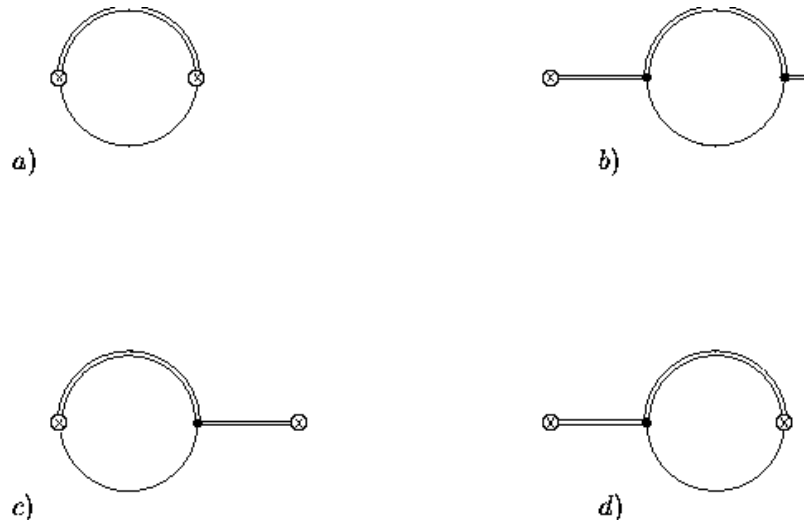

Figure 5.1: The vector-vector correlator topologies at 1-loop

5.4 The vector-vector correlator at one-loop

The main object of study in this work is the two-point function built from the I=1 part of the electromagnetic current,

$$\begin{aligned} \Pi^{33}_{\mu\nu}(q^2) &= i\int d^4x\, e^{iqx}\langle 0|\, T\,[\, V^3_\mu(x)\, V^3_\nu(0)\,]\,|0\rangle \\ &= (q_\mu q_\nu - q^2 g_{\mu\nu})\;\Pi(q^2)\,, \end{aligned} \tag{5.7}$$

with the vector current given by

$$V^3_\mu = \frac{\delta S^\chi_R}{\delta v^\mu_3}\,, \tag{5.8}$$

being S^χ_R the effective action associated to $\mathcal{L}_R + \mathcal{L}^{(2)}_\chi$, and the external vector field $v_\mu \equiv \frac{\lambda^a}{2} v^a_\mu$. Current conservation has been used to extract the tensor structure of the correlator in Eq. (5.7). The observable quantity we shall derive from the Π^{33} correlator is the inclusive hadronic cross section in the I=1 channel:

$$R^{\rm I=1}_{had} = \frac{\sigma^{\rm I=1}(e^+e^-\to hadrons)}{\sigma(e^+e^-\to\mu^+\mu^-)} = 12\,\pi\,{\rm Im}\,\Pi^{33}(q^2)\,.$$

At the 1-loop level and following the effective Lagrangian described in Section 5.3, two different types of absorptive terms contribute to the imaginary part of the correlator: loops with two pseudoscalars, arising from $\mathcal{L}_2(V)$ and $\mathcal{L}^{(2)}_\chi$, and loops with one internal resonance (Fig. 5.1), originated by $\mathcal{L}^{\rm odd}_R$; both can be attached to a ρ-like meson or directly to the V^3_μ currents to build up the correlator. Loops with only pseudoscalars have been previously considered in the literature (see e.g. [75], [76]), and we will turn to them when necessary. Other contributions, like the loop with two internal vector resonances arising from the kinetic term of the resonance Lagrangian

$\mathcal{L}_{\rm Kin}$, will not be not considered here; its absorptive part encodes information about the $2\pi^0\pi^+\pi^-$ channel, but its contribution to $\sigma(e^+e^- \to 2\pi^0\pi^+\pi^-)$ is very small in the 1 GeV region [63]. Moreover, loop contributions directly connected to the external currents will not enter in the resummation carried out in Section 5.6 and can be added to our correlator independently (as it also happens with the amplitude depicted in Fig. 5.1b). Let us focus now on the loops arising from the odd-intrinsic-parity couplings.

The four allowed topologies are shown in Fig. 5.1. Each of the resonance lines can belong to any of the vector multiplets, V_i, $i = 1, \dots N$. Therefore we have N^3 possible diagrams with topology a), N for b), and N^2 for both c) and d). We shall denote by $\mathcal{W}_0^{(ijk)}$, $\mathcal{W}_1^{(i)}$ and $\mathcal{W}_2^{(ij)}$ the invariant functions associated to the loops a), b) and c), respectively, with $i, j, k = 1, \dots N$ labelling the vector multiplets which enter the diagrams in order. Note that the invariant function for diagram d) is equal to that of diagram c) with multiplets $i\,, j$ interchanged. For each of these diagrams, we can still choose which resonance is running inside the loop among an ω, which will be accompanied by a π^0, and a charged or neutral K^*, with the corresponding $\overline{K}$. The five possibilities will be subscript-labelled in the scalar functions $\mathcal{W}$ with the character $P = \pi^0, K^+, K^-, K^0, \overline{K}^0$.

In terms of the invariant functions just introduced, the correlator built from the diagrams of Fig. 5.1, which we denote as $\Sigma^{\mu\nu}$, reads:

$$\Sigma^{\mu\nu} = (q^2 g^{\mu\nu} - q^\mu q^\nu) \sum_{P=\pi^0\,,K} \frac{C_P^2}{F^2} \left\{ \sum_{ijk}^{N} \frac{F_{V_i} F_{V_j}}{(M_{V_i}^2 - q^2)(M_{V_j}^2 - q^2)}\, \mathcal{W}_{0,P}^{(ijk)}(q^2) \right. \\ \left. + \sum_i \mathcal{W}_{1,P}^{(i)}(q^2) + \sum_{i,j} 4\, \frac{F_{V_i}}{(M_{V_i}^2 - q^2)}\, \mathcal{W}_{2,P}^{(ij)}(q^2) \right\}, \tag{5.9}$$

where the indices i, j, k refer to any of the three resonance nonets, with corresponding masses M_{V_i}. The constants C_P take the values

$$C_P \;\equiv\; \begin{cases} 2/\sqrt{3} & P = \pi^0 \\ 1 & P = K^+, K^- \\ -1 & P = K^0, \bar{K}^0 \end{cases} . \tag{5.10}$$

Full expressions for the functions $\mathcal{W}_{i,P}(q^2)$ can be found in Appendix A.

5.5 Regularization of the loop functions

The functions $\mathcal{W}_{i,P}(q^2)$ as calculated within perturbation theory are divergent quantities which need to be regularized. The expressions given for these functions in the Appendix A have been obtained following the $\overline{\rm MS}$ subtraction scheme. The

absorption of the infinities that arise is a rather involved task, as the renormalization of RχT remains an unexplored issue.

Alternatively, we can bypass the lack of a consistent renormalization procedure by using a dispersion technique to regularize the real part of the functions $\mathcal{W}_i$ from their well-defined imaginary parts. The number of subtraction constants needed depends on the behaviour of the spectral densities $\mathrm{Im}\,\mathcal{W}_i(q^2)$ at large q^2. Let us go on with the discussion by considering only the loops arising from the resonances of the lowest-lying nonet[3]. The associated spectral densities read:

$$\begin{aligned}
\mathrm{Im}\,\mathcal{W}_{0,P}(q^2) &= -\frac{2\,\lambda(q^2,m_P^2,M_V^2)}{M_V^2\,q^2}\,\Big\{(d_1+8d_2-d_3)m_P^2+d_3(M_V^2+q^2)\Big\}^2 \\
&\quad\times \mathrm{Im}\,B_0[q^2,M_V^2,m_P^2]\,, \\
\mathrm{Im}\,\mathcal{W}_{1,P}(q^2) &= -\frac{\lambda(q^2,m_P^2,M_V^2)}{M_V^4\,q^2}\Big\{(c_1+c_2+8c_3-c_5)m_P^2+(c_1-c_2+c_5)q^2 \\
&\quad+(-c_1+c_2+c_5-2c_6)M_V^2\Big\}^2\,\mathrm{Im}\,B_0[q^2,M_V^2,m_P^2]\,, \\
\mathrm{Im}\,\mathcal{W}_{2,P}(q^2) &= \frac{\lambda(q^2,m_P^2,M_V^2)}{\sqrt{2}M_V^3\,q^2}\,\Big\{(d_1+8d_2-d_3)m_P^2+d_3(M_V^2+q^2)\Big\} \\
&\quad\times\Big\{(c_1+c_2+8c_3-c_5)m_P^2+(c_1-c_2+c_5)q^2 \\
&\quad+(-c_1+c_2+c_5-2c_6)M_V^2\Big\}\,\mathrm{Im}\,B_0[q^2,M_V^2,m_P^2]\,. \qquad (5.11)
\end{aligned}$$

Quite remarkably, the combinations of odd–intrinsic–parity couplings appearing in $\mathrm{Im}\,\mathcal{W}_i$ get fixed by the short distance conditions, Eqs. (4.24). This fact has already been noticed in Ref. [79], where full predictions from the QCD matching were given to the tree-level diagrams which make up $\mathrm{Im}\,\mathcal{W}_i$ upon squaring. This is an important result in our work, meaning that we know all the analytic structure of the functions $\mathcal{W}_i$ except for a polynomial whose coefficients are the subtraction constants encoding our lack of knowledge on the renormalization procedure. The properly regularized dispersion relations are thus written as:

$$\begin{aligned}
\mathcal{W}_{0,P}(s) &= \sum_{k=0}^{3} a_0^{(k)}\,s^k+\frac{s^4}{\pi}\int_{(M_V+m_P)^2}^{\infty} ds'\frac{\mathrm{Im}\,\mathcal{W}_{0,P}(s')}{s'^4(s'-s)}\,, \\
\mathcal{W}_{1,P}(s) &= \sum_{k=0}^{1} a_1^{(k)}\,s^k+\frac{s^2}{\pi}\int_{(M_V+m_P)^2}^{\infty} ds'\frac{\mathrm{Im}\,\mathcal{W}_{1,P}(s')}{s'^2(s'-s)}\,, \\
\mathcal{W}_{2,P}(s) &= \sum_{k=0}^{2} a_2^{(k)}\,s^k+\frac{s^3}{\pi}\int_{(M_V+m_P)^2}^{\infty} ds'\frac{\mathrm{Im}\,\mathcal{W}_{2,P}(s')}{s'^3(s'-s)}\,. \qquad (5.12)
\end{aligned}$$

[3]We shall drop the labels $i=j=k=1$ from the $\mathcal{W}$ functions and from the masses and couplings of the first multiplet to simplify the notation throughout this section ($M_{V_1}\equiv M_V$, $c_a^{(1)}\equiv c_a$, $d_a^{(1)}\equiv d_a$).

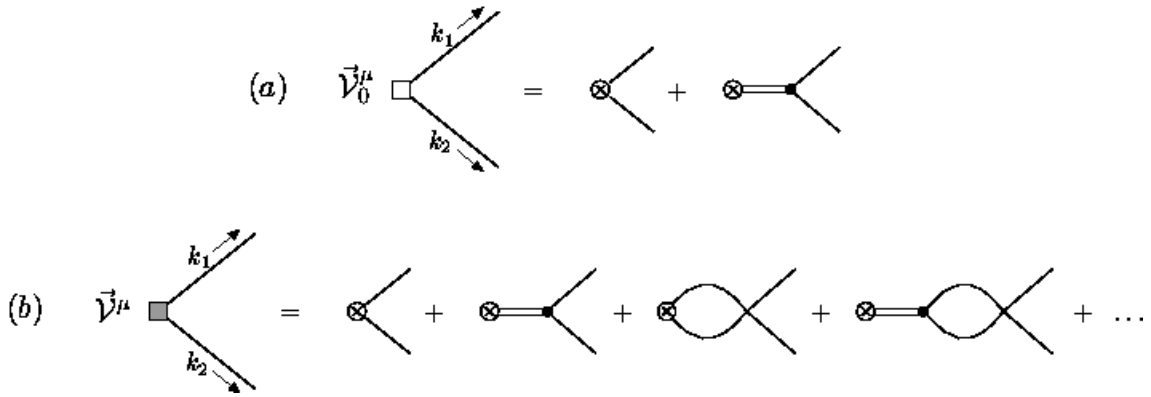

Figure 5.2: Definition of the off-shell effective current vertices

To end with this Section, let us briefly mention what happens in the case of several multiplets. The short distance conditions extracted from the VVP correlator with the lowest-lying octet do not longer apply and must be reanalyzed by extending the study of Ref. [79] beyond the single resonance saturation assumption. In addition, considering other relevant Green's functions may yield further constraints among the couplings of higher multiplets. These studies are, however, beyond the scope of this work.

5.6 Resummation of the 1-loop topologies

The bare resonances acquire a finite width through resummation of quantum loops in perturbation theory. These effects are subleading in the $1/N_C$ counting, but must be accounted for to avoid the singularities arising at energies close to the bare pole of resonance propagators. The way in which loop effects shift the position of the off-shell pole within perturbation theory clearly depends on the diagrams entering the summation. A satisfactory definition for the $\rho(770)$ width was given in [75] through the analysis of the vector-vector correlator $\Pi^{33}_{\mu\nu}$ built from the effective theory with the lowest resonance multiplet. Our case is more involved, as several resonances contribute to the same channel -$\rho(770), \rho(1450)$ and $\rho(1700)$- and loops can induce mixing effects among them, thus making the definition of an off-shell width for each individual resonance far from obvious. Instead, we shall avoid the ambiguities related with the latter by seeking a resummed expression for the full correlator, which contains the observable quantity we are interested in, $\mathrm{Im}\,\Pi(q^2)$. With this aim, we rely on the procedure followed by the authors of Ref. [76], who performed the Dyson-Schwinger summation of pseudoscalar loops in the vector form factor, and afterwards we will extend their limits of applicability by explicitly including the loops of Fig. 5.1 in the resummed expression. Let us first revisit the method of Ref. [76]. For the sake of clarity we restrict the derivation in this section to just one multiplet, and leave aside the general result for Appendix B.

The vector form factor is defined from the matrix element of production of two pseudoscalars ($P = \pi^+, K^+, K^0$) in the $I = 1$ channel:

$$\langle\, P(k_1)\bar{P}(k_2)|\, V_3^\mu \,|\, 0\rangle = (k_1 - k_2)^\mu\, \mathcal{F}^{(P)}(q^2)\,, \tag{5.13}$$

$$q = k_1 + k_2\,.$$

In the framework of Resonance Chiral Theory, this form factor can be perturbatively calculated. At leading order in $1/N_C$ (no loops), the result comes from the sum of diagrams in the r.h.s. of Fig. 5.2a, giving

$$\vec{\mathcal{F}}_0(q^2) \;\equiv\; \left(\begin{array}{c} \mathcal{F}_0^{(\pi)}(q^2) \\ \mathcal{F}_0^{(K)}(q^2) \\ \mathcal{F}_0^{(K^0)}(q^2) \end{array}\right) \;=\; \left\{1 \,+\, \frac{F_V G_V}{F^2}\,\frac{q^2}{M_V^2 - q^2}\right\} \left(\begin{array}{c} 1 \\ \frac{1}{2} \\ \frac{1}{2} \end{array}\right). \tag{5.14}$$

(We borrow the notation from [76], and define $\mathcal{F}_0$ and related quantities as a vector whose components correspond to the $\pi^+\pi^-$, K^+K^- and $K^0\bar{K}^0$ channels respectively). If pseudoscalars are off-shell we shall write the off-shell effective current vertex defined in Fig. 5.2a,

$$\vec{\mathcal{V}}_0^\mu = \left[\, \vec{\mathcal{F}}_0(q^2)\, P_T^{\mu\nu} + \vec{\mathcal{G}}_0(q^2)\, P_L^{\mu\nu} \,\right]\, (k_1 - k_2)_\nu\ , \tag{5.15}$$

in terms of the transverse and longitudinal Lorentz projectors, $P_T^{\mu\nu} = g^{\mu\nu} - \frac{q^\mu q^\nu}{q^2}$ and $P_L^{\mu\nu} = \frac{q^\mu q^\nu}{q^2}$ respectively, with

$$\vec{\mathcal{G}}_0(q^2) = \left(\begin{array}{c} 1 \\ \frac{1}{2} \\ \frac{1}{2} \end{array}\right).$$

The contraction $P_L^{\mu\nu}\,(k_1 - k_2)_\nu$ vanishes for both pseudoscalars on-shell, and Eq. (5.13) is restored.

Beyond the leading-N_C approximation, the absorptive cut with two pseudoscalars is the first to consider. The sequence of diagrams with an arbitrary number of pseudoscalar loops connected by resonance-exchange or through elastic rescattering, sketched in Fig. 5.2b, defines a resummed off-shell effective vertex $\vec{\mathcal{V}}^\mu$:

$$\vec{\mathcal{V}}^\mu = \left[\, \vec{\mathcal{F}}(q^2)\, P_T^{\mu\nu} + \vec{\mathcal{G}}(q^2)\, P_L^{\mu\nu} \,\right]\, (k_1 - k_2)_\nu\,. \tag{5.16}$$

It was first proved in [75] and afterwards in [76], than this sum is a geometrical series, which results in

$$\vec{\mathcal{F}}(q^2) \;=\; \frac{\vec{\mathcal{F}}_0(q^2)}{1 \,+\, \left(1 + \frac{2G_V^2}{F^2}\frac{q^2}{M_V^2 - q^2}\right)\frac{2q^2}{F^2}\,\overline{B}_{22}}\,, \tag{5.17}$$

with

$$\overline{B}_{22} \equiv B_{22}[\, q^2, m_\pi^2, m_\pi^2] + \frac{1}{2}\, B_{22}[\, q^2, m_K^2, m_K^2]\,. \tag{5.18}$$

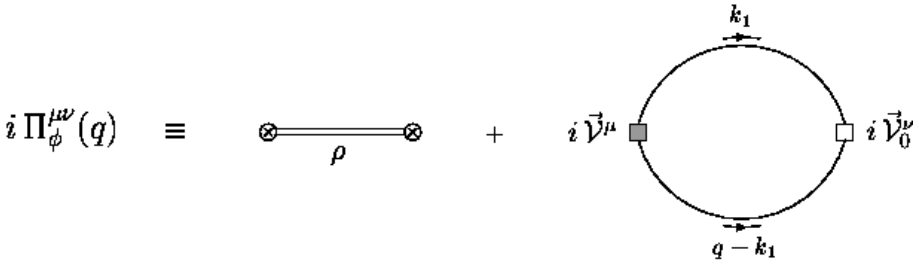

Figure 5.3: The $\Pi_\phi^{\mu\nu}(q)$ vector-vector correlator with resummed pseudoscalar loops

The $B_{22}[q^2, m^2, m^2]$ function has been defined in Appendix A. The factor

$$\left(1 + \frac{2G_V^2}{F^2}\frac{q^2}{M_V^2 - q^2}\right)\frac{2q^2}{F^2}\,, \tag{5.19}$$

appearing in the denominator of Eq. (5.17) is (up to a kinematic factor) the $\pi^+\pi^-$ elastic scattering amplitude in the $I = J = 1$ partial-wave (called $T^s_{\rm LO}$ in Ref. [76]).

The resummed expression for the off-shell effective vertex $\vec{\mathcal{V}}^\mu$ is all we need to perform the corresponding Dyson-Schwinger summation on the vector-vector correlator (see Fig. 5.3):

$$i\,\Pi_\phi^{\mu\nu}(q^2) = -i\,\Pi_0(q^2)\,q^2 P_T^{\mu\nu} + i\,\mathcal{I}^{\mu\nu}(q^2)\,, \tag{5.20}$$

$$\Pi_0(q^2) = \frac{F_V^2}{M_V^2 - q^2}\,, \tag{5.21}$$

$$\mathcal{I}^{\mu\nu}(q^2) = \sum_{P=\pi,K}\int\frac{d^4k_1}{i(2\pi)^4}\,\frac{\mathcal{V}^{\mu(P)}(k_1, q-k_1)\,\mathcal{V}_0^{\nu(P)}(k_1, q-k_1)}{(k_1^2 - m_P^2)\,[(q-k_1)^2 - m_P^2]}\,.$$

The first term in the r.h.s. of Eq. (5.20) is the tree level contribution of Fig. 5.3, and the integral arises when the pseudoscalar lines which come out the effective current vertices $\vec{\mathcal{V}}^\mu$ and $\vec{\mathcal{V}}_0^\mu$, are closed. The integration can be worked out easily:

$$\begin{aligned}
\mathcal{I}^{\mu\nu}(q^2) &= \sum_{P=\pi,K}\left[\,\mathcal{F}^{(P)}(q^2)\,P_T^{\mu\sigma} + \mathcal{G}^{(P)}(q^2)\,P_L^{\mu\sigma}\,\right]\left[\,\mathcal{F}_0^{(P)}(q^2)\,P_T^{\rho\nu} + \mathcal{G}_0^{(P)}(q^2)\,P_L^{\rho\nu}\,\right] \\
&\quad\times\int\frac{d^4k_1}{i(2\pi)^4}\,\frac{(2k_1-q)_\sigma(2k_1-q)_\rho}{(k_1^2 - m_\pi^2)\,[(q-k_1)^2 - m_\pi^2]} \\
&= \sum_{P=\pi,K}\left[\,\mathcal{F}^{(P)}\,P_T^{\mu\sigma} + \mathcal{G}^{(P)}\,P_L^{\mu\sigma}\,\right]\left[\,4B_{22}^{(P)}\,q^2\,P_{T,\sigma\rho} + \ldots\,P_{L,\sigma\rho}\,\right] \\
&\quad\times\left[\,\mathcal{F}_0^{(P)}\,P_T^{\rho\nu} + \mathcal{G}_0^{(P)}\,P_L^{\rho\nu}\,\right] \\
&= \sum_{P=\pi,K}\left[\,4B_{22}^{(P)}\,\mathcal{F}^{(P)}\mathcal{F}_0^{(P)}q^2 P_T^{\mu\nu} + \ldots P_L^{\mu\nu}\,\right]\,.
\end{aligned} \tag{5.22}$$

The off-shell form factors $\vec{\mathcal{G}}_0$, $\vec{\mathcal{G}}$ only contribute to the longitudinal component of the resummed function $\mathcal{I}^{\mu\nu}(q^2)$, which we do not need to compute. Recall that the correlator $\Pi^{\mu\nu}$ is transversal and therefore longitudinal pieces must cancel when all diagrams at a given order are considered. The resummed two-point function finally reads

$$\Pi_\phi(q^2) \;=\; \frac{\left(1 \,+\, \frac{F_V G_V}{F^2}\,\frac{q^2}{M_V^2-q^2}\right)^2}{1 \,+\, \left(1+\frac{2G_V^2}{F^2}\frac{q^2}{M_V^2-q^2}\right)\frac{2q^2}{F^2}\,\bar{B}_{22}}\,\left(-4\bar{B}_{22}\right) + \frac{F_V^2}{M_V^2-q^2}\;, \tag{5.23}$$

and agrees with the expression found in Ref. [75] after the constraints [49]

$$F_V G_V = F^2 \;\;,\;\; F_V = 2G_V\,,$$

are enforced in Eq. (5.23).

At this stage, it is rather easy to incorporate the resonance loops from the odd-intrinsic-parity Lagrangian, Fig. 5.1, in the resummed expression Eq. (5.23). Note that those loops have the structure of either a self energy correction of the ρ propagators, Fig. 5.1a, or a vertex-loop correction, Figs. 5.1b and 5.1c. We first analyse how the vector meson propagator gets modified by the effects of loops.

5.6.1 $\omega - \pi$ and $K^* - K$ loops in the ρ propagator

It is convenient for our purposes to write the free vector resonance propagator, within the antisymmetric formulation, in the following tensor basis:

$$\langle 0|T\{V_{\mu\nu}(x), V_{\rho\sigma}(y)\}|0\rangle = i\int \frac{d^4q}{(2\pi)^4} e^{-iq(x-y)}\left[\frac{2\mathcal{A}_{\mu\nu,\rho\sigma}}{M_V^2-q^2-i\varepsilon} + \frac{2\,\Omega^{\top}_{\mu\nu,\rho\sigma}}{M_V^2}\right], \tag{5.24}$$

with

$$\begin{aligned}
\mathcal{A}_{\mu\nu,\rho\sigma} &= \frac{1}{2q^2}\left(g_{\mu\rho}q_\nu q_\sigma - g_{\nu\rho}q_\mu q_\sigma - g_{\mu\sigma}q_\nu q_\rho + g_{\nu\sigma}q_\mu q_\rho\right)\,,\\
\Omega^{\top}_{\mu\nu,\rho\sigma} &= -\mathcal{A}_{\mu\nu,\rho\sigma} + \frac{1}{2}\left(g_{\mu\rho}g_{\nu\sigma} - g_{\mu\sigma}g_{\nu\rho}\right)\,.
\end{aligned}$$

The tensors $\mathcal{A}_{\mu\nu,\rho\sigma}$ and $\Omega^{\top}_{\mu\nu,\rho\sigma}$ are projectors, satisfying:

$$\begin{aligned}
\mathcal{A}_{\mu\nu,\rho\sigma}\Omega^{\top\rho\sigma}{}_{\alpha\beta} &= 0\,,\\
\mathcal{A}_{\mu\nu,\rho\sigma}\mathcal{A}^{\rho\sigma}{}_{\alpha\beta} &= \mathcal{A}_{\mu\nu,\alpha\beta}\;,\\
\Omega^{\top}_{\mu\nu,\rho\sigma}\Omega^{\top,\rho\sigma}{}_{\alpha\beta} &= \Omega^{\top}_{\mu\nu,\alpha\beta}\,.
\end{aligned} \tag{5.25}$$

The loop of Fig. 5.1a with resonance legs amputated, can also be decomposed in the same tensor basis

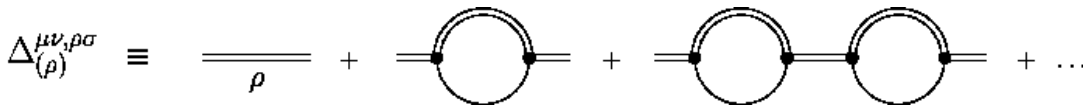

Figure 5.4: The ρ propagator with $\omega-\pi$ and K^*-K loop insertions

$$\mathcal{S}^{\mu\nu,\rho\sigma}_{0,P}(q^2) = \frac{\mathcal{W}_{0,P}(q^2)}{2}\,\mathcal{A}^{\mu\nu,\rho\sigma} + \frac{\mathcal{T}_{0,P}(q^2)}{2}\,\Omega^{\top\mu\nu,\rho\sigma}\,. \tag{5.26}$$

The orthogonality of the projectors $\mathcal{A}_{\mu\nu,\rho\sigma}$ and $\Omega^{\top}_{\mu\nu,\rho\sigma}$ guarantee that the Dyson-Schwinger summation shown in Fig. 5.4 holds independently for the invariant functions $\mathcal{W}_{0,P}$ and $\mathcal{T}_{0,P}$. The ρ propagator with an infinite number of $\omega-\pi$ and K^*-K loop insertions thus gives, in momentum space,

$$\Delta^{\mu\nu,\rho\sigma}_{(\rho)}(q^2) = 2\,i\mathcal{A}^{\mu\nu,\rho\sigma}\,\frac{1}{M_V^2 - q^2 + \mathcal{W}_0(q^2)} + 2\,i\,\Omega^{\top\mu\nu,\rho\sigma}\,\frac{1}{M_V^2 + \mathcal{T}_0(q^2)}\,, \tag{5.27}$$

The condensed notation

$$\mathcal{W}_0(q^2) = \sum_{P=\pi^0,K}\frac{C_P^2}{F^2}\,\mathcal{W}_{0,P}(q^2) \quad , \quad \mathcal{T}_0(q^2) = \sum_{P=\pi^0,K}\frac{C_P^2}{F^2}\,\mathcal{T}_{0,P}(q^2)\,. \tag{5.28}$$

collects all $\mathcal{W}_{0,P}$ functions.

The piece accompanying the $\Omega^{\top}_{\mu\nu,\rho\sigma}$ tensor does not contribute to the vector-vector correlator. The reason is that this piece vanishes when the ρ propagator is connected to two pseudoscalars, even if these are off-shell, and also when we attach the ρ to the external V_3^μ current, because the latter involves a derivative coupling and $\Omega^{\top}_{\mu\nu,\rho\sigma}$ satisfies that $q^\mu\Omega^{\top}_{\mu\nu,\rho\sigma} = 0$. Hence, from Eq. (5.27), we see that the effect of the inserted $\omega-\pi$ and K^*-K loops in the ρ propagators is just a shift of the position of the corresponding pole:

$$M_V^2 \to M_V^2 + \mathcal{W}_0(q^2)\,.$$

Making this replacement inside the propagators appearing in the vector form factors $\vec{\mathcal{F}}_0$ and $\vec{\mathcal{F}}$,

$$\vec{\mathcal{F}}(q^2) \;=\; \frac{\vec{\mathcal{F}}_0}{1 + \left(1 + \frac{2G_V^2}{F^2}\frac{q^2}{M_V^2 - q^2 + \mathcal{W}_0(q^2)}\right)\frac{2q^2}{F^2}\,\bar{B}_{22}}\,, \tag{5.29}$$

$$\vec{\mathcal{F}}_0(q^2) \;=\; \left\{1 + \frac{F_V G_V}{F^2}\,\frac{q^2}{M_V^2 - q^2 + \mathcal{W}_0(q^2)}\right\}\begin{pmatrix} 1 \\ \frac{1}{2} \\ \frac{1}{2}\end{pmatrix}\,, \tag{5.30}$$

the expression for the two point-function with pseudoscalar mesons $\Pi_\phi(q^2)$, Eq. (5.23), automatically incorporates the loops of Fig. 5.1a inserted in all possible ways. The result, together with the vertex loop corrections, is given below, Eq. (5.34).

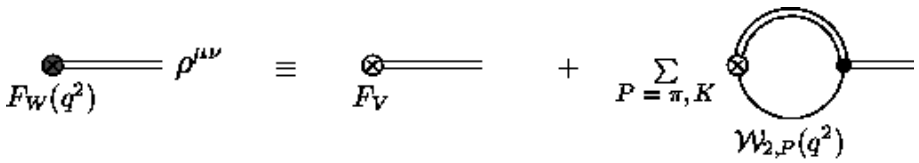

Figure 5.5: The vertex loop correction

5.6.2 Vertex loop corrections

Let us now turn over to the effects of the loops of Fig. 5.1c and Fig. 5.1d. These loops represent corrections to the coupling of the ρ resonance to the external current. The modified Feynman rule for a ρ resonance connected to a V_3^μ external current including the loop correction comes up from the sum of diagrams in Fig. 5.5:

$$iV_3^\mu|\rho\rangle = \left\{F_V + 2\sqrt{2}\sum_{P=\pi^0,K}\frac{C_P^2}{F^2}\,\mathcal{W}_{2,P}(q^2)\right\} q_\alpha\, g^\mu{}_\beta\,|\rho^{\alpha\beta}\rangle\,. \tag{5.31}$$

We observe that defining a q^2-dependent coupling to the external current,

$$F_W(q^2) = F_V + 2\sqrt{2}\sum_{P=\pi^0,K}\frac{C_P^2}{F^2}\,\mathcal{W}_{2,P}(q^2)\,, \tag{5.32}$$

the effect of the vertex loop correction translates directly to the tree level form factor $\vec{\mathcal{F}}_0$ (5.14), and to the tree level 2-point function $\Pi_0(q^2)$, Eq. (5.21):

$$\begin{aligned}
\vec{\mathcal{F}}_0(q^2) \;&\Longrightarrow\; \left\{1 + \frac{F_W(q^2)\,G_V}{F^2}\,\frac{q^2}{M_V^2-q^2}\right\}\begin{pmatrix}1\\ \frac{1}{2}\\ \frac{1}{2}\end{pmatrix}\,,\\
\Pi_0(q^2) \;&\Longrightarrow\; \frac{F_W^2(q^2)}{M_V^2-q^2}\,,
\end{aligned} \tag{5.33}$$

and, hence, to the resummed correlator $\Pi_\phi(q^2)$, Eq. (5.23).

Including both the vertex loop corrections and the $\omega-\pi$ and K^*-K loops, we finally obtain a analytical expression for the $\Pi(q^2)$ two-point function which accounts for both the pseudoscalar loops and the two-particle absorptive cuts emerged from the odd-intrinsic-parity sector:

$$\begin{aligned}
\Pi(q^2) \;=\; & \frac{\left(1 + \frac{F_W(q^2)G_V}{F^2}\,\frac{q^2}{M_V^2-q^2+\mathcal{W}_0}\right)^2}{1 + \left(1+\frac{2G_V^2}{F^2}\frac{q^2}{M_V^2-q^2+\mathcal{W}_0}\right)\frac{2q^2}{F^2}\,\bar{B}_{22}}\left(-4\bar{B}_{22}\right) + \frac{F_W^2(q^2)}{M_V^2-q^2+\mathcal{W}_0}\\
& + \sum_{P=\pi^0,K}\frac{C_P^2}{F^2}\,\mathcal{W}_{1,P}(q^2)\,.
\end{aligned} \tag{5.34}$$

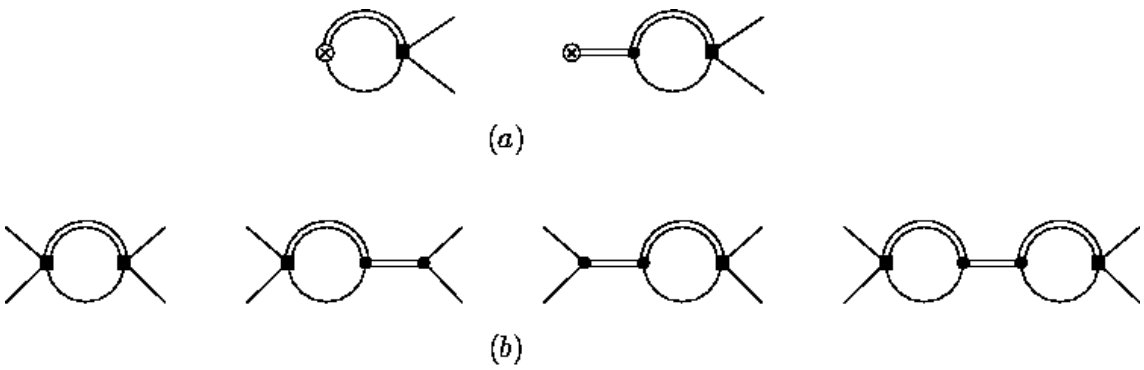

Figure 5.6: Loops arising from the V3P vertices. Diagrams in (a) modify the tree-level form factor $\vec{\mathcal{F}}_0$, while those of (b) represent corrections to the tree-level pseudoscalar scattering

5.7 Missing contributions

Going beyond 1-loop level, we can find contributions which have not been included in the resummed expression (5.34) derived in last section. Two different sources of missing terms with similar absorptive content as our previous results may be considered.

5.7.1 Direct vertices V3P

These terms mix a loop with two pseudoscalars with a $\omega - \pi$ or a $K^* - K$ loop when plugged inside the correlator. The importance of the V3P direct vertices has been pointed out in Section 4.4. There it was shown that the decay $\omega \to 3\pi$ is not dominated by the intermediate ρ-exchange (VMD hypothesis), but rather the local contributions compete in size with the $\rho\omega\pi$ couplings. Accordingly, we find no reason to neglect the $\pi\pi \to \omega\pi$ scattering vertices with respect the $\rho \to \omega\pi$ ones already included in the perturbative calculation of the vector form factor and the correlator.

The operators responsible for the V3P vertices also belong to the odd–intrinsic–parity–sector, but a complete basis in the antisymmetric formulation has not been written down to the best of our knowledge. The terms can be derived from the VJP terms introduced in Eq. (4.9), substituting the external vector source $f_+^{\mu\nu}$ by $[u^\mu, u^\nu]$, and thus they are of the same order in the chiral counting. Important information about the values of their couplings could be extracted by studying the four-point function $\langle \mathrm{VPPP} \rangle$ for instance, following the methodology employed in Chapter 4 for the $\langle \mathrm{VPP} \rangle$ correlator. The list of operators and the later study will be given elsewhere [81]. Let us, nevertheless, explain how these new contributions would enter in the resummation of Section 5.6 .

The loops arising from these V3P vertices which are relevant for the resummation are displayed in Fig. 5.6. The diagrams in the first line are connected to the external

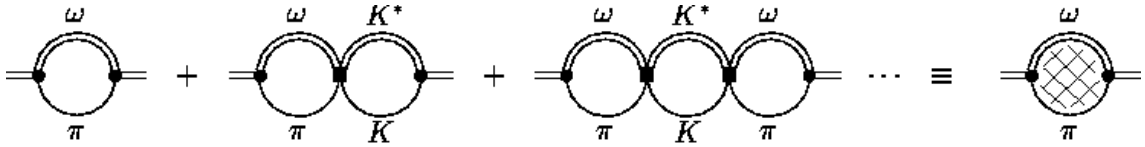

Figure 5.7: Missing contributions generated by the $\omega\pi \to K^*K$ vertices. The resonance-legs at the edges can be substituted by two pseudoscalars to give additional contributions

V_μ^3 current, and should be added to the tree level form factor defined in Eq. (5.15), thus modifying $\vec{\mathcal{F}}_0$. Diagrams in the second line represent loop corrections to the tree-level two-pseudoscalar scattering vertex defined in [76] by the sum of the $\mathcal{L}_\chi^{(2)}$ contribution plus the resonance exchange. The corresponding s-channel $I = J = 1$ partial-wave amplitude, Eq. (5.19), of LO in $1/N_C$, gets thus modified by the NLO terms above. Injecting the new partial-wave amplitude in the resummation procedure of Ref. [76] yields a new expression for $\vec{\mathcal{F}}$ (and consequently for $\Pi_{\mu\nu}^{33}$) which accounts for these new features.

5.7.2 $\omega\pi \to K^*K$ vertices

These vertices originate from the kinetic term $\mathcal{L}_{\rm Kin}(V)$ of the resonance Lagrangian and give rise to direct interaction among $\omega - \pi$ and $K^* - K$ loops, as shown in Fig. 5.7 Note that a vertex $\omega\pi \to \omega\pi$ (equivalently $K^*K \to K^*K$) does not show up when expanding $\mathcal{L}_{\rm Kin}(V)$, and thus the $\omega\pi$ loop can only be joined to a K^*-K and vice versa. This characteristic feature means that these contributions are not present if kaons are switched off from the theory. Zweig's rule predicts that the $I = 1$ ρ-resonances decays into kaons should be very much suppressed with respect to non-strange decay channels. The latter is confirmed experimentally, and therefore leaving aside intermediate states of kaons should not affect the $\sigma(e^+e^- \to \text{hadrons})$ description proposed in this work.

The Dyson-Schwinger summation sketched in Fig. 5.7 defines a dressed $\omega - \pi$ loop which would replace the bare one already included in our $\Pi(q^2)$ expression (and similarly for the K^*K loop). This is enough to account for the new loops. We should note, however, that the diagrammatic sum of Fig. 5.7 cannot be easily performed due to the non-trivial structure of the $\omega\pi \to K^*K$ vertices, thus requiring a careful study not performed here.

The kinetic term is also a source of $\rho\rho \to \pi\pi$ vertices, which produce loop contributions with two internal vector resonances attached to two pseudoscalars or directly to the external current. As commented in Section 5.4. the absorptive part of these loops is highly supressed due to phase space availability.

To be consistent, the inclusion of the VVPP vertices coming from the $\mathcal{L}_{\rm Kin}(V)$ piece in our analysis would demand that all the chiral allowed VVPP operators (with the same chiral counting) were built in the resonance Lagrangian.

5.8 Conclusions

We have presented in this work the first stage of a rather ambitious project. Our goal is to provide a description of the hadronic cross section in the resonance region using the effective realization of QCD at those energies, and well-known features from the phenomenology. Following the optical theorem we extract $\sigma(e^+e^- \to \text{hadrons})$ from the imaginary part of the two-point function built from the I=1 part of the electromagnetic current ($\Pi^{33}_{\mu\nu}$). We focus on the I=1 part of this observable, since resonances in this channel are broad and it is crucial to keep under control their off-shell behaviour beyond the *ad hoc* assumptions of conventional parameterizations.

The framework has been set up above. We rely on RχT and we add two extra vector nonets to account for the $\rho(1450)$ and $\rho(1700)$ resonances, which characterize the hadronic spectrum between 1 and 2 GeV. The perturbative evaluation within the effective theory has been improved with respect to previous works on the pion vector form factor by including $\omega - \pi$ and $K^* - K$ resonance loops whose absorptive part is related with the intermediate states $2\pi^0\pi^+\pi^-$ and $K\overline{K}\pi$, respectively. The vertices that generate the aforementioned loops belong to the odd–intrinsic–parity sector and had been generalized to allow interactions among different multiplets.

We have proved that the series of $\omega - \pi$ loop insertions in ρ propagators can be summed up into an analytic expression which also includes loops with two pseudoscalars, already accounted for in previous works. The new loops modify the off-shell width of ρ propagators and hence the vector form factor and the $\Pi(q^2)$ correlator, for which we have given complete expressions in this work.

Several issues must be addressed before we can make use of the expressions obtained above. First, the number of couplings introduced through the VJP and VVP terms of the odd–intrinsic–parity Lagrangian for the three proposed nonets is too large to handle, even if we plan to fit the data in the 1-2 GeV energy region. The study of relevant Green's functions and the comparison with short-distance QCD, as done in the analysis of the VVP three-point Green's function for the lowest-lying octet in Chapter 4, may yield additional information on the remaining couplings. This method appears as a very promising way to enforce the QCD requirements in the low-energy interactions, and should be pushed forward in future works. Alternatively, the relative strength of the odd–intrinsic–parity interactions among multiplets might be inferred by careful comparison with the available experimental information, thus allowing to neglect some terms from the beginning.

Restricting our work by the lowest meson dominance hypothesis, which may be a good approximation for energies below the $\rho(1450)$, our knowledge on the odd–intrinsic–parity–couplings of the first multiplet does not allow us, however, to have full predictive power in our results, since the subtraction constants of the regularization procedure remain as free parameters. Progress in this direction does not seem clear, as we would need to deal first with the renormalization of RχT.

In addition, the missing V3P vertices cannot be ignored and must be included in the resummation procedure to complete our work. As explained, this is feasible,

but introduces new unknown couplings that will require further investigations on the asymptotic behaviour of the relevant Green's functions.

Appendices

A Expressions for the 1-loop functions

The 1-loop diagrams collected in this Appendix have been regularized within dimensional regularization in D dimensions and $\Delta = 2\mu^{D-4}/(D-4) + \gamma_E - \ln(4\pi)$, with μ the renormalization scale. The following scalar one-point and two-point functions will appear in the 1-loop amplitudes:

$$\begin{aligned}
A_0[m^2] &= \int \frac{d^D\ell}{i(2\pi)^D}\,\frac{1}{\ell^2-m^2} = -\frac{m^2}{16\pi^2}\left(\Delta + \ln\frac{m^2}{\mu^2} - 1\right) \\
B_0[q^2,M^2,m^2] &= \int \frac{d^D\ell}{i(2\pi)^D}\,\frac{1}{[\ell^2-M^2]\,[(\ell+q)^2-m^2]} \\
&= -\frac{1}{16\pi^2}\left[\Delta - 2 + \frac{q^2-M^2+m^2}{2q^2}\,\ln\frac{m^2}{\mu^2} + \frac{q^2+M^2-m^2}{2q^2}\,\ln\frac{M^2}{\mu^2}\right. \\
&\qquad -\frac{\lambda^{1/2}(q^2,m^2,M^2)}{2q^2}\,\ln\frac{q^2-m^2-M^2-\lambda^{1/2}(q^2,m^2,M^2)}{q^2-m^2-M^2+\lambda^{1/2}(q^2,m^2,M^2)} \\
&\qquad \left. -i\pi\,\frac{\lambda^{1/2}(q^2,m^2,M^2)}{q^2}\right] \quad , \quad q^2 > (m+M)^2\,, \qquad \text{(A.5.1)}
\end{aligned}$$

where $\lambda(x,y,z) = (x-y-z)^2 - 4yz$. Also the loop function $B_{22}[q^2,m^2,m^2]$ has been used in the text; it is defined from the tensor two-point function

$$\int \frac{d^D\ell}{i(2\pi)^D}\,\frac{\ell^\mu\ell^\nu}{[\ell^2-m^2]\,[(\ell-q)^2-m^2]} \equiv B_{21}[q^2,m^2,m^2]q^\mu q^\nu + q^2 B_{22}[q^2,m^2,m^2]g^{\mu\nu}$$

with

$$q^2\,B_{22}[q^2,m^2,m^2] = \frac{1}{D-1}\left[\frac{A_0[m^2]}{2} + \left(m^2 - \frac{q^2}{4}\right)B_0[q^2,m^2,m^2]\right], \qquad \text{(A.5.2)}$$

written in terms of the scalar functions introduced above.

The functions $\mathcal{W}_{i,P}(q^2)$ only depend on the mass of the internal resonance, which we shall denote as M instead of M_{V_i} to shorten the notation of this Appendix, and on the pseudoscalar mass running inside the loop, called m in what follows.

The function $\mathcal{W}_{0,P}^{(ijk)}$ correspond to the diagram of Fig. 5.1a with resonance legs amputated, and has been defined in Eq. (5.9), (see also Eq. (5.26) for the tensor decomposition). Let us give the general result for multiplets i and k in the external legs and multiplet j running inside, with $i \neq j$ and $j \neq k$.

$$\mathcal{W}_{0,P}^{(ijk)} = \frac{(2\pi)^{D-4}}{4\,M^2\,q^2}\Big\{\mathcal{C}_0 + A_0[m^2]\,\mathcal{C}_m + A_0[M^2]\,\mathcal{C}_M + B_0[q^2,M^2,m^2]\,\mathcal{C}_B\Big\}, \quad \text{(A.5.3)}$$

$$d_n \equiv d_n^{(ij)} \qquad , \qquad \widetilde{d}_n \equiv d_n^{(jk)}$$

$$\begin{aligned}
\mathcal{C}_0 \;=\; & \frac{2}{3}\,q^8\;\Big\{\;\frac{d_3}{2}\,(\widetilde{d}_3+4\widetilde{d}_5-4\widetilde{d}_6)+2\,d_5\,(\widetilde{d}_5-2\,\widetilde{d}_6)+2\,d_6\,\widetilde{d}_6\;\Big\}\\
& +\frac{2}{3}\,q^6\;\Big\{\;\Big[-\frac{d_3}{2}\,(5\widetilde{d}_3+16\,\widetilde{d}_5)-6\,d_5\;\widetilde{d}_5+(\;d_1\;+8\,d_2\;)\,(\widetilde{d}_3+2\,\widetilde{d}_5-2\,\widetilde{d}_6)\\
& \qquad +2(4\,d_3\;+6\,d_5\;-6\,d_6\;)\,\widetilde{d}_6\Big]\,m^2\;-\Big[\,10\,d_5\,(\widetilde{d}_5-2\,\widetilde{d}_6)+10\,d_6\,\widetilde{d}_6\\
& \qquad +\frac{d_3}{2}\,(\widetilde{d}_3+12\,\widetilde{d}_5-12\,\widetilde{d}_6)\Big]\,M^2\;\Big\}\\
& +\frac{q^4}{6}\;\Big\{\;\Big[\,128\,d_2\,(\,\widetilde{d}_2-\widetilde{d}_3)+\;\frac{d_3}{2}\,(37\,\widetilde{d}_3-18\,\widetilde{d}_4)-\frac{9}{2}\,d_4\,\widetilde{d}_4+(-192\,d_2\;+60\,d_3\\
& \qquad +36\,d_5\,)\,\widetilde{d}_5+6\,(32\,d_2\;-7\,d_3\;+3\,d_4\;-12\,d_5\;+3\,d_6\,)\,\widetilde{d}_6+2\,d_1\,(\,\widetilde{d}_1\\
& \qquad +16\,\widetilde{d}_2-8\,\widetilde{d}_3-12\,\widetilde{d}_5+12\,\widetilde{d}_6\,)\,\Big]\,m^4\;-8\,\Big[\,\frac{d_3}{2}\,(\widetilde{d}_3-8\,\widetilde{d}_5)-6\,d_5\,\widetilde{d}_5\\
& \qquad +(\;d_1\;+8\,d_2\,)(\widetilde{d}_3+4\,\widetilde{d}_5-4\,\widetilde{d}_6)+2(\;2\,d_3\;+6\,d_5\;-3\,d_6\,)\,\widetilde{d}_6\,\Big]\,M^2\,m^2\\
& \qquad -2\Big[\,28\,d_5\,(\,\widetilde{d}_5-2\,\widetilde{d}_6)-28\,d_6\,\widetilde{d}_6+\frac{9}{2}\,d_1\,(\,\widetilde{d}_1+4\,\widetilde{d}_5-4\,\widetilde{d}_6)\\
& \qquad +\frac{d_3}{2}\,(\,\widetilde{d}_3-28\,\widetilde{d}_5+28\,\widetilde{d}_6\,)\Big]\,M^4\;\Big\}\\
& -q^2\;\Big\{\;\Big[\,16\,d_2\,(\,4\,\widetilde{d}_2-\widetilde{d}_3)+d_3\,\widetilde{d}_3+\frac{3}{2}(-16\,d_2\;+2\,d_3\;+\;d_4\,)\,\widetilde{d}_4+6\,(\,8\,d_2\;-\;d_3\\
& \qquad -\,d_4\;+d_5\,)\,\widetilde{d}_5+\;d_1\,(\,\widetilde{d}_1+16\,\widetilde{d}_2-2\,\widetilde{d}_3-3\,\widetilde{d}_4+6\,\widetilde{d}_5\,)\Big]\,m^6\\
& \qquad +\Big[\,\frac{1}{2}\,d_3\,\widetilde{d}_3+d_1\,(\,\widetilde{d}_1+16\,\widetilde{d}_2-4\,\widetilde{d}_5+4\,\widetilde{d}_6\,)+2\,d_3\,(\,\widetilde{d}_6-\widetilde{d}_5\,)\\
& \qquad +32\,d_2\,(\,2\widetilde{d}_2-\;\widetilde{d}_5+\widetilde{d}_6\,)+6\,d_5\,(\,\widetilde{d}_5-2\,\widetilde{d}_6\,)+6\,d_6\,\widetilde{d}_6\,\Big]\,M^2\,m^4\\
& \qquad +\Big[\,\frac{1}{2}\,d_3\,\widetilde{d}_3+4\,d_5\,\widetilde{d}_5-8\,d_2\,(\,\widetilde{d}_3+4\,\widetilde{d}_5-4\,\widetilde{d}_6\,)-4(\,2\,d_5\;-\;d_6\,)\,\widetilde{d}_6\\
& \qquad +\frac{d_1}{2}\,(\,3\,\widetilde{d}_1+48\,\widetilde{d}_2-2\,\widetilde{d}_3-8\,\widetilde{d}_5+8\,\widetilde{d}_6\,)\Big]\,M^4\,m^2+\Big[\,\frac{3}{2}\,d_1\,(\,\widetilde{d}_1-4\,\widetilde{d}_5
\end{aligned}$$

$$+2\,\widetilde{d}_6\,) - \frac{d_3}{2}\,(\,\widetilde{d}_3 - 4\,\widetilde{d}_5 + 4\,\widetilde{d}_6\,) + 4\,d_5\,(\,\widetilde{d}_5 - 2\,\widetilde{d}_6\,) + 4\,d_6\,\widetilde{d}_6\,\Big]\,M^6\,\Big\}$$

$$+\,\Big\{\,d_n \leftrightarrow\,\widetilde{d}_n\,\Big\}\,, \tag{A.5.4}$$

$$\begin{aligned}
\mathcal{C}_m \;=\;& 2\,q^6\,\Big\{\;\frac{d_3}{2}\,(\,\widetilde{d}_3 + 4\,\widetilde{d}_5 - 4\,\widetilde{d}_6\,) + 2\,d_5\,(\,\widetilde{d}_5 - 2\,\widetilde{d}_6\,) + 2\,d_6\,\widetilde{d}_6\,\Big\} \\
&+ q^4\,\Big\{\;\Big[-\frac{d_3}{2}\,(\,11\,\widetilde{d}_3 + 6\,\widetilde{d}_4 + 24\,\widetilde{d}_5\,) - \frac{3}{2}\,d_4\,\widetilde{d}_4 - 8\,d_5\,\widetilde{d}_5 + 2\,(\,d_1 + 8\,d_2\,) \\
&\qquad \times(\,\widetilde{d}_3 + 2\,\widetilde{d}_5 - 2\,\widetilde{d}_6\,) + \,2\,(\,9\,d_3 + 3\,d_4 + 8\,d_5 - 7\,d_6\,)\,\widetilde{d}_6\,\Big]\,m^2 \\
&\qquad +2\,\Big[\,\frac{d_3}{2}\,(\,\widetilde{d}_3 - 4\,\widetilde{d}_5 + 4\,\widetilde{d}_6\,) - 6\,d_5\,(\,\widetilde{d}_5 - 2\,\widetilde{d}_6\,) - 6\,d_6\,\widetilde{d}_6\,\Big]\,M^2\,\Big\} \\
&- 2\,q^2\,\Big\{\;\Big[\,\frac{d_1}{2}\,(\,5\,\widetilde{d}_1 + 80\,\widetilde{d}_2 - 12\,\widetilde{d}_3 - 6\,\widetilde{d}_4 + 8\,\widetilde{d}_5 + 4\,\widetilde{d}_6\,\Big] + 8\,d_2\,(\,20\,\widetilde{d}_2 - 6\,\widetilde{d}_3 \\
&\qquad -3\,\widetilde{d}_4 + 4\,\widetilde{d}_5 + 2\,\widetilde{d}_6\,) + \frac{d_3}{2}\,(7\,\widetilde{d}_3 + 6\,\widetilde{d}_4 - 8\,\widetilde{d}_5 - 4\,\widetilde{d}_6\,) + \frac{3}{2}\,d_4\,(\,\widetilde{d}_4 \\
&\qquad -4\,\widetilde{d}_5\,)\,\Big]\,m^4 \;-\; \Big[\,-4(\,d_1 + 8\,d_2 - d_5\,)(\,\widetilde{d}_5 - \widetilde{d}_6\,) + \frac{d_3}{2}\,(\,5\widetilde{d}_3 - 4\,\widetilde{d}_5 \\
&\qquad +4\,\widetilde{d}_6\,) + 2\,d_6\,\widetilde{d}_6\,\Big]\,M^2\,m^2 \;+\; \Big[\,\frac{d_3}{2}\,(\,\widetilde{d}_3 + 4\,\widetilde{d}_5 - 4\,\widetilde{d}_6\,) \\
&\qquad -6\,d_5\,(\,\widetilde{d}_5 - 2\,\widetilde{d}_6\,) - 6\,d_6\,\widetilde{d}_6\,\Big]\,M^4\,\Big\} \\
&+ 2\,(m^2 - M^2)\,\Big\{\,\Big[\,\frac{d_1}{2}\,(\,\widetilde{d_1} + 16\,\widetilde{d_2} - 2\,\widetilde{d_3}\,) + 4\,d_2\,(\,\widetilde{d}_2 - 2\,\widetilde{d}_3\,) + \frac{1}{2}d_3\,\widetilde{d}_3\,\Big]\,m^4 \\
&\qquad +\Big[\,\frac{1}{2}\,(d_1 + 8\,d_2 - d_3\,)(\,\widetilde{d}_3 - 4\,\widetilde{d}_5 + 4\,\widetilde{d}_6\,) - \frac{1}{2}d_3\,\widetilde{d}_3\,\Big]\,m^2\,M^2 \\
&\qquad +\Big[\,\frac{d_3}{2}\,(\widetilde{d}_3 - 4\,\widetilde{d}_5 + 4\,\widetilde{d}_6\,) + 2\,d_5\,(\,\widetilde{d}_5 - 2\,\widetilde{d}_6\,) + 2\,d_6\,\widetilde{d}_6\,\Big]\,M^4\,\Big\} \\
&+\,\Big\{\,d_n \leftrightarrow\,\widetilde{d}_n\,\Big\}\,,
\end{aligned} \tag{A.5.5}$$

$$\begin{aligned}
\mathcal{C}_M \;=\;& 2\,q^6\,\Big\{\;\frac{d_3}{2}\,(\,\widetilde{d}_3 + 4\,\widetilde{d}_5 - 4\,\widetilde{d}_6\,) + 2\,d_5\,(\,d_5 - 2\,\widetilde{d}_6\,) + 2\,d_6\,\widetilde{d}_6\Big\} \\
&+ q^4\,\Big\{\;\Big[-\frac{d_3}{2}\,(\,3\,\widetilde{d}_3 - 8\,\widetilde{d}_5\,) + (\,d_1 + 8\,d_2\,)(\,\widetilde{d}_3 + 2\,\widetilde{d}_5 - 2\,\widetilde{d}_6\,) + 2\,(\,2\,d_3 \\
&\qquad +2\,d_5 - d_6\,)\,\widetilde{d}_6\,\Big]\,m^2 \;+\; \Big[\,-2\,d_5\,(\,\widetilde{d}_5 - 2\,\widetilde{d}_6\,) - 2\,d_6\,\widetilde{d}_6 + \frac{3}{2}\,d_1\,(\,\widetilde{d}_1 + 4\widetilde{d}_5
\end{aligned}$$

$$
\begin{aligned}
&-4\,\widetilde{d}_6\,)-4\,d_3\,(\,\widetilde{d}_5-\widetilde{d}_6\,)\Big]\,M^2\Big\}\\
&+q^2\,\Big\{\,\Big[16\,d_2\,(\,2\,\widetilde{d}_2-\widetilde{d}_3-\widetilde{d}_5+\widetilde{d}_6\,)+\frac{d_3}{2}\,(\,3\,\widetilde{d}_3+4\,\widetilde{d}_5-4\,\widetilde{d}_6\,)+\frac{d_1}{2}\,(\,\widetilde{d}_1+16\,\widetilde{d}_2\\
&-4\,\widetilde{d}_3-4\,\widetilde{d}_5+4\,\widetilde{d}_6\,)\Big]\,m^4\,+\Big[\,\frac{3}{2}\,d_1\,(\,\widetilde{d}_1+16\,\widetilde{d}_2\,)-(\,2\,d_1+16\,d_2\\
&+3\,d_3\,)\,\frac{\widetilde{d}_3}{2}+4\,d_5\,(\,\widetilde{d}_5-2\,\widetilde{d}_6\,)+4\,d_6\,\widetilde{d}_6\Big]\,M^2\,m^2\,+\,\Big[\,4\,d_3\,(\,\widetilde{d}_5-\widetilde{d}_6\,)\\
&+\frac{3}{2}\,d_1\,(\,\widetilde{d}_1-4\,\widetilde{d}_5+4\,\widetilde{d}_6\,)-2\,d_5\,(\,\widetilde{d}_5-2\,\widetilde{d}_6\,)-2\,d_6\,\widetilde{d}_6\Big]\,M^4\Big\}\,q^2\\
&-2\,(m^2-M^2)\Big\{\,\Big[\,\frac{d_1}{2}\,(\,\widetilde{d}_1+16\,\widetilde{d}_2-2\,\widetilde{d}_3\,)+8\,d_2\,(\,4\,\widetilde{d}_2-\widetilde{d}_3\,)+\frac{1}{2}\,d_3\,\widetilde{d}_3\Big]\,m^4\\
&+\Big[\,\frac{1}{2}\,(\,2\,d_1+16\,d_2-d_3\,)(\,\widetilde{d}_3-2\,\widetilde{d}_5+2\,\widetilde{d}_6\,)-\frac{1}{2}\,d_3\,\widetilde{d}_3\Big]\,m^2\,M^2\\
&+\Big[\,\frac{1}{2}\,d_3\,(\,\widetilde{d}_3-4\,\widetilde{d}_5+4\,\widetilde{d}_6\,)+2\,d_5\,(\,\widetilde{d}_5-2\,\widetilde{d}_6\,)+2\,d_6\,\widetilde{d}_6\Big]\Big\}\\
&+\Big\{\,d_n\leftrightarrow\,\widetilde{d}_n\,\Big\}\,,
\end{aligned}
\tag{A.5.6}
$$

$$
\begin{aligned}
\mathcal{C}_B\;\;=\;\;&-2\,\lambda(q^2,m^2,M^2)\,\Big[\,(\,d_1+8\,d_2-d_3\,)\,m^2\,+\,d_3\,(\,M^2+q^2\,)\\
&-2\,(\,d_5-d_6\,)(\,M^2-q^2\,)\,\Big]\Big[\,(\,\widetilde{d}_1+8\,\widetilde{d}_2-\widetilde{d}_3\,)\,m^2\\
&+\widetilde{d}_3\,(\,M^2+q^2\,)-2\,(\,\widetilde{d}_5-\widetilde{d}_6\,)(\,M^2-q^2\,)\,\Big]\,.
\end{aligned}
\tag{A.5.7}
$$

If $i=j$ then the following replacements on Eqs. (A.5.4-A.5.7) must be imposed to obtain the result for the new configuration:

$$
\begin{aligned}
d_1^{(ij)}\;&\to\;2\,d_1^{(i)}\\
d_2^{(ij)}\;&\to\;2\,d_2^{(i)}\\
d_3^{(ij)}\;&\to\;2\,d_3^{(i)}\\
d_4^{(ij)}\;&\to\;2\,d_4^{(i)}\\
d_5^{(ij)}\;&\to\;0\\
d_6^{(ij)}\;&\to\;0\,,
\end{aligned}
\tag{A.5.8}
$$

and similarly if $j=k$.

For the function $\mathcal{W}_{1,P}^{(i)}$ the loop calculation gives:

$$\mathcal{W}_{1,P}^{(i)} = \frac{(2\pi)^{D-4}}{M^4\, q^2}\left\{\mathcal{D}_0 + A_0[m^2]\,\mathcal{D}_m + A_0[M^2]\,\mathcal{D}_M + B_0[q^2, M^2, m^2]\,\mathcal{D}_B\right\}, \quad \text{(A.5.9)}$$

$$c_n \;\equiv\; c_n^{(i)}$$

$$\begin{aligned}
\mathcal{D}_0 \;=\;& \frac{q^8}{3}\left\{\,(\,c_1 - c_2 + c_5\,)^2\,\right\} \\
&- \frac{q^6}{3}\left\{\,(\,c_1 - c_2 + c_5\,)\Big[\,(\,c_1 - 5\,c_2 - 16\,c_3 + 5\,c_5\,)\,m^2\right. \\
&\qquad\left. +(\,5\,c_1 - 5\,c_2 + c_5 + 4\,c_6\,)\,M^2\,\Big]\,\right\} \\
&- \frac{q^4}{6}\left\{\,\Big[\,c_1(\,c_1 + 14\,c_2 + 64\,c_3 - 14\,c_5\,) + c_2\,(-23\,c_2 - 128\,c_3 + 46\,c_5\,)\right. \\
&\qquad -128\,c_3\,(\,c_3 - c_5\,) + c_5\,(-5\,c_5 + 36\,c_7\,) + 18\,c_7^2\,\Big]\,m^4 \\
&\quad + 4\,\Big[\,c_1\,(\,c_1 + 6\,c_2 + 32\,c_3 - 2\,c_5 - 4\,c_6\,) + c_2\,(-7\,c_2 - 32\,c_3 + 6\,c_5 + 8\,c_6\,) \\
&\qquad +16\,c_3\,(\,c_5 + c_6\,) + c_5\,(\,c_5 - 8\,c_6\,)\,\Big]\,M^2\,m^2 \\
&\quad + \Big[\,c_1\,(\,13\,c_1 + 46\,c_2 - 14\,c_5 - 32\,c_6\,) + c_2\,(-23\,c_2 + 14\,c_5 + 32\,c_6\,) \\
&\qquad \left. + c_5\,(\,c_5 - 16\,c_6\,) - 8\,c_6^2\,\Big]\,M^4\right\} \\
&- \frac{q^2}{2}\left\{\,\Big[\,c_1\,(11\,c_1 - 2\,c_2 + 80\,c_3 - 22\,c_5 - 24\,c_7\,) + \,c_2\,(\,-c_2 + 2\,c_5 - 16\,c_3\,)\right. \\
&\qquad +16\,c_3\,(\,8\,c_3 - 5\,c_5 - 6\,c_7\,) + c_5\,(\,11\,c_5 + 24\,c_7\,) + 12\,c_7^2\,\Big]\,m^6 \\
&\quad + \Big[\,c_1\,(\,c_1 - 2\,c_2 - 2\,c_5 + 4\,c_6\,) + c_2\,(\,9\,c_2 + 64\,c_3 + 2\,c_5 - 20\,c_6\,) \\
&\qquad +64\,c_3\,(2\,c_3 - c_6\,) + c_5\,(\,c_5 - 4\,c_6\,) + 12\,c_6^2\,\Big]\,M^2\,m^4 \\
&\quad + \Big[\,c_1\,(\,c_1 + 2\,c_2 + 16\,c_3 - 2\,c_5\,) + c_2\,(\,9\,c_2 + 80\,c_3 - 2\,c_5 - 16\,c_6\,) \\
&\qquad -16\,c_3\,(\,c_5 + 4\,c_6\,) + c_5^2 + 8\,c_6^2\,\Big]\,M^4\,m^2 \\
&\quad - \Big[\,c_1\,(\,c_1 - 2\,c_2 - 2\,c_5 + 4\,c_6\,) + c_2\,(-11\,c_2 + 2\,c_5 + 20\,c_6\,)
\end{aligned}$$

$$+ c_5\,(\,c_5 - 4\,c_6\,) - 8\,c_6^2\Big]\,M^6\Big\}\,, \tag{A.5.10}$$

$$\begin{aligned}
\mathcal{D}_m \;=\;& q^6\,\Big\{\,(\,c_1 - c_2 + c_5\,)^2\,\Big\} \\
& - q^4\,\Big\{\,2\Big[\,2\,c_2\,(\,c_2 + 4\,c_3 - 2\,c_5\,) + c_5\,(\,5\,c_5 - 8\,c_3 + 6\,c_7\,) + 3\,c_7^2 \\
& \qquad -2\,c_1\,(\,c_2 + 4\,c_3 - c_5\,)\Big]\,m^2 \\
& \qquad +(\,c_1 - c_2 + c_5\,)(\,3\,c_1 - 3\,c_2 - c_5 + 4\,c_6\,)\,M^2\,\Big\} \\
& - q^2\,\Big\{\,\Big[\,4\,c_1\,(\,3\,c_1 + c_2 + 28\,c_3 - 7\,c_5 - 6\,c_7\,) + c_2\,(\,c_2 + 12\,c_3 - 2\,c_5\,) \\
& \qquad + 4\,c_3\,(\,20\,c_3 - 9\,c_5 - 6\,c_7\,) + 2\,c_5\,(\,2\,c_5 + 3\,c_7\,) + 3\,c_7^2\Big]\,m^4 \\
& \qquad +\Big[\,c_1\,(3\,c_1 + 2\,c_2 + 32\,c_3 + 2\,c_5 - 4\,c_6\,) + c_2\,(-5\,c_2 - 32\,c_3 - 2\,c_5 + 12\,c_6\,) \\
& \qquad -5\,c_5^2 + 12\,c_6\,(\,c_5 - c_6\,)\Big]\,M^2\,m^2 \\
& \qquad -\Big[\,(\,c_1 - c_2 - c_5 + 2\,c_6\,)(\,3\,c_1 - 3\,c_2 + c_5 + 2\,c_6\,)\Big]\,M^4\,\Big\} \\
& + (m^2 - M^2)\Big[\,(\,c_1 + c_2 + 8\,c_3 - c_5\,)\,m^2 - (\,c_1 - c_2 - c_5 + 2\,c_6\,)\,M^2\,\Big]^2\,,
\end{aligned} \tag{A.5.11}$$

$$\begin{aligned}
\mathcal{D}_M \;=\;& q^6\,\Big\{\,(\,c_1 - c_2 + c_5\,)^2\,\Big\} \\
& - q^4\,\Big\{\,-\Big[\,(\,c_1 + 3\,c_2 + 16\,c_3 - 3\,c_5\,)(\,c_1 - c_2 + c_5\,)\Big]\,m^2 \\
& \qquad + 4\Big[\,c_1\,(\,-2\,c_1 - 2\,c_2 + c_5 + c_6\,) + (\,c_2 - c_5\,)(\,c_2 - c_6\,)\Big]\,M^2\,\Big\} \\
& - q^2\,\Big\{\,\Big[\,(\,c_1 + c_2 + 8\,c_3 - c_5\,)(\,c_1 - 3\,c_2 - 8\,c_3 + 3\,c_5\,)\Big]\,m^4 \\
& \qquad -4\Big[\,c_1\,(\,-c_1 + 2\,c_2 + c_5 - 3\,c_6\,) + (\,c_2 - c_6\,)(\,2\,c_2 - c_5 - c_6\,)\Big]\,M^4 \\
& \qquad -\Big[\,c_1\,(\,5\,c_1 + 2\,c_2 + 48\,c_3 - 2\,c_5\,) + c_2\,(\,5\,c_2 + 48\,c_3 - 2\,c_5 - 8\,c_6\,) \\
& \qquad -16\,c_3\,(\,c_5 - 2\,c_6\,) + c_5\,(-3\,c_5 + 8\,c_6\,)\Big]\,m^2\,M^2\,\Big\}
\end{aligned}$$

$$- (m^2 - M^2) \Big[(c_1 + c_2 + 8\, c_3 - c_5)\, m^2 - (c_1 - c_2 - c_5 + 2\, c_6)\, M^2 \Big]^2 , \tag{A.5.12}$$

$$\begin{aligned} \mathcal{D}_B \;\; = \;\; & -\lambda(q^2, m^2, M^2) \Big[(c_1 + c_2 + 8\, c_3 - c_5)\, m^2 - (c_1 - c_2 - c_5 + 2\, c_6)\, M^2 \\ & + (c_1 - c_2 + c_5)\, q^2 \Big]^2 . \end{aligned} \tag{A.5.13}$$

Finally, the function $\mathcal{W}_{2,P}^{(ij)}$, Fig. 5.1c with the resonance leg on the right amputated, results in:

$$\mathcal{W}_{2,P}^{(ij)} = \frac{(2\pi)^{D-4}}{2\sqrt{2}\, M^3\, q^2} \Big\{ \mathcal{E}_0 + A_0[m^2]\, \mathcal{E}_m + A_0[M^2]\, \mathcal{E}_M + B_0[q^2, M^2, m^2]\, \mathcal{E}_B \Big\} , \tag{A.5.14}$$

$$c_n \;\equiv\; c_n^{(i)} \qquad , \qquad d_n \;\equiv\; d_n^{(ij)}$$

$$\begin{aligned} \mathcal{E}_0 \;\; = \;\; & -\frac{q^8}{3} \Big\{ \; (c_1 - c_2 + c_5)(d_3 + 2\, d_5 - 2\, d_6) \Big\} \\ & -\frac{q^6}{3} \Big\{ \Big[c_1 (d_1 + 8\, d_2 - 3\, d_3 - 4\, d_5 + 4\, d_6) + 8\, c_3 (d_3 + 2\, d_5 - 2\, d_6) \\ & \qquad -(c_2 - c_5)(d_1 + 8\, d_2 - 5\, d_3 - 8\, d_5 + 8\, d_6) \Big] m^2 \\ & \qquad - \Big[(c_1 - c_2) (d_3 + 10\, d_5 - 10\, d_6) + c_5 (d_3 + 6\, d_5 - 6\, d_6) \\ & \qquad\quad + c_6 (2\, d_3 + 4\, d_5 - 4\, d_6) \Big] M^2 \Big\} \\ & +\frac{q^4}{6} \Big\{ \Big[c_1 (4\, d_1 + 32\, d_2 - 7\, d_3 - 6\, d_5 + 6\, d_6) + c_2 (-8\, d_1 - 64\, d_2 + 23\, d_3 \\ & \qquad +30\, d_5 - 30\, d_6) + 16\, c_3 (-d_1 - 8\, d_2 + 4\, d_3 + 6\, d_5 - 6\, d_6) + c_5 (8\, d_1 \\ & \qquad +64\, d_2 - 14\, d_3 + 9\, d_4 - 30\, d_5 + 12\, d_6) + 9\, c_7 (d_3 + d_4 - 2\, d_6) \Big] m^4 \\ & \qquad +4 \Big[c_1 (2\, d_1 + 16\, d_2 - d_3 - 2\, d_5 + 2\, d_6) + c_2 (-2\, d_1 - 16\, d_2 + 3\, d_3 \\ & \qquad\quad +10\, d_5 - 10\, d_6) + 8\, c_3 (d_3 + 4\, d_5 - 4\, d_6) + c_5 (d_1 + 8\, d_2 + d_3 \\ & \qquad\quad -4\, d_5 + 4\, d_6) + c_6 (d_1 + 8\, d_2 - 4\, d_3 - 6\, d_5 + 6\, d_6) \Big] M^2\, m^2 \\ & \qquad + \Big[c_1 (18\, d_1 - 7\, d_3 - 10\, d_5 + 10\, d_6) + c_2 (7\, d_3 + 46\, d_5 - 46\, d_6) \end{aligned}$$

$$+c_5\,(\,d_3-14\,d_5+14\,d_6\,)+8\,c_6\,(-d_3-4\,d_5+4\,d_6\,)\,\Big]\,M^4\Big\}$$

$$+\frac{q^2}{2}\,\Big\{\,\Big[\,(\,c_1-c_5\,)\,(\,5\,d_1+40\,d_2-5\,d_3-6\,d_4+12\,d_5\,)+c_2\,(-d_1-8\,d_2+d_3\,)$$

$$+8\,c_3\,(\,2\,d_1+16\,d_2-2\,d_3-3\,d_4+6\,d_5\,)-6\,c_7\,(\,d_1+8\,d_2-d_3$$

$$-d_4+2\,d_5\,)\,\Big]\,m^6+\Big[\,-\,(\,c_1-c_5\,)(\,d_3-2\,d_5+2\,d_6\,)+c_2\,(\,4\,d_1$$

$$+32\,d_2+d_3-10\,d_5+10\,d_6\,)+16\,c_3\,(\,d_1+8\,d_2-2\,d_5+2\,d_6\,)$$

$$-2\,c_6\,(\,2\,d_1+16\,d_2+d_3-6\,d_5+6\,d_6\,)\,\Big]\,M^2\,m^4\;+\;\Big[\,c_1\,(\,d_1+8\,d_2-d_3\,)$$

$$+c_2\,(\,5\,d_1+40\,d_2-d_3-8\,d_5+8\,d_6\,)+8\,c_3\,(\,3\,d_1-d_3-4\,d_5+4\,d_6\,)$$

$$+c_5\,(-d_1-8\,d_2+d_3\,)+4\,c_6\,(-d_1-8\,d_2+2\,d_5-2\,d_6\,)\,\Big]\,M^4\,m^2$$

$$+\Big[\,(\,c_1-c_5\,)(\,d_3-2\,d_5+2\,d_6\,)+c_2\,(\,6\,d_1-d_3-10\,d_5+10\,d_6\,)$$

$$+2\,c_6\,(-3\,d_1+d_3+4\,d_5-4\,d_6\,)\,\Big]\,M^6\,\Big\}\,, \qquad \text{(A.5.15)}$$

$$\mathcal{E}_m\;=\;-\,q^6\,\Big\{\,(\,c_1-c_2+c_5\,)(\,d_3+2\,d_5-2\,d_6\,)\,\Big\}$$

$$-\,q^4\,\Big\{\,\Big[\,c_1\,(\,d_1+8\,d_2-2\,d_3-2\,d_5+2\,d_6\,)-c_2\,(\,d_1+8\,d_2-4\,d_3-6\,d_5+6\,d_6\,)$$

$$+8\,c_3\,(\,d_3+2\,d_5-2\,d_6\,)+c_5\,(\,d_1+8\,d_2-7\,d_3-3\,d_4-6\,d_5+6\,d_6\,)$$

$$-3\,c_7\,(\,d_3+d_4-2\,d_6\,)\,\Big]\,m^2+\Big[\,(\,c_2-c_1\,)(\,d_3+6\,d_5-6\,d_6\,)$$

$$+c_5\,(\,d_3-2\,d_5+2\,d_6\,)-2\,c_6\,(\,d_3+2\,d_5-2\,d_6\,)\,\Big]\,M^2\,\Big\}$$

$$+\,q^2\,\Big\{\,\Big[\,c_1\,(\,7\,d_1+56\,d_2-8\,d_3-6\,d_4+10\,d_5+2\,d_6\,)+c_2\,(\,3\,d_1+24\,d_2-4\,d_3$$

$$-2\,d_5+2\,d_6\,)+8\,c_3\,(\,5\,d_1+40\,d_2-6\,d_3-3\,d_4+4\,d_5+2\,d_6\,)$$

$$+c_5\,(-9\,d_1-72\,d_2+10\,d_3+6\,d_4-10\,d_5-2\,d_6\,)-6\,c_7\,(\,d_1+8\,d_2$$

$$-d_3-d_4+2\,d_5\,)\,\Big]\,m^4\;+\;\Big[\,c_1\,(\,2\,d_1+16\,d_2+d_3+2\,d_5-2\,d_6\,)$$

$$-c_2\,(\,2\,d_1+16\,d_2+d_3-6\,d_5+6\,d_6\,)+32\,c_3\,(\,d_5-d_6\,)$$

$$-c_5\,(\,5\,d_3-2\,d_5+2\,d_6\,)+2\,c_6\,(\,d_1+8\,d_2+3\,d_3-4\,d_5+4\,d_6\,)\,\Big]\,M^2\,m^2$$

$$+\Big[\, c_1\,(\,d_3-6\,d_5+6\,d_6\,)-c_2\,(\,d_3-6\,d_5+6\,d_6\,)+c_5\,(\,d_3+2\,d_5-2\,d_6\,)$$
$$-8\,c_6\,(\,d_5-d_6\,)\Big]\,M^4\Big\}$$
$$-\,(m^2-M^2)\Big[\,(\,c_1+c_2+8\,c_3-c_5\,)\,m^2-(\,c_1-c_2-c_5+2\,c_6\,)\,M^2\Big]$$
$$\times\Big[\,(\,d_1+8\,d_2-d_3\,)\,m^2+(\,d_3-2\,d_5+2\,d_6\,)\,M^2\Big]\Big\}, \quad \text{(A.5.16)}$$

$$\mathcal{E}_M \;=\; -\,q^6\,\Big\{\,(\,c_1-c_2+c_5\,)(\,d_3+2\,d_5-2\,d_6\,)\Big\}$$
$$+\,q^4\,\Big\{\,-\Big[\,c_1\,(\,d_1+8\,d_2-d_3\,)-c_2\,(\,d_1+8\,d_2-3\,d_3-4\,d_5+4\,d_6\,)$$
$$+8\,c_3\,(\,d_3+2\,d_5-2\,d_6\,)+c_5\,(\,d_1+8\,d_2-3\,d_3-4\,d_5+4\,d_6\,)\Big]\,m^2$$
$$-2\,\Big[\,c_1\,(\,3\,d_1-d_3+2\,d_5-2\,d_6\,)+c_2\,(\,d_3+4\,d_5-4\,d_6\,)+2\,c_5\,(\,d_6-d_5\,)$$
$$-c_6\,(\,d_3+2\,d_5-2\,d_6\,)\Big]\,M^2\Big\}$$
$$+\,q^2\,\Big\{\,-\Big[\,-\,c_1\,(\,d_3+2\,d_5-2\,d_6\,)+c_2\,(\,2\,d_1+16\,d_2-3\,d_3-2\,d_5+2\,d_6\,)$$
$$+8\,c_3\,(\,d_1+8\,d_2-2\,d_3-2\,d_5+2\,d_6\,)+c_5\,(-2\,d_1-16\,d_2+3\,d_3$$
$$+2\,d_5-2\,d_6\,)\Big]\,m^4-\Big[\,c_1\,(\,3\,d_1+24\,d_2-d_3+4\,d_5-4\,d_6\,)$$
$$+c_2\,(\,3\,d_1+24\,d_2-d_3-4\,d_5+4\,d_6\,)+8\,c_3\,(\,3\,d_1-d_6\,)$$
$$-c_5\,(\,d_1+8\,d_2+3\,d_3\,)-2\,c_6\,(\,d_1+8\,d_2-2\,d_3-2\,d_5\;+2\,d_6\,)\Big]\,M^2\,m^2$$
$$-2\,\Big[\,c_1\,(\,d_3-4\,d_5+4\,d_6\,)+c_2\,(\,3\,d_1-d_3-2\,d_5+2\,d_6\,)+2\,c_5\,(\,d_5-d_6\,)$$
$$+c_6\,(\,d_3-3\,d_1\,)\Big]\,M^4\Big\}$$
$$+\,(m^2-M^2)\Big[\,(\,c_1+c_2+8\,c_3-c_5\,)\,m^2-(\,c_1-c_2-c_5+2\,c_6\,)\,M^2\Big]$$
$$\times\Big[\,(\,d_1+8\,d_2-d_3\,)\,m^2+(\,d_3-2\,d_5+2\,d_6\,)\,M^2\Big]\Big\}, \quad \text{(A.5.17)}$$

$$\mathcal{E}_B \;=\; \lambda(q^2,m^2,M^2)\Big[\,(\,c_1+c_2+8\,c_3-c_5\,)\,m^2-(\,c_1-c_2-c_5+2\,c_6\,)\,M^2$$
$$+\,(\,c_1-c_2+c_5\,)\,q^2\,\Big]\Big[\,(\,d_1+8\,d_2-d_3\,)\,m^2$$

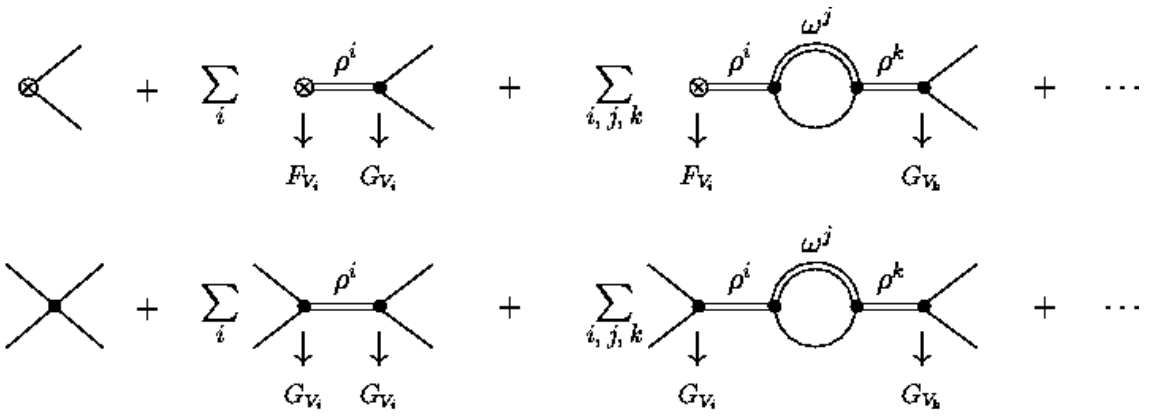

Figure 5.8: Resumming $\omega - \pi$ loops for N different multiplets

$$+(d_3 - 2\,d_5 + 2\,d_6)\,M^2 + (d_3 + 2\,d_5 - 2\,d_6)\,q^2 \Big] . \tag{A.5.18}$$

The set of conditions A.5.8 also apply for the function $\mathcal{W}_{2,P}^{(ij)}$ if $j = i$.

B Resummation for several multiplets

Let us analyse in this Appendix how the resummation explained in Section 5.6 gets modified when N different resonance octets are introduced in the theory. First note that $\omega - \pi$ (or $K^* - K$) loop insertions in the ρ propagators are not longer just self-energy corrections, as the intermediate ω^j (K^{*j}) resonance can couple to ρ's from different multiplets, thus inducing a mixing. The situation is sketched in Fig. 5.8: The series of the first line generalizes the result of $\vec{\mathcal{F}}_0$ in (5.30), which now has to account for any resonance occurring in the intermediate states:

$$\begin{aligned} \vec{\mathcal{F}}_0(q^2) \;\; = \;\; & \left\{ 1 + \sum_i \frac{F_{V_i} G_{V_i}}{F^2} \, \frac{q^2}{M_{V_i}^2 - q^2} + \right. \\ & \left. \sum_{i,j,k} \frac{F_{V_i} G_{V_k}}{F^2} \, \frac{-q^2}{(M_{V_i}^2 - q^2)(M_{V_k}^2 - q^2)} \, \mathcal{W}_0^{(ijk)}(q^2) \, + \, \ldots \right\} \begin{pmatrix} 1 \\ \frac{1}{2} \\ \frac{1}{2} \end{pmatrix} , \end{aligned} \tag{B.5.1}$$

with $i, j, k = 1, \ldots N$ and

$$\mathcal{W}_0^{(ijk)}(q^2) = \sum_{P=\pi^0,K} \frac{C_P^2}{F^2} \, \mathcal{W}_{0,P}^{(ijk)}(q^2) \; .$$

Introducing the matrix notation,

$$\vec{F}_V = \begin{pmatrix} F_{V_1} \\ F_{V_2} \\ \vdots \end{pmatrix} \ , \ \vec{G}_V = \begin{pmatrix} G_{V_1} \\ G_{V_2} \\ \vdots \end{pmatrix} \ ,$$

$$\mathrm{D} = \begin{pmatrix} (M_{V_1} - q^2)^{-1} & 0 & \cdots \\ 0 & (M_{V_2} - q^2)^{-1} & \cdots \\ \vdots & \vdots & \ddots \end{pmatrix} \ , \ \mathrm{W} = \begin{pmatrix} -\sum_j \mathcal{W}_0^{(1j1)} & -\sum_j \mathcal{W}_0^{(1j2)} & \cdots \\ -\sum_j \mathcal{W}_0^{(2j1)} & -\sum_j \mathcal{W}_0^{(2j2)} & \cdots \\ \vdots & \vdots & \ddots \end{pmatrix}$$

the sum of Eq. (B.5.1) can be written in a more compact form:

$$\begin{aligned} \vec{\mathcal{F}}_0(q^2) &= \left\{ 1 + \frac{q^2}{F^2} \vec{F}_V^{\top} \cdot \mathrm{D} \cdot \vec{G}_V + \frac{q^2}{F^2} \vec{F}_V^{\top} \cdot \mathrm{D} \cdot \mathrm{W} \cdot \mathrm{D} \cdot \vec{G}_V + \ldots \right\} \begin{pmatrix} 1 \\ \frac{1}{2} \\ \frac{1}{2} \end{pmatrix} \\ &= \left\{ 1 + \frac{q^2}{f^2} \vec{F}_V^{\top} \cdot \mathrm{D} \cdot (1 - \mathrm{W} \cdot \mathrm{D})^{-1} \cdot \vec{G}_V \right\} \begin{pmatrix} 1 \\ \frac{1}{2} \\ \frac{1}{2} \end{pmatrix} \\ &= \left\{ 1 + \frac{q^2}{F^2} \vec{F}_V^{\top} \cdot \mathrm{P} \cdot \vec{G}_V \right\} \begin{pmatrix} 1 \\ \frac{1}{2} \\ \frac{1}{2} \end{pmatrix} , \end{aligned} \tag{B.5.2}$$

which substitutes the expression of $\vec{\mathcal{F}}_0$ for just one multiplet, Eq. (5.30). Also note that the matrix W is symmetric,

$$\sum_j \mathcal{W}_0^{(ijk)}(q^2, M_{V_j}) = \sum_j \mathcal{W}_0^{(kji)}(q^2, M_{V_j}) \, ,$$

as the function $\mathcal{W}_0^{(ijk)}$ is symmetric under the exchange of the couplings $d_n^{(ij)}$ for $d_n^{(jk)}$.

We also need to generalize the $\omega - \pi$ and $K^* - K$ loop insertions which can happen between pseudoscalar scattering (see Fig. 5.8) to the case of several multiplets. The series shown in the second line of Fig. 5.8 is the pseudoscalar scattering amplitude in the $I = J = 1$ channel which, in the one-multiplet case, produces the term

$$\left(1 + \frac{2G_V^2}{F^2} \frac{q^2}{M_V^2 - q^2 + \mathcal{W}_0(q^2)} \right)$$

in the denominator of $\vec{\mathcal{F}}$, Eq. (5.29). For N multiplets the above result gets replaced by:

$$1 + \sum_i \frac{2G_{V_i}^2}{F^2} \frac{q^2}{M_{V_i}^2 - q^2} + \sum_{i,j,k} \frac{2G_{V_i} G_{V_k}}{F^2} \frac{-q^2}{(M_{V_i}^2 - q^2)(M_{V_k}^2 - q^2)} \mathcal{W}_0^{(ijk)}(q^2) + \ldots$$

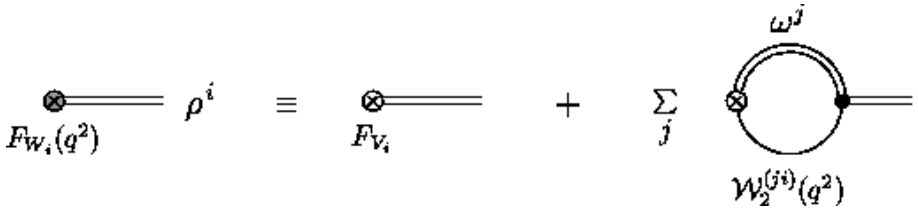

Figure 5.9: Vertex loop corrections for several resonance multiplets

$$
\begin{aligned}
&= 1 + \frac{2q^2}{F^2}\,\vec{G}_V^{\,\top}\cdot \mathrm{D}\cdot\vec{G}_V + \frac{2q^2}{F^2}\,\vec{G}_V^{\,\top}\cdot \mathrm{D}\cdot \mathrm{W}\cdot \mathrm{D}\cdot\vec{G}_V + \ldots \\
&= 1 + \frac{2q^2}{F^2}\,\vec{G}_V^{\,\top}\cdot \mathrm{P}\cdot\vec{G}_V\,, \qquad \text{(B.5.3)}
\end{aligned}
$$

using the matrix notation just introduced. Translating this result to the expression for the vector form factor $\vec{\mathcal{F}}$ we have

$$
\vec{\mathcal{F}}(q^2) = \frac{\vec{\mathcal{F}}_0}{1 + \left(1 + \frac{2q^2}{F^2}\,\vec{G}_V^{\,\top}\cdot \mathrm{P}\cdot\vec{G}_V\right)\frac{2q^2}{F^2}\,\bar{B}_{22}}\,. \qquad \text{(B.5.4)}
$$

We now turn over vertex loop corrections. By inspecting Fig. 5.9 we see that the q^2-dependent coupling to the external coupling defined in Eq. (5.32) must be now written as a vector with N components:

$$
\vec{F}_W(q^2) \;=\; \vec{F}_V + 2\sqrt{2}\,\vec{\mathcal{W}}_2(q^2)\,, \qquad \text{(B.5.5)}
$$

with

$$
\vec{\mathcal{W}}_2(q^2) = \begin{pmatrix} \sum_i \mathcal{W}_2^{(i\,1)} \\ \sum_i \mathcal{W}_2^{(i\,2)} \\ \vdots \end{pmatrix}\,,
$$

and

$$
\mathcal{W}_2^{(i\,j)}(q^2) \;=\; \sum_{P=\pi^0,K} \frac{C_P^2}{F^2}\,\mathcal{W}_{2,P}^{(i\,j)}(q^2)\,.
$$

The resummed $\omega-\pi$ loop insertions in the resonance propagators, Eq. (B.5.2), and the result (B.5.5) yield the final expression for the quantity $\vec{\mathcal{F}}_0$ which includes both features:

$$
\vec{\mathcal{F}}_0(q^2) \;=\; \left\{1 + \frac{q^2}{F^2}\,\vec{F}_W^{\,\top}\cdot \mathrm{P}\cdot\vec{G}_V\right\}\begin{pmatrix} 1 \\ \frac{1}{2} \\ \frac{1}{2} \end{pmatrix}\,. \qquad \text{(B.5.6)}
$$

Accordingly, the final expression for the vector form factor $\vec{\mathcal{F}}$ is obtained by inserted the result for $\vec{\mathcal{F}}_0$ above in Eq. (B.5.4).

Finally, it is straightforward to write down the resummed two-point function $\Pi(q^2)$ for the case of several multiplets:

$$\Pi(q^2) \;=\; \frac{\left(1+\frac{q^2}{F^2}\,\vec{F}_W^{\,\top}\cdot \mathrm{P}\cdot\vec{G}_V\right)^2}{1\,+\,\left(1+\frac{2q^2}{F^2}\,\vec{G}_V^{\,\top}\cdot \mathrm{P}\cdot\vec{G}_V\right)\frac{2q^2}{F^2}\,\bar{B}_{22}}\left(-4\bar{B}_{22}\right)\,+\,\vec{F}_W^{\,\top}\cdot \mathrm{P}\cdot\vec{F}_W$$

$$+\sum_i \frac{2\,\mathcal{W}_1^{(i)}(q^2)}{M_{V_i}^2}\;, \tag{B.5.7}$$

where

$$\mathcal{W}_1^{(i)}(q^2) \;=\; \sum_{P=\pi^0,K}\frac{C_P^2}{F^2}\,\mathcal{W}_{1,P}^{(i)}(q^2)\,.$$

We have also included the various contributions from different multiplets to the amplitude of Fig. 5.1d, given by the functions $\mathcal{W}_1^{(i)}(q^2)$.

Conclusiones

Resumimos a continuación las conclusiones más relevantes que pueden extraerse de las discusiones de los capítulos precedentes.

La producción de fermiones pesados

Los procesos de producción de fermiones pesados a partir de la aniquilación electrón-positrón han sido objeto de estudio recurrente en los últimos años. Este interés recoge multiples aspectos y un rango de energías enorme, desde la zona umbral a los colisionadores de alta energía. Entre las posibilidades de esta exploración, podemos destacar aspectos cruciales de la fenomenología, como la medida precisa de las masas de los fermiones (como el τ o el quark top), y la posibilidad de explorar Nueva Física más allá del Modelo Estándar. LEP y LEP2 nos han proporcionado la herramienta apropiada para perseguir este objetivo. Además es de esperar que este proceso sea uno de los que tengan una seccción eficaz más alta en un futuro colisionador lineal que funcione en la región de energía de 0.5 TeV a 1 TeV, como podrían ser TESLA y NLC/JLC-X, o CLIC a energías superiores. Para poder analizar convenientemente los datos experimentales se hace necesario que se calculen e implementen dentro del Modelo Estándar órdenes perturbativos completos. Proyectos como ZFITTER [18] y el CalcPHEP [19, 20], en pleno funcionamiento, persiguen crear el marco teórico adecuado para este propósito.

Las correcciones de QED no parecen ser especialmente interesantes para explorar efectos de la Teoría Cuántica dentro del Modelo Estándar, pero es evidente que su contribución, aunque pequeña, debe considerarse para investigar posibles efectos de Nueva Física. Además, si se quiere tener un conocimiento más profundo de los parámetros físicos de los fermiones pesados, la producción electromagnética de $\tau^+\tau^-$ o de quarks pesados $Q\overline{Q}$ cerca del umbral nos provee de la información necesaria.

Desde un punto de vista teórico, el cálculo de las secciones eficaces de $e^+e^- \to f\bar{f}$ cerca del umbral en teoría de perturbaciones es delicado, debido a la presencia en el sistema de una variable cinemática del mismo orden que la constante de la teoría *gauge*: la velocidad β del par de fermiones pesados en el centro de masas. Así, cuando $\beta \sim \alpha$, debemos tener cuidado en resumar los términos $(\alpha/\beta)^n$ o $(\alpha \ln \beta)^n$, que puedan dar contribuciones potencialmente grandes. Recientemente el desarrollo de las teorías de campos efectivas no-relativistas de QED y QCD implementan

el procedimiento sistemático adecuado. Instalaciones como la Factoría *Tau-Charm* propuesta en el pasado, un colisionador de e^+e^- de alta luminosidad con una energía de centro de masas cercana al umbral de producción de $\tau^+\tau^-$ [22], podrían proporcionar información vital sobre la masa de este leptón [24]. Además, una determinación precisa de la masa del quark *top* (dificil de conseguir en los próximos aceleradores hadrónicos), requiere el uso de un futuro colisionador de leptones en el umbral de $t\bar{t}$ [23]. Como consecuencia, se hace imprescindible un análisis exhaustivo de la contribuciones no-relativistas a $\sigma(e^+e^- \to f\bar{f})$.

En el Capítulo 2 hemos evaluado los diagramas tipo caja con dos fotones en QED, que contribuyen a $\sigma(e^+e^- \to f\bar{f})$ con fermiones finales masivos ($m_e \ll M$), proporcionando las expresiones analíticas completas. También se ha estudiado su contribución en la región cercana al umbral de producción, demostrándose que es despreciable por la supresión que produce la dependencia en la velocidad. Este analísis no-relativista complementa el llevado a cabo en la Referencia [24] (resumido al principio del capítulo), y muestran que la amplitud caja de QED no modifica las conclusiones alcanzadas allí.

Para finalizar con este cálculo hemos analizado el comportamiento a bajas velocidades usando la estrategia de regiones para expandir las integrales de Feynman cerca del umbral, confirmando, además, que dicha expansión puede aplicarse también a diagramas que involucran a la vez fermiones pesados y ligeros. Esta técnica permite identificar y evaluar las contribuciones a los diagramas de producción y aniquilación de fermiones pesados mediados por fermiones ligeros a un orden determinado en la velocidad.

En el capítulo siguiente hemos dirigido nuestra atención a la técnica usual para estudiar la producción de quarks pesados: las reglas de suma. Los análisis basados en las reglas de suma han usado de forma intensiva de la relación que existe entre el correlador de las corrientes electromagnéticas de quarks y la sección eficaz de $e^+e^- \to$ *hadrones* bajo la hipótesis de dualidad entre las descripciones en términos de quarks o de hadrones, para extraer información fundamental sobre los sistemas hadrónicos a partir de la fenomenología. Aplicadas a la producción de quarks pesados, las reglas de suma se han derivado empleando únicamente el correlador simétrico que se construye a partir de la corriente vectorial con los campos de quarks pesados. Sin embargo, a medida que se aumenta el orden perturbativo de este análisis, la consistencia del método exige que se estudien nuevos aspectos en la parte teórica de las reglas de suma de quarks pesados que no han sido considerados en trabajos anteriores.

De esta cuestión nos hemos ocupado en el Capítulo 3. Mientras que a $\mathcal{O}(\alpha_s)$ el correlador de dos corrientes de quarks pesados contiene toda la información perturbativa, se ha señalado que a $\mathcal{O}(\alpha_s^2)$ hay que tener en cuenta la posibilidad de que un par de quarks pesados $Q\overline{Q}$ sea radiado de los sabores ligeros en el correlador de dos corrientes de quarks ligeros. A $\mathcal{O}(\alpha_s^3)$ las dificultades crecen con el papel esencial que juegan los correladores asimétricos. El delicado problema de la discontinuidad de tres gluones que aparece en el correlador de corrientes de quarks pesados a $\mathcal{O}(\alpha_s^3)$, anticipado por Groote y Pivovarov, está muy relacionado con todo lo anterior.

Hemos mostrado cómo los resultados rigurosos de la teoría general de singularidades en teoría de perturbaciones proporcionan las herramientas esenciales para analizar las nuevas contribuciones. De esta forma se hace posible la inclusión o exclusión de alguna de las discontinuidades específicas en la parte perturbativa, exigiendo esta elección una definición clara de la información experimental que se introduce en la parte fenomenológica de las reglas de suma.

A $\mathcal{O}(\alpha_s^3)$ se ha propuesto una solución al problema expuesto por Groote and Pivovarov. Concluimos que el procedimiento apropiado para obtener información sobre los parámetros de quarks pesados debe hacer uso de momentos convenientemente corregidos en la zona infrarroja, los cuales satisfacen la regla de suma modificada del Capítulo 3. La incertidumbre asociada con la hadronización de los tres gluones es pequeña, aunque debe tenerse en cuenta.

El análisis llevado a cabo es completamente general, ya que se basa únicamente en la teoría de singularidades de las amplitudes perturbativas, y proporciona una herramienta muy eficaz para estudios futuros de las reglas se suma de quarks pesados.

Teorías efectivas en la descripción de quarks ligeros

Las teorías efectivas de QCD poseen todas las características cruciales de la teoría subyacente para describir la dinámica de hadrones en el régimen perturbativo. El sector de paridad intrínseca negativa ha sido estudiado en teoría quiral de perturbaciones, pero su extensión a la región de energía de las resonancias requiere que se implementen correctemente los grados de libertad activos, y que se genere la teoría efectiva correspondiente mediante un procedimiento capaz de implementar la física de QCD en las constantes de acoplamiento. Esta tarea se ha llevado a cabo en el Capítulo 4. Tras considerar cuáles son los operadores del Lagrangiano que respetan las simetrías globales de QCD, se ha procedido a trasladar la información de la teoría subyaciente a los acoplamientos, mediante un *matching* del comportamiento dominante de la expansión de producto de operadores en la función de Green vector-vector-pseudoscalar calculada en el límite quiral.

En primer lugar hemos introducido el Lagrangiano a orden más bajo con las interacciones entre un bosón de Goldstone y dos partículas vectoriales dentro de la Teoría Quiral con Resonancias en la formulación antisimétrica. A continuación se ha calculado la función de tres puntos $\langle \mathrm{VVP} \rangle$ a orden árbol con el nuevo sector añadido al Lagrangiano de resonancias. Asumiendo que la técnica de *matching* entre el resultado obtenido con la acción efectiva por un lado, y con QCD con quarks sin masa por otro, es válida para momentos grandes, hemos derivado un conjunto de relaciones entre los parámetros del sector de paridad intrínseca negativa.

En contraste con el resultado de la Referencia [50], en la que las resonancias son descritas como campos de Proca, la expresión para la función de Green $\langle \mathrm{VVP} \rangle$ obtenida con el Lagrangiano con campos antisimétricos es perfectamente compatible con las restricciones que impone QCD a cortas distancias, y se reduce al *ansatz*

sugerido por la hipótesis de *lowest meson dominance* (LMD) en el límite de gran número de colores de QCD, un resultado éste que ha sido probado con éxito en trabajos anteriores [52, 54].

En el camino hemos descubierto que las mismas combinaciones de acoplamientos que aparecen en las condiciones de cortas distancias de QCD, surgen en las amplitudes para los procesos $\omega \to \pi\gamma$ y $\rho \to \pi\gamma$ calculados con el Lagrangiano de resonancias, lo que nos permite dar una predicción completa para estas desintegraciones. El acuerdo con los valores experimentales es notable, considerando las limitaciones impuestas por la aproximación de gran N_C. Además, el cálculo de $\omega \to \pi\gamma$ muestra una característica importante: la contribución de un vértice directo $\omega\pi\gamma$ es más grande de lo esperado por la hipótesis de LMD. De hecho, esta pieza supone más de un 50% del resultado de esta amplitud. Ésto concuerda con las predicciones del contaje $1/N_C$, ya que ambos mecanismos contribuyen al mismo orden.

La conclusión anterior tiene importantes consecuencias para otros canales donde se pensaba que el mecanismo relevante de desintegración estaba dictado por VMD. Para que sirva de ejemplo, hemos mostrado que, dentro de nuestro formalismo, el intercambio de un meson intermedio $\omega \to \rho\pi \to 3\pi$ no puede dominar el proceso $\omega \to 3\pi$, siendo imprescindible la contribución local.

Nuestro estudio ha puesto de manifiesto que el uso de las teorías efectivas de QCD en la región de energías intermedias, poblada por resonancias, nos abastece de toda la información básica para obtener descripciones cuantitativas y cualitativas de la fenomenología hadrónica de una forma independiente de modelo.

El Capítulo 5 presenta la primera fase de un proyecto más ambicioso. Nuestro objetivo es obtener una descripción de la sección eficaz hadrónica en la región de las resonancias empleando la realización efectiva de QCD a esas energías junto a aspectos bien conocidos de la fenomenología.

A nivel teórico el conocimiento sobre esta región, alejada de los dominios de la simetría quiral ($E \ll M_\rho$, siendo M_ρ la masa de la resonancia $\rho(770)$), es muy deficiente debido a las complicaciones de la dinámica no-perturbativa de QCD. El método convencional para extraer los elementos de matriz hadrónicos de las corrientes de QCD se ha basado en la información experimental disponible, como los datos de $e^+e^- \to hadrones$ y de desintegraciones semileptónicas. A partir de estos datos, los observables hadrónicos se han obtenido típicamente por integración directa de los mismos o empleando parametrizaciones *ad hoc* vagamente inspiradas en QCD. Ambos procedimientos tienen una contrapartida clara: no nos dicen mucho sobre la física subyacente. Incluso cuando puede obviarse la interpretación física, tenemos que tener en mente que los métodos de ajuste (o de integración) heredan todas las incertidumbres asociadas con los datos experimentales, haciendo difícil el definir la precisión de los resultados. La estimación de los errores teóricos introducidos por estas técnicas es siempre objeto de discusión. Recuérdese, por ejemplo, la evolución de la constante de estructura fina de QED $\alpha(s)$ y el momento magnético anómalo del muón. Éstos son observables cuyas predicciones teóricas están limitadas por los efectos de los *loops* de la polarización hadrónica. Ambas magnitudes se relacionan via relaciones de dispersión con la tasa de produción hadrónica en la aniquilación

e^+e^-, que puede determinarse usando los datos de e^+e^- y de las desintegraciones hadrónicas del τ. Es claro que la aparente discrepancia entre el valor medido para el momento magnético anómalo del muón [70] y la predicción del Modelo Estándar [71] requiere una revisión cuidadosa de las incertidumbres teóricas asociadas a la contribución hadrónica, con el fin de determinar de forma precisa el tamaño de dicha desviación. Un análisis de estos observables de una forma independiente de modelo podría ayudar a clarificar esta cuestión.

Los intentos basados en las acciones efectivas de QCD han alcanzado un éxito considerable en la descripción de los datos para energías hasta 1 GeV y, de hecho, sugieren que este enfoque puede continuarse a energías más altas. El factor de forma vectorial a muy bajas energías se ha calculado en teoría quiral de perturbaciones, permitiendo describir los datos de $e^+e^- \to \pi^+\pi^-$ en esta región de forma muy precisa con los valores actuales de los parámetros quirales [72, 73]. En lo que respecta al momento magnético anómalo del muón, el uso de la expansión quiral para la contribución de dos piones a $E \leq 0.5$ GeV ha hecho disminuir drásticamente su error, en comparación con estimaciones anteriores obtenidas directamente de los datos. A energías superiores ($E \sim M_\rho$), el formalismo adecuado para implementar la información de QCD es RχT. Éste ha sido el punto de partida de varios trabajos dedicados al estudio del factor de forma del pion en la región cercana a la masa de la $\rho(770)$ [74, 75, 76], que también han implementado aspectos relevantes de la expansión de $1/N_C$, técnicas de resumación y otros requirimientos importantes, como analiticidad y unitariedad. La expresión para el correlador de corrientes vector-vector en la región de 1-2 GeV que proponemos en el Capítulo 5 sigue métodos similares a los de los trabajos mencionados. Nuestro análisis podría arrojar algo de luz sobre el citado asunto del momento magnético anómalo del muón, para el que alrededor del 90% del total de la contribución hadrónica proviene de la zona de energías por debajo de 2 GeV.

De acuerdo con el teorema óptico, extraemos $\sigma(e^+e^- \to \text{hadrones})$ de la parte imaginaria de la función de dos puntos $\Pi^{33}_{\mu\nu}(q^2)$ construida a partir de la parte de isospin uno de la corriente electromagnética. Nos centramos en la parte $I = 1$ de este observable ya que las resonancias en este canal son anchas y es crucial tener bajo control su comportamiento fuera de la capa de masas más alla de las aproximaciones de las parametrizaciones convencionales.

El formalismo se ha descrito previamente. Tomamos como base RχT y añadimos dos nonetes vectoriales extra para introducir las resonancias $\rho(1450)$ y $\rho(1700)$, que caracterizan el espectro hadrónico entre 1 y 2 GeV. Se mejora el cálculo perturbativo con la teoría efectiva respecto a trabajos anteriores sobre el factor de forma vectorial del pion incluyendo *loops* de resonancias $\omega \to \pi$ y $K^* \to K$, cuya parte absortiva está relacionada con los estados intermedios $2\pi^0\pi^+\pi^-$ y $2K\pi$, respectivamente. Los vértices que generan los *loops* mencionados pertenecen al sector de paridad intrínseca negativa, que se ha generalizado para permitir las interacciones entre distintos multipletes.

Se ha probado que la serie de inserciones de *loops* $\omega - \pi$ en los propagadores de las resonancias vectoriales puede sumarse, resultando una expresión analítica que

también incorpora los *loops* con dos pseudoscalares considerados en trabajos anteriores. Los nuevos *loops* modifican la anchura de los propagadores de las resonancias vectoriales fuera de la capa de masas y, por tanto, el factor de forma vectorial y el correlador $\Pi^{33}_{\mu\nu}(q^2)$, para los que hemos proporcionado expresiones completas en este capítulo.

Varias cuestiones han de ser abordadas antes de que podamos hacer uso de las expresiones obtenidas. Para empezar, el número de acoplamientos introducidos a través de los términos VJP y VVP del Lagrangiano de paridad intrínseca negativa para los tres nonetes propuestos es demasiado grande para hacer el formalismo viable, aun incluso si planeamos hacer un ajuste a los datos en la región de energías de 1 a 2 GeV. El estudio de las funciones de Green relevantes y su comparación con QCD a cortas distancias, tal y como se ha hecho en el análisis de la función de tres puntos VVP para el octete más ligero en el Capítulo 4, podría arrojar información adicional sobre los acoplamientos restantes. Éste parece un método muy prometedor para incorporar los requerimientos de QCD en las interacciones de baja energía, y debe avanzarse en esta dirección en trabajos futuros. Alternativamente se podría intentar inferir la importancia relativa de las interacciones de paridad intrínseca negativa entre los multipletes mediante un examen cuidadoso de la información experimental disponible, lo que permitiría despreciar algunos términos directamente.

Si restringimos nuestro trabajo a la hipótesis LMD, lo cuál puede ser una buena aproximación para energías por debajo de la $\rho(1450)$, nuestro conocimiento sobre los acoplamientos de paridad intrínseca negativa del primer multiplete, no nos permite, sin embargo, tener completo poder predictivo en nuestros resultados, ya que las constantes de substracción del procedimiento de regularización siguen siendo parámetros libres. No parece evidente cómo progresar en esta dirección, pues necesitaríamos primero ocuparnos de la renormalización de RχT [82].

Por último, los vértices V3P no incluídos no pueden ignorarse, y han de ser incluidos en nuestra resumación para completar el trabajo. Como se ha explicado, ésto es factible, pero introduce nuevas constantes desconocidas que requieren que se investigue el comportamiento asintótico de otras funciones de Green relevantes.

Bibliography

[1] M.E. Luke and A.V. Manohar, *Phys. Rev.* **D55** (1997) 4129;
A.V. Manohar, *Phys. Rev.* **D56** (1997) 230;
A. Pineda and J. Soto, *Nucl. Phys. Proc. Suppl.* **64** (1998) 428;
M. Beneke and V.A. Smirnov, *Nucl. Phys.* **B522** (1998) 321;
H.W. Griesshammer, *Phys. Rev.* **D58** (1998) 094027.

[2] A. Pich, arXiv:hep-ph/9806303.

[3] W. E. Caswell and G. P. Lepage, *Phys. Lett.* **B167** (1986) 437.

[4] M.E. Luke, A.V. Manohar and I.Z. Rothstein, *Phys. Rev.* **D61** (2000) 074025;
N. Brambilla, A. Pineda, J. Soto and A. Vairo, Nucl. Phys. B **566** (2000) 275 [arXiv:hep-ph/9907240];
A.V. Manohar, J. Soto, I.W. Stewart, *Phys.Lett.* **B486** (2000) 400.

[5] P. Labelle, *Phys. Rev.* **D58** (1998) 093913.

[6] N. Brambilla, arXiv:hep-ph/0012026.

[7] A. H. Hoang, arXiv:hep-ph/0204299.

[8] S. Coleman, J. Wess and B. Zumino, Phys. Rev. **177** (1969) 2239;
C.G. Callan, S. Coleman, J. Wess and B. Zumino, Phys. Rev. **177** (1969) 2247.

[9] S. Weinberg, Phys. Rev. **166** (1968) 1568.

[10] A. V. Manohar, arXiv:hep-ph/9606222.

[11] S. Weinberg, Physica **96A** (1979) 327.

[12] J. Gasser and H. Leutwyler, Ann. of Phys. (NY) **158** (1984) 142.

[13] J. Gasser and H. Leutwyler, Nucl. Phys. **B250** (1985) 465.

[14] G. Ecker, Prog. Part. Nucl. Phys. **35** (1995) 1;
H. Leutwyler, arXiv:hep-ph/9406283.

[15] G. 't Hooft, Nucl. Phys. B **72** (1974) 461.

[16] E. Witten, Nucl. Phys. B **160** (1979) 57.

[17] S. R. Coleman and E. Witten, Phys. Rev. Lett. **45** (1980) 100.

[18] D. Y. Bardin, P. Christova, M. Jack, L. Kalinovskaya, A. Olchevski, S. Riemann and T. Riemann, Comput. Phys. Commun. **133** (2001) 229.

[19] D. Y. Bardin, L. Kalinovskaya and G. Nanava, "An electroweak library for the calculation of EWRC to e+ e- → f anti-f within the topfit project," arXiv:hep-ph/0012080.

[20] A. Andonov, D. Bardin, S. Bondarenko, P. Christova, L. Kalinovskaya and G. Nanava, "Further study of the e+ e- → f anti-f process with the aid of CalcPHEP system," arXiv:hep-ph/0202112.

[21] R. Barbieri, P. Christillin and E. Remiddi, Phys. Rev. A **8** (1973) 2266.

[22] J. M. Jowett, "Initial Design Of The Cern Tau Charm Factory," CERN-LEP-TH/87-56;
A. Pich,"Perspectives on tau charm factory physics," arXiv:hep-ph/9312270.

[23] A. H. Hoang, A. V. Manohar, I. W. Stewart and T. Teubner, Phys. Rev. Lett. **86** (2001) 1951.

[24] P. Ruiz-Femenia and A. Pich, Phys. Rev. D **64** (2001) 053001.

[25] W. Beenakker, S. C. van der Marck and W. Hollik, Nucl. Phys. B **365** (1991) 24.

[26] P. Ruiz-Femenía, "La sección eficaz de producción de $\tau^+\tau^-$ en el umbral", Trabajo de Investigación de 3^{er} Ciclo, Dpto. de Física Teòrica - Univ. València, Julio 2000.

[27] E.A. Kuraev and V.S. Fadin, *Yad. Fiz.* **41** (1985) 733 [*Sov. J. Nucl. Phys.* **41** (1985) 466].

[28] A. Sommerfeld, *Atombau und Spektrallinien*, Vol.II, Vieweg, Braunschweig, 1939.

[29] A. H. Hoang and T. Teubner, *Phys. Rev.* **D58** (1998) 114023; A. A. Penin and A. A. Pivovarov, *Phys. Lett.* **B435** (1998) 413.

[30] M. Beneke and V. A. Smirnov, Nucl. Phys. B **522** (1998) 321.

[31] Z. Bern, L. J. Dixon and D. A. Kosower, Phys. Lett. B **302** (1993) 299, [Erratum-ibid. B **318** (1993) 649].

[32] J. Portolés and P. D. Ruiz-Femenía, Eur. Phys. J. C **25** (2002) 553.

[33] R. Mertig, M. Bohm and A. Denner, Comput. Phys. Commun. **64** (1991) 345, http://www.feyncalc.org.

[34] G. t' Hooft and M. Veltman, Nucl. Phys. B **153** (1979) 365.

[35] R. Barbieri, J. A. Mignaco and E. Remiddi, Nuovo Cim. A **11** (1972) 824.

[36] D. R. Yennie, S. C. Frautschi and H. Suura, Annals Phys. **13** (1961) 379;
N. Meister and D. R. Yennie, Phys. Rev. **130** (1963) 1210;
S. Weinberg, Phys. Rev. **140** (1965) B516.

[37] S. Groote and A. A. Pivovarov, JETP Lett. **75** (2002) 221 [Pisma Zh. Eksp. Teor. Fiz. **75** (2002) 267].

[38] S. Groote and A. A. Pivovarov, Eur. Phys. J. C **21** (2001) 133.

[39] T. Appelquist and H. Georgi, Phys. Rev. **D8** (1973) 4000;
A. Zee, Phys. Rev. **D8** (1973) 4038.

[40] L. D. Landau, Nucl. Phys. **13** (1959) 181;
J. C. Taylor, Phys. Rev. **117** (1960) 261;
R. E. Cutkosky, J. Math. Phys. **1** (1960) 429;
R. E. Cutkosky, Rev. Mod. Phys. **33** (1961) 448.

[41] M. A. Shifman, A. I. Vainshtein and V. I. Zakharov, Nucl. Phys. B **147** (1979) 385;
M. A. Shifman, A. I. Vainshtein and V. I. Zakharov, Nucl. Phys. B **147** (1979) 448;
L. J. Reinders, H. Rubinstein and S. Yazaki, Phys. Rept. **127** (1985) 1;
M. Jamin and A. Pich, Nucl. Phys. B **507** (1997) 334;
A. H. Hoang, Phys. Rev. D **59** (1999) 014039;
M. Beneke and A. Signer, Phys. Lett. B **471** (1999) 233;
M. Eidemuller and M. Jamin, Phys. Lett. B **498** (2001) 203.

[42] A. H. Hoang, M. Jezabek, J. H. Kuhn and T. Teubner, Phys. Lett. B **338** (1994) 330.

[43] D. J. Miller and M. H. Seymour, Phys. Lett. B **435** (1998) 213;
R. Barate *et al.* [ALEPH Collaboration], Phys. Lett. B **434** (1998) 437;
P. Abreu *et al.* [DELPHI Collaboration], Phys. Lett. B **462** (1999) 425.

[44] K. G. Chetyrkin, J. H. Kuhn and M. Steinhauser, Nucl. Phys. B **482** (1996) 213;
K. G. Chetyrkin, R. Harlander, J. H. Kuhn and M. Steinhauser, Nucl. Phys. B **503** (1997) 339.

[45] D. Z. Freedman, K. Johnson and J. I. Latorre, Nucl. Phys. B **371** (1992) 353;
D. Z. Freedman, G. Grignani, K. Johnson and N. Rius, Annals Phys. **218** (1992) 75.

[46] J. Portoles and P. D. Ruiz-Femenia, Eur. Phys. J. C **24** (2002) 439.

[47] J. Portoles and P. D. Ruiz-Femenia, J. Phys. G **29** (2003) 349.

[48] G. Ecker, J. Gasser, A. Pich and E. de Rafael, Nucl. Phys. **B321** (1989) 311.

[49] G. Ecker, J. Gasser, H. Leutwyler, A. Pich and E. de Rafael, Phys. Lett. **B223** (1989) 425.

[50] M. Knecht and A. Nyffeler, Eur. Phys. J. C **21** (2001) 659.

[51] J. Bijnens, E. Gamiz, E. Lipartia and J. Prades, JHEP **0304** (2003) 055.

[52] B. Moussallam, Phys. Rev. D **51** (1995) 4939.

[53] B. Moussallam, Nucl. Phys. B **504** (1997) 381.

[54] M. Knecht, S. Peris, M. Perrottet and E. de Rafael, Phys. Rev. Lett. **83** (1999) 5230.

[55] J. Wess and B. Zumino, Phys. Lett. **B37** (1971) 95;
E. Witten, Nucl. Phys. B **223** (1983) 22.

[56] D. Issler,"Nonrenormalization Of The Chiral Anomaly In Chiral Perturbation Theory," SLAC-PUB-4943;
R. Akhoury and A. Alfakih, Annals Phys. **210** (1991) 81.

[57] J. Bijnens, L. Girlanda and P. Talavera, Eur. Phys. J. C **23** (2002) 539.

[58] J. Bijnens, G. Ecker and J. Gasser, "Chiral perturbation theory", arXiv:hep-ph/9411232.

[59] E. Pallante and R. Petronzio, Nucl. Phys. B **396** (1993) 205.

[60] J. Prades, Z. Phys. C **63** (1994) 491 [Erratum-ibid. C **11** (1999) 571].

[61] J. Bijnens, Int. J. Mod. Phys. A **8** (1993) 3045.

[62] K. Hagiwara *et al.* [Particle Data Group Collaboration], Phys. Rev. D **66** (2002) 010001.

[63] G. Ecker and R. Unterdorfer, Eur. Phys. J. C **24** (2002) 535.

[64] S. L. Adler, Phys. Rev. **177** (1969) 2426;
J. S. Bell and R. Jackiw, Nuovo Cim. A **60** (1969) 47;
W. A. Bardeen, Phys. Rev. **184** (1969) 1848.

[65] J. F. Donoghue, B. R. Holstein and Y. C. Lin, Phys. Rev. Lett. **55** (1985) 2766.

[66] J. Bijnens, A. Bramon and F. Cornet, Phys. Rev. Lett. **61** (1988) 1453;
J. Bijnens, A. Bramon and F. Cornet, Z. Phys. C **46** (1990) 599.

[67] Joaquim Prades, private communication.

[68] G. P. Lepage and S. J. Brodsky, Phys. Lett. **B87** (1979) 359;
G. P. Lepage, S. J. Brodsky, Phys. Rev. D **22** (1980) 2157;
S. J. Brodsky and G. P. Lepage, Phys. Rev. D **24** (1981) 1808.

[69] J. Gronberg et *al.*, Phys. Rev. D **57** (1998) 33.

[70] G. W. Bennett *et al.* [Muon g-2 Collaboration], Phys. Rev. Lett. **89** (2002) 101804 [Erratum-ibid. **89** (2002) 129903].

[71] M. Davier, S. Eidelman, A. Hocker and Z. Zhang, arXiv:hep-ph/0308213.

[72] J. Gasser and H. Leutwyler, Nucl. Phys. B **250** (1985) 517.

[73] J. Bijnens, G. Colangelo and P. Talavera, JHEP **9805** (1998) 014.

[74] F. Guerrero and A. Pich, Phys. Lett. B **412** (1997) 382.

[75] D. Gomez Dumm, A. Pich and J. Portolés, Phys. Rev. D **62** (2000) 054014.

[76] J. J. Sanz-Cillero and A. Pich, Eur. Phys. J. C **27** (2003) 587.

[77] J. J. Sakurai, Currents and Mesons (University of Chicago press, Chicago, IL, 1969).

[78] D. Gomez Dumm, A. Pich and J. Portolés, "$\tau \to \pi\pi\nu_\tau$ decays in the Resonance Effective Theory", IFIC/03-38.

[79] P. D. Ruiz-Femenía, A. Pich and J. Portolés, JHEP **0307** (2003) 003.

[80] B. Ananthanarayan and B. Moussallam, JHEP **0205** (2002) 052.

[81] J. Portolés and P. D. Ruiz-Femenía, work in preparation.

[82] A. Pich, I. Rosell and J. Sanz-Cillero, work in preparation.